Published for SISSA by Springer

Received: November 3, 2025
Accepted: February 9, 2026
Published: April 10, 2026

Inclusive and differential measurements of the $t\bar{t}\gamma$ cross section and the $t\bar{t}\gamma/t\bar{t}$ cross section ratio in proton-proton collisions at $\sqrt{s} = 13$ TeV

The CMS collaboration

Full author list at the end of the paper

E-mail: cms-publication-committee-chair@cern.ch

Abstract: Inclusive and differential cross section measurements of top quark pair ($t\bar{t}$) production in association with a photon (γ) are performed as a function of lepton, photon, top quark, and $t\bar{t}$ kinematic observables, using data from proton-proton collisions at $\sqrt{s} = 13$ TeV, corresponding to an integrated luminosity of 138 fb^{-1}, collected at the CERN LHC with the CMS detector. Events containing two leptons (electrons or muons) and a photon in the final state are considered. The fiducial cross section of $t\bar{t}\gamma$ is measured to be 137 ± 8 fb, in a phase space including events with a high momentum, isolated photon. The fiducial cross section of $t\bar{t}\gamma$ is also measured to be 56 ± 5 fb when considering only events where the photon is emitted in the production part of the process. Both measurements are in agreement with the theoretical predictions, of 126 ± 19 fb and 57 ± 5 fb, respectively. Differential measurements are performed at the particle and parton levels. Additionally, inclusive and differential ratios between the cross sections of $t\bar{t}\gamma$ and $t\bar{t}$ production are measured. The inclusive ratio is found to be 0.0133 ± 0.0005, in agreement with the standard model prediction of 0.0127 ± 0.0008. The top quark charge asymmetry in $t\bar{t}\gamma$ production is also measured to be -0.012 ± 0.042, compatible with both the standard model prediction and with no asymmetry.

Keywords: Hadron-Hadron Scattering, Particle and Resonance Production, Top Physics

ArXiv ePrint: 2511.01995

https://doi.org/10.1007/JHEP04(2026)086

JHEP04(2026)086

Contents

JHEP04(2026)086

1 Introduction

Precision measurements of top quark production can be used to test the standard model (SM) of particle physics. The associated production of a top quark-antiquark pair ($t\bar{t}$) with a photon (γ), is of particular interest as it is sensitive to new phenomena in the top quark electromagnetic coupling to the photon. Unlike other processes that offer sensitivity to new phenomena only at higher orders in perturbation theory [1–3], in $t\bar{t}\gamma$ production these effects are present already at leading order (LO) in perturbative quantum chromodynamics (QCD). New t-γ interactions can be targeted in dedicated differential cross section measurements, for example, as a function of the photon momentum. Moreover, differential measurements provide useful information on the modelling of the $t\bar{t}\gamma$ production process.

In $t\bar{t}\gamma$ events, the photon can originate from initial-state radiation (ISR), intermediate-state particles, such as the top quarks, or final-state radiation (FSR) from the top quark decay products. Some examples of Feynman diagrams for $t\bar{t}\gamma$ production at LO in QCD are

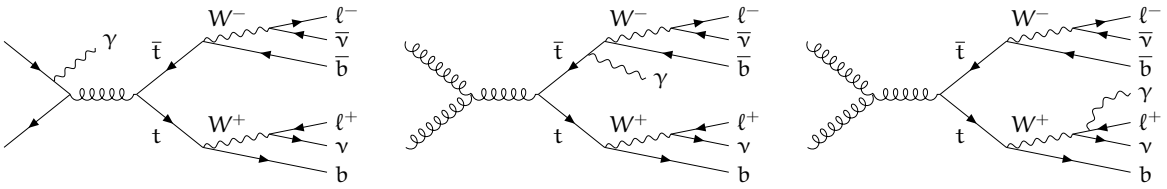

Figure 1. Example Feynman diagrams for the production of $t\bar{t}\gamma$, where both top quarks decay leptonically. The photon can be emitted from the initial state (left), from an off-shell top quark (centre), or from a top quark decay product (right).

shown in figure 1, with the top quarks decaying leptonically. Events consisting of a $t\bar{t}$ pair with a photon emission during the hadronization stage are commonly treated as background. It has been shown in theoretical studies [4, 5] that, in the narrow-width approximation, the cross section of the $t\bar{t}\gamma$ process with a high-momentum photon can be factorized into two parts: the first part describes the process where a photon is emitted from ISR or from an off-shell top quark (referred to as $t\bar{t}\gamma$ production), and the second part describes the process where a photon is emitted from an on-shell top quark or from the top quark decay products (referred to as $t\bar{t}\gamma$ decay). While the $t\bar{t}\gamma$ production process is the one offering sensitivity to the t-γ coupling, and therefore the most interesting from a physics perspective, both processes have similar experimental signatures and thus the analysis reported in this paper aims to measure both. Single top quark production in association with a W boson and a photon ($tW\gamma$) is another process that can be categorized in the same way into production and decay. In the following, it is treated as an irreducible background.

The interference between diagrams where the photon is emitted from one of the initial-state quarks and diagrams where it is radiated from one of the top quarks introduces a charge asymmetry in $t\bar{t}\gamma$ production at LO in QCD. This asymmetry induces an anisotropy in the rapidity distributions of the top quark and antiquark, where the top quark tends to scatter more centrally than the antiquark. A similar effect, but with gluon emission and in the opposite direction, is also present in $t\bar{t}$ production, but the latter takes place only at next-to-LO (NLO) in QCD. The charge asymmetry in $t\bar{t}\gamma$ production can be more pronounced than that of $t\bar{t}$ production [6, 7], partly because the contribution of quark-initiated production in the $t\bar{t}\gamma$ process is enhanced by about 60% (at LO) when compared to $t\bar{t}$ [8].

Regardless of the photon origin, top quarks in $t\bar{t}\gamma$ events are mainly produced via QCD interactions, through similar diagrams as the standard $t\bar{t}$ production at the CERN LHC. The ratio of the cross section of $t\bar{t}\gamma$ to that of $t\bar{t}$, R_γ, benefits from the cancellation of several systematic uncertainties and yields an observable that can probe theory predictions more precisely. Differential measurements of R_γ bring additional insight into the $t\bar{t}\gamma$ process [9], as new physics effects can depend on the phase space. Such measurements can be used to place strong constraints on new t-γ couplings in the context of SM effective field theory [3, 10].

The $t\bar{t}\gamma$ process was observed for the first time by the CDF Collaboration at the Fermilab Tevatron [11]. It was later observed at the LHC by the ATLAS Collaboration at $\sqrt{s} = 7\,\text{TeV}$ [12], and by both the ATLAS and CMS Collaborations at 8 TeV [13, 14]. At $\sqrt{s} = 13\,\text{TeV}$, the ATLAS and CMS Collaborations have each measured the inclusive $t\bar{t}\gamma$ cross section, as well as differential distributions of lepton and photon observables [15–19].

JHEP04(2026)086

The ATLAS Collaboration has also performed a measurement of the charge asymmetry in $\mathrm{t\bar{t}\gamma}$ events [20]. To date, no differential measurements have been reported for R_γ, nor for $\mathrm{t\bar{t}\gamma}$ as a function of observables related to the kinematic properties of the top quarks.

In this paper, we report the first differential measurements of the $\mathrm{t\bar{t}\gamma}$ cross section as a function of top quark and $\mathrm{t\bar{t}}$ system observables, using proton-proton (pp) collision data recorded with the CMS detector at $\sqrt{s} = 13\,\mathrm{TeV}$ between 2016 and 2018, corresponding to an integrated luminosity of $138\,\mathrm{fb}^{-1}$. Inclusive and differential R_γ measurements are also presented, and the top quark charge asymmetry is determined in $\mathrm{t\bar{t}\gamma}$ events. The measurements are performed using events with two oppositely charged leptons and a photon. In this paper, leptons refer to electrons or muons, unless otherwise specified. Events with τ leptons are only considered if the τ leptons decay into electrons or muons passing the selection criteria. Throughout the paper, the designation "top quark" includes both the quark and the antiquark, unless otherwise indicated. These results are also tabulated in the HEPData record for this analysis [21].

The paper is organized as follows. In section 2, an overview of the CMS detector is given. Subsequently, in section 3, the data sets and Monte Carlo (MC) simulation samples used for the analysis are described. The criteria to reconstruct and select the physics objects and to select the events are discussed in sections 4 and 5, respectively. Section 6 describes the methods used to estimate the background contributions, focusing on the backgrounds arising from misidentified photons and photons produced in hadron decays, using control samples in data. The systematic uncertainties are reported in section 7. The statistical analysis is introduced in section 8, while the results for the inclusive and differential cross section measurements are presented in section 9. The results for R_γ are reported in section 10. Section 11 presents the top quark charge asymmetry measurement in $\mathrm{t\bar{t}\gamma}$ events, and a summary of the paper is given in section 12.

2 The CMS experiment

The central feature of the CMS apparatus is a superconducting solenoid of 6 m internal diameter, providing a magnetic field of 3.8 T. Within the solenoid volume are a silicon pixel and strip tracker, a lead tungstate crystal electromagnetic calorimeter (ECAL), and a brass and scintillator hadron calorimeter (HCAL), each composed of a barrel and two endcap sections. The ECAL consists of 75 848 lead tungstate crystals, which provide coverage in absolute pseudorapidity $|\eta| < 1.48$ in the barrel region (EB) and $1.48 < |\eta| < 3.0$ in the two endcap regions (EE). Preshower detectors consisting of two planes of silicon sensors interleaved with a total of three radiation lengths of lead are located in front of each EE detector.

Forward calorimeters extend the pseuddorapidity coverage provided by the barrel and endcap detectors. Muons are measured in gas-ionization detectors embedded in the steel flux-return yoke outside the solenoid, using three technologies: drift tubes, cathode strip chambers, and resistive plate chambers. A more detailed description of the CMS detector, together with a definition of the coordinate system used and the relevant kinematic variables, can be found in refs. [22, 23].

Events of interest are selected using a two-tiered trigger system. The first level (L1), composed of custom hardware processors, uses information from the calorimeters and muon

JHEP04(2026)086

detectors to select events at a rate of around 100 kHz within a fixed latency of about 4 μs [24]. The second level, known as the high-level trigger (HLT), consists of a farm of processors running a version of the full event reconstruction software optimized for fast processing, and reduces the event rate to a few kHZ before data storage [25, 26].

3 Data and simulated samples

Events from pp collision data are selected using a combination of single- and double-lepton triggers. The online selection requirements on leptons depend on the trigger type and vary according to the data-taking conditions. The threshold on transverse momentum p_T ranges from 27 (24) GeV to 35 (27) GeV for electrons (muons) in single-lepton triggers. In dilepton triggers, the p_T of the leading (subleading) lepton must exceed the threshold of 23 (12) and 17 (8) GeV in the dielectron and dimuon paths, respectively. In the electron-muon paths, the leading lepton must have p_T above 23 GeV, while the subleading lepton must have p_T above 12 GeV if it is an electron, or above 8 GeV if it is a muon.

Monte Carlo simulations are used to estimate the contributions from both signal and background processes. Since the CMS detector configuration has undergone some changes between 2016 and 2018, samples are simulated for different data-taking periods separately. The $\mathrm{t\bar{t}\gamma}$ production process is modelled as a 2→3 process ($\mathrm{pp} \to \mathrm{t\bar{t}\gamma}$) with two on-shell top quarks using the MadGraph5_aMC@NLO (v2.9.18) [27] MC generator, at NLO accuracy in QCD, with up to one additional jet at LO. Only photons with $p_T > 10$ GeV and $|\eta| < 2.6$ are accepted. They must have an angular separation from other generated particles of $\Delta R > 0.05$, where $\Delta R = \sqrt{(\Delta\eta)^2 + (\Delta\phi)^2}$, and ϕ is azimuthal angle, as defined in ref. [28], with $\varepsilon_\gamma = 1$, and $n = 1$. Top quark decays are simulated via MADSPIN [29]. A similar procedure is followed to simulate $\mathrm{tW\gamma}$ production events at NLO accuracy in QCD, except that only one on-shell top quark must be present at matrix-element (ME) level, and no additional jets are simulated at ME level. The $\mathrm{tW\gamma}$ and $\mathrm{t\bar{t}\gamma}$ samples contain some overlap, which is removed using the diagram removal (DR) method [30].

To model the $\mathrm{t\bar{t}\gamma}$ decay process, a sample simulating the 2→2→7 ($\mathrm{pp} \to \mathrm{t\bar{t}} \to \ell^+\ell^-\nu\bar{\nu}\mathrm{b\bar{b}\gamma}$) process at LO accuracy in QCD is produced with MadGraph5_aMC@NLO, and the cross section is scaled to the NLO value of 2220.37 fb using a K-factor of 1.48, computed in ref. [16]. Simulated events in this sample contain a photon with $p_T > 10$ GeV and $|\eta| < 5$, isolated from other particles within a fixed cone of radius $R = 0.1$. An alternative model for the $\mathrm{t\bar{t}\gamma}$ decay process is provided by a $\mathrm{t\bar{t}}$ sample produced with the POWHEG (v2.0) MC event generator [31–33] at NLO accuracy in QCD and filtered for events with a "signal" photon, generated in the parton shower (PS), emitted from particles involved in the decay of one of the top quarks, before hadronization. "Signal" photons are defined as photons with generated $p_T > 20$ GeV, isolated from nearby particles, and not emitted in hadron decays. The sample produced with MadGraph5_aMC@NLO is taken as the reference, and is designated as the "nominal sample" throughout the paper, but all the differential results are also compared with the POWHEG model, designated as the "alternative sample".

The $\mathrm{t\bar{t}}$ process with no additional photons is simulated using the same sample produced with POWHEG, mentioned above, but vetoing any "signal" photons in the event. For this sample, the inclusive $\mathrm{t\bar{t}}$ cross section (before any photon veto) is scaled to the most precise

JHEP04(2026)086

theoretical prediction at next-to-NLO (NNLO) accuracy in QCD, 832 ± 42 pb, which is calculated using the TOP++ (v2.0) program [34]. The calculation also includes the resummation of next-to-next-to-leading-logarithm (NNLL) soft-gluon terms [35–39]. The $\mathrm{t\bar{t}}$ and $\mathrm{t\bar{t}\gamma}$ decay simulated events are reweighted in order to account for a known mismodelling of the top quark p_{T}, $p_{\mathrm{T}}(\mathrm{t})$, in the simulation at NLO, due to missing higher order corrections. This procedure is also referred to as "NNLO QCD reweighting" [40], and is performed using FASTNLO tables [41–43] to compute the $p_{\mathrm{T}}(\mathrm{t}/\bar{\mathrm{t}})$ distribution in fixed-order QCD at NNLO.

The $\mathrm{tW\gamma}$ decay process is modelled with a tW sample also produced with the POWHEG event generator and filtered in the same way as the $\mathrm{t\bar{t}}$ sample. The tW process without additional photons is obtained using the same tW sample, but vetoing events with "signal" photons. Other processes involving top quarks are produced with MADGRAPH5_aMC@NLO at LO or at NLO accuracy in QCD, depending on the process.

The MADGRAPH5_aMC@NLO event generator is used for the remaining background processes, except for diboson processes with massive vector bosons (ZZ, WZ, and WW) processes, which are generated at LO accuracy in QCD with PYTHIA (v8.240) [44]. The production of Drell-Yan events with up to four additional jets (DY+jets) is modelled at LO for dilepton invariant masses of $10 < m(\ell\ell) < 50$ GeV and at NLO for $m(\ell\ell) > 50$ GeV. The associated production of a Z (W) boson and a photon, with up to one additional jet, $\mathrm{Z\gamma}$+jets ($\mathrm{W\gamma}$+jets), as well as triboson processes are generated at NLO. The overlap between $\mathrm{Z\gamma}$+jets and DY+jets, and $\mathrm{W\gamma}$+jets and W+jets, is removed, by requiring that the events in the DY+jets and W+jets samples have no generated photons within the phase spaces generated in the $\mathrm{Z\gamma}$+jets and $\mathrm{W\gamma}$+jets samples, respectively.

For all simulated samples involving top quarks, the top quark mass is set to 172.5 GeV [45]. All processes are interfaced with PYTHIA using the CP5 tune [46–48] to model the hadronization, PS, and underlying event. The NNPDF parton distribution functions (PDFs) version 3.1 [49] at NNLO are used. The MLM [50] (FxFx [51]) matching scheme is used at LO (NLO) to account for the double-counting of jets from the ME calculations and the PS. Generated events are passed through the full description of the CMS detector, implemented in GEANT4 [52]. Multiple simultaneous pp collisions occur within the same bunch crossing (about 27–38 on average in 2016–2018). To model the effect of pileup caused by these additional collisions, as well as collisions from bunch crossings nearby in time, minimum bias interactions are simulated and superimposed on the hard-scattering events. Simulated events are then reweighted to reproduce the distribution of the number of interactions in each bunch crossing [53] observed in data.

4 Object reconstruction and selection

The signature of the $\mathrm{t\bar{t}\gamma}$ signal consists of a high-p_{T} photon, together with the decay products of $\mathrm{t\bar{t}}$ in the dilepton final state, i.e., two oppositely-charged leptons (e or μ), two jets originating from b quarks, and a p_{T} imbalance due to the presence of neutrinos.

Events are required to contain a primary vertex (PV), taken to be the vertex in which the p_{T} sum of the associated physics objects is the largest, as described in section 9.4.1 of ref. [54]. The particle-flow (PF) algorithm [55] aims to reconstruct and identify each

JHEP04(2026)086

individual particle in an event, with an optimized combination of information from the various elements of the CMS detector.

The energy of electrons is evaluated from a combination of the electron momentum at the PV as determined by the tracker, the energy of the corresponding ECAL cluster, and the energy sum of all bremsstrahlung photons spatially compatible with originating from the electron track. The momentum resolution for electrons with $p_{\mathrm{T}} \approx 45\,\mathrm{GeV}$ from $\mathrm{Z} \to \mathrm{e}^{+}\mathrm{e}^{-}$ decays ranges from 1.6 to 5.0%, depending on the electron η [56, 57]. Electrons are selected with $p_{\mathrm{T}} > 25\,\mathrm{GeV}$ if they are the leading lepton in the event, and with $p_{\mathrm{T}} > 20\,\mathrm{GeV}$ otherwise. They are required to lie within $|\eta| < 2.5$, excluding candidates that are reconstructed in the ECAL superclusters (SC) located in the transition region between the barrel and endcap, $1.44 < |\eta_{\mathrm{SC}}| < 1.57$. Electron identification requirements are based on the shower shape, the track-cluster matching, the hadronic over electromagnetic energy ratio, and the incompatibility with originating from a photon conversion. The isolation variable I_{rel} is calculated by summing the transverse energy deposited by other particles in a cone of radius $\Delta R = 0.3$ centered around the lepton, normalized to the lepton p_{T}. The contribution of charged particles from pileup is suppressed by requiring the charged particles to be associated with the PV. An average pileup energy is subtracted from the total energy of neutral particles and photons within the isolation cone. To select electron candidates, p_{T}- and η-dependent maximum values are set on I_{rel} in the range of 5–10%. A set of identification and isolation criteria are chosen such that genuine electrons are selected with an efficiency of about 70% [56].

Muons are measured in the range $|\eta| < 2.4$, and their momentum is obtained from the curvature of the corresponding track. Matching muons to tracks measured in the silicon tracker results in a relative p_{T} resolution, for muons with p_{T} up to 100 GeV, of 1% in the barrel and 3% in the endcaps [58]. Muons are selected with $p_{\mathrm{T}} > 25$ (15) GeV, if they are the leading (subleading) lepton in the event. Identification requirements are based on the quality of the geometrical matching between the measurements of the tracker and the muon system. The identification efficiency varies between 95 and 99%, depending on η, where the data and simulation agree within 1–3% [58]. The misidentification rate for pions and kaons was found to be below 0.3%. Muons are further required to be isolated with $I_{\mathrm{rel}} < 0.15$ where the isolation cone is of radius $\Delta R = 0.4$.

Photons are selected with $|\eta| < 2.5$, excluding the ECAL transition region, and with $p_{\mathrm{T}} > 20\,\mathrm{GeV}$, where the energy of the photon is obtained from the ECAL measurement [59]. Photon identification is based on the shower shape information, the hadronic to electromagnetic energy ratio, and a p_{T}- and η-dependent isolation from nearby charged and neutral reconstructed particles. A "medium" identification working point that is 80% efficient for selecting genuine photons is used [56, 60, 61]. Photon candidates are rejected if a track in the silicon tracker is found to be compatible with the photon cluster (pixel seed veto), thus reducing the number of electrons misidentified as photons. Finally, photons must be well separated from all selected leptons in the event, fulfilling the criterion $\Delta R(\gamma, \ell) > 0.4$.

Jets are reconstructed by clustering the PF candidates using the anti-k_{T} algorithm [62, 63] with a distance parameter of 0.4. The energy of neutral hadrons is obtained from the corresponding corrected ECAL and HCAL energies. The energy of charged hadrons is determined from a combination of their momentum measured in the tracker and the matching

JHEP04(2026)086

ECAL and HCAL energy deposits, corrected for the response function of the calorimeters to hadronic showers. Contamination from pileup and electronic noise is subtracted using the charged-hadron subtraction method [55]. An η-dependent uncertainty is added to the jet energy in simulated events to better describe the data resolution [64, 65]. Jets are selected with $p_{\mathrm{T}} > 30\,\mathrm{GeV}$ and $|\eta| < 2.4$, and are required to be away from leptons by $\Delta R(\ell, \mathrm{jet}) > 0.4$, and photons by $\Delta R(\gamma, \mathrm{jet}) > 0.4$.

The DeepJet b tagging algorithm [66–68] is used to identify jets originating from b quarks in $\mathrm{t\bar{t}}$ decays. The medium working point of the algorithm is chosen, corresponding to an efficiency of 80% and a misidentification rate of 1% for light-quark and gluon jets.

The missing transverse momentum vector $\vec{p}_{\mathrm{T}}^{\,\mathrm{miss}}$ is computed as the negative vector sum of the transverse momenta of all the PF candidates in an event, and its magnitude is denoted as $p_{\mathrm{T}}^{\mathrm{miss}}$ [69], and it is a measure of the momentum imbalance in an event. This quantity is used to reconstruct the $\mathrm{t\bar{t}}$ system in the events, as described in section 5. The $\vec{p}_{\mathrm{T}}^{\,\mathrm{miss}}$ is modified to account for corrections to the energy scale of the reconstructed jets in the event. This observable is sensitive to pileup interactions, inefficiencies in reconstruction, energy calibrations, and detector effects.

Differences between data and simulation arising in lepton reconstruction, identification, and triggering efficiencies, the energy scale and resolution of jets, and the response of the DeepJet algorithm are accounted for through corrections applied to the simulated samples. These corrections are typically at the level of a few percent [66, 69, 70] and are measured using a variety of SM processes, such as $\mathrm{Z} \to \mathrm{e^+e^-}$, $\mathrm{Z} \to \mu^+\mu^-$, $\mathrm{t\bar{t}}$, and γ+jets production.

5 Event reconstruction and selection

Following the HLT selection of events, a variety of offline requirements are made. Each event must have at least two charged leptons, and the two highest p_{T} (leading) leptons are required to have opposite charge and an invariant mass $m(\ell\ell)$ greater than 40 GeV. Events where the two leading leptons are of the same flavour are rejected if $m(\ell\ell)$ is compatible, within a $\pm 15\,\mathrm{GeV}$ window, with the mass of the Z boson, m_{Z}. Events are then required to have exactly one photon satisfying the criteria defined in section 4. For same-flavour lepton events, the invariant mass of the photon and two leading leptons, $m(\ell\ell\gamma)$, must not be compatible with originating from a Z boson, $m_{\mathrm{Z}} \pm 15\,\mathrm{GeV}$. This is to reject the background from the $\mathrm{Z} \to \ell\ell\gamma$ process. At least two jets must be present in the event, where at least one is identified as a b jet. No explicit requirement on $p_{\mathrm{T}}^{\mathrm{miss}}$ is applied. The $\mathrm{t\bar{t}}\gamma$ events with only one generated lepton that pass the selection are considered as background in the analysis and grouped with the "Others" category in the figures, since their contribution is rather small.

Figure 2 shows comparisons between the data and the predictions, for several distributions, after the fit to the data to measure the production component of $\mathrm{t\bar{t}}\gamma$, described in section 9.3. The predictions for signal and most background processes are taken from MC simulations, as described above. The contribution labelled as "$\mathrm{t\bar{t}}\gamma$ prod." corresponds to the $\mathrm{t\bar{t}}\gamma$ production process, while the one labelled as "$\mathrm{t\bar{t}}\gamma$ decay" corresponds to the $\mathrm{t\bar{t}}\gamma$ decay process, as defined in section 3. Background events containing nonprompt photons are estimated from the data, as described in section 6, and labelled as "Nonprompt". The data and the estimated signal and background contributions after the fit are found to be consistent.

JHEP04(2026)086

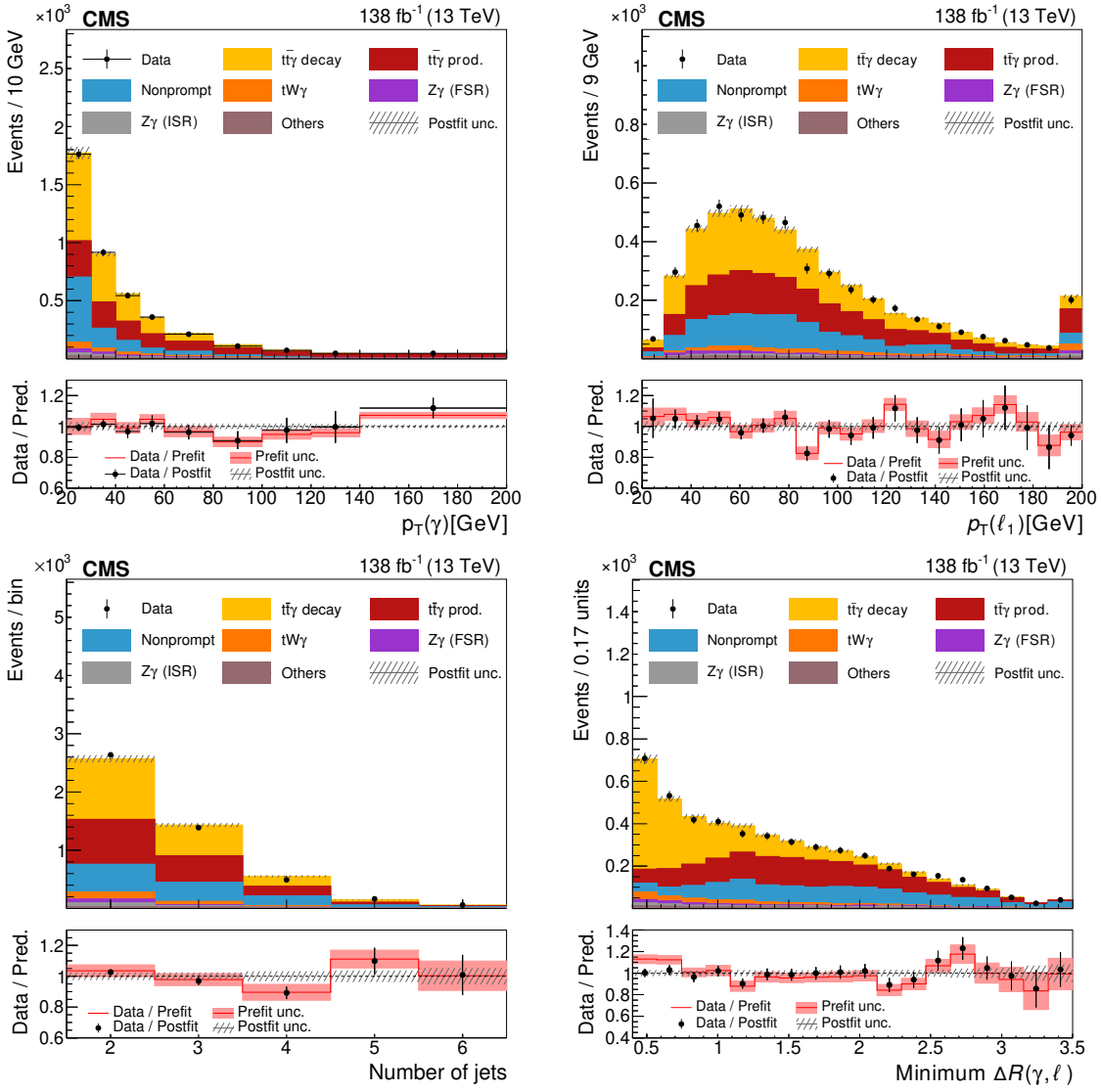

Figure 2. Distributions after the event selection for: the p_{T} of the photon (upper left), the p_{T} of the lepton with the highest p_{T} (upper right), the number of jets (lower left), and the minimum $\Delta R(\gamma, \ell)$ (lower right). The data and their statistical uncertainties are indicated by black points and error bars, respectively. The postfit prediction for the $\mathrm{t\bar{t}}\gamma$ process is shown in red and yellow, after the fit to the production component of $\mathrm{t\bar{t}}\gamma$, described in section 9.3. The hatched area indicates the total uncertainty in the prediction. The lower panels show the ratio of the data to the sum of the postfit predictions (points) and the ratio of the data to the sum of the prefit predictions (red line). The black (red) hatched areas represent the postfit (prefit) uncertainties. The last bin includes all events above the plotted range.

JHEP04(2026)086

For the selected events, the kinematic properties of the top quarks and the $\mathrm{t\bar{t}}$ system are reconstructed. The four-momenta of the top quark and antiquark in each event are estimated using a kinematic reconstruction algorithm, extensively described in ref. [71]. The main challenge is to accurately estimate the four-momenta of the neutrinos that collectively give rise to the $\vec{p}_{\mathrm{T}}^{\,\mathrm{miss}}$ of the event. The reconstructed jets and leptons in each event are assigned to the b quarks and leptons from the top quark decays, in all possible combinations. These combinations are inserted into a set of energy-momentum conservation equations. Constraints in those equations are the mass of the W boson, $m_{\mathrm{W}} = 80.4\,\mathrm{GeV}$ [72], and the mass of the top (anti)quark, $m_{\mathrm{t}} = 172.5\,\mathrm{GeV}$. The assumed value of m_{W} is varied according to a simulated Breit-Wigner distribution, with a width of 2.1 GeV [72]. It is also assumed that the $\vec{p}_{\mathrm{T}}^{\,\mathrm{miss}}$ originates only from the neutrinos. To account for the detector effects, the measured energy and the direction of the reconstructed jets and leptons are randomly smeared according to their simulated resolutions. The combination providing a neutrino solution that minimizes the invariant mass of the $\mathrm{t\bar{t}}$ system is chosen. More details can be found in ref. [73]. The reconstruction efficiency in $\mathrm{t\bar{t}}$, defined as the fraction of events where a solution is found, is about 90% in both data and simulation. Events where no real solution can be found for the neutrino momenta are discarded. The presence of the photon is not considered explicitly in the reconstruction, but this is shown to have a negligible effect on the event reconstruction efficiency. The reconstruction efficiency was checked as a function of photon kinematic observables, and minimal dependence was observed. In $\mathrm{t\bar{t}}\boldsymbol{\gamma}$ events with at least two leptons, the reconstruction efficiency ranges from more than 95% to about 80% for the leading lepton p_{T} between 25 and 400 GeV. Figure 3 shows the p_{T} distribution of the reconstructed leading top quark ($p_{\mathrm{T}}(\mathrm{t}_1)$), the invariant mass distribution of the reconstructed $\mathrm{t\bar{t}}$ system ($m(\mathrm{t\bar{t}})$), and the difference between the absolute rapidities of the reconstructed top quark and antiquark ($\Delta|y|(\mathrm{t},\bar{\mathrm{t}})$), in data and simulation, after the fit.

6 Background determination

A variety of background processes have a similar signature to the signal, and events from these processes can pass the event selection. They can be categorized into processes with prompt or nonprompt photons, depending on the nature of the reconstructed photon. Each reconstructed photon is matched to the nearest generator-level particle within a cone of $\Delta R < 0.3$, and with a p_{T} that agrees within 50% with that of the photon. The photon is labelled as prompt if the generator-level particle is a photon radiated from either a lepton, a quark, or a boson; whereas it is considered nonprompt if the generator-level particle is a photon originating from hadronic sources, e.g. a $\pi^0 \to \gamma\gamma$ decay, if it is not a photon, e.g. an electron that is misidentified as a photon, or if no match is found (for instance, photons from pileup interactions).

Among the background sources with prompt photons, the highest contribution arises from the $\mathrm{Z}\boldsymbol{\gamma}$+jets process, where the Z boson decays into pairs of leptons. The $\mathrm{Z}\boldsymbol{\gamma}$+jets contribution is split into $\mathrm{Z}\boldsymbol{\gamma}$+jets (FSR) and $\mathrm{Z}\boldsymbol{\gamma}$+jets (ISR) components, based on generator-level information related to the photon origin. The contribution from this process is estimated from simulation, and is constrained using a dedicated control region (CR). The CR is defined by selecting same-flavour lepton events with the same requirements as the signal region (SR),

JHEP04(2026)086

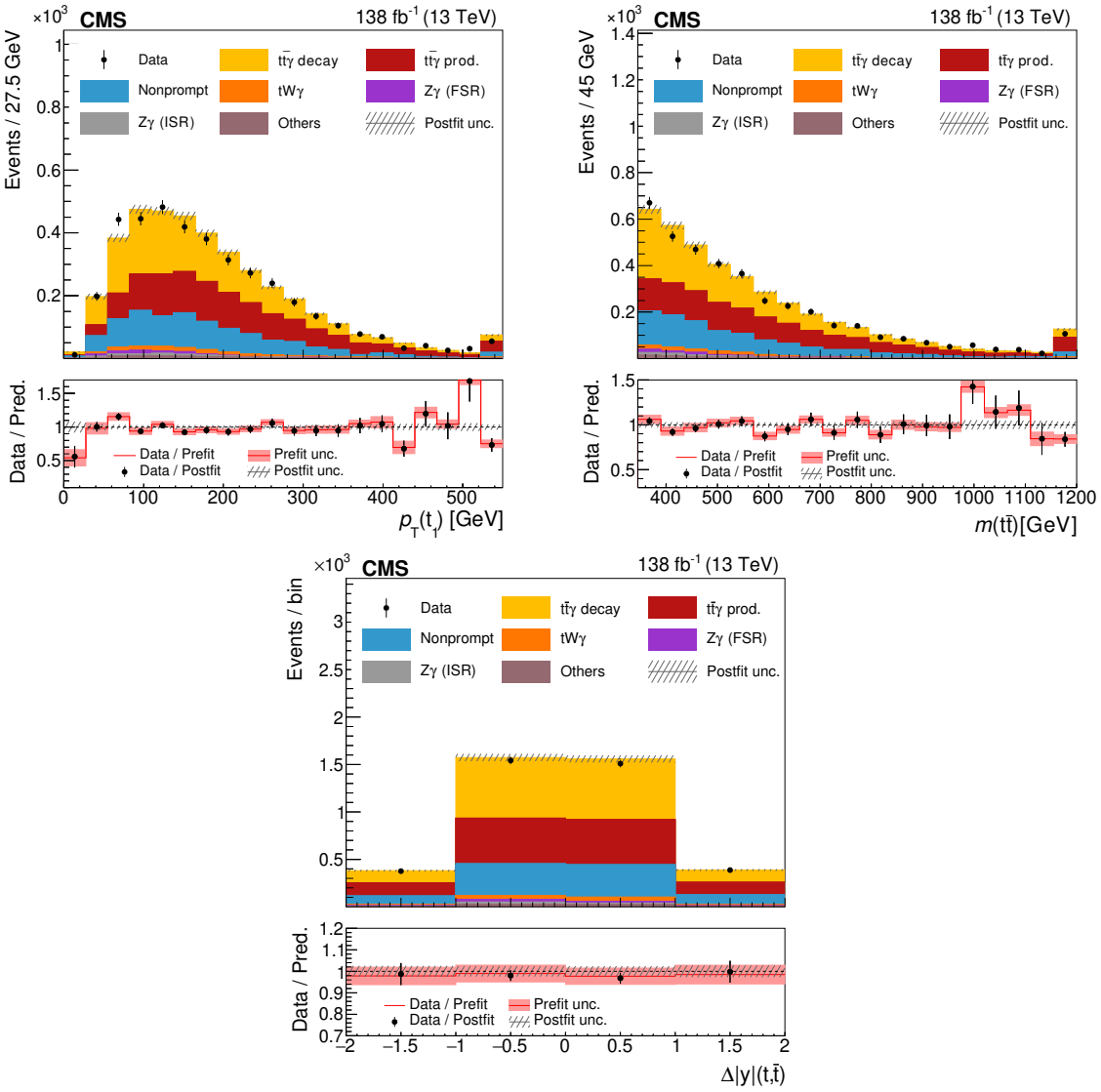

Figure 3. The $p_{\mathrm{T}}(\mathrm{t}_1)$ (upper left), $m(\mathrm{t\bar{t}})$ (upper right), and $\Delta|y|(\mathrm{t},\bar{\mathrm{t}})$ (lower) distributions in data and simulation, after the fit to the production component of $\mathrm{t\bar{t}}\gamma$, described in section 9.3. The hatched area indicates the total uncertainty in the prediction. The lower panels show the ratio of the data to the sum of the postfit predictions (points) and the ratio of the data to the sum of the prefit predictions (red line). The black (red) hatched areas represent the postfit (prefit) uncertainties. The last bin includes all events above the plotted range and, where applicable, the first bin includes all events below the plotted range.

JHEP04(2026)086

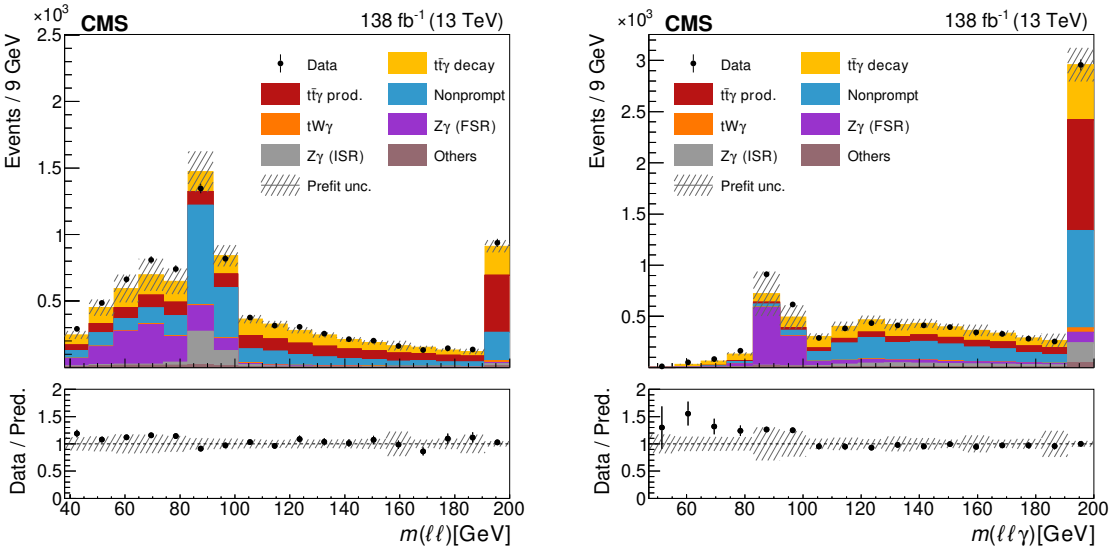

Figure 4. Distributions of the invariant mass of the two leptons (left) and two leptons + photon (right) system, for events with two same-flavour leptons, as estimated by the simulation before the fit. These distributions are shown after requiring that the events pass the full event selection, but excluding the requirement that both invariant masses are reconstructed with a value not compatible with m_{Z}, within 15 GeV. The data and their statistical uncertainties are indicated by the black points and error bars, respectively. The hatched area indicates the total prefit uncertainty in the prediction. The last bin includes all events above the plotted range.

but with $m(\ell\ell\gamma)$ enforced to be compatible with m_{Z} within a ± 15 GeV window. Because of this requirement on the invariant mass, the photon in the CR mostly originates from FSR. Figure 4 shows the distributions of $m(\ell\ell)$ and $m(\ell\ell\gamma)$ after the full event selection except for the requirements on these two variables, for events with two same-flavour leptons. The Zγ+jets CR is included in the fit to the data, and the rates of the Zγ+jets (FSR) and Zγ+jets (ISR) processes are controlled by constrained nuisance parameters. Different nuisance parameters are defined for events with different jet multiplicities, to account for an observed mismodelling of this observable in the CR. All other backgrounds with prompt photons are estimated from simulation.

Due to its potentially unreliable description in simulation, the contribution arising from processes with nonprompt photons is estimated from data using the so-called ABCD method, with a similar strategy to that of ref. [15]. Four exclusive regions (A through D) are defined, based on two variables that provide good discrimination between prompt and nonprompt photons, namely the photon PF charged isolation (I_{ch}) and the width of the electromagnetic shower measured in the ECAL ($\sigma_{i\eta i\eta}$) [56], as illustrated in figure 5. The I_{ch} is obtained by summing the p_{T} of charged hadrons inside an isolation cone of $\Delta R < 0.3$ with respect to the photon direction. These variables present a low correlation between them, below 2 (7)% for photons reconstructed in the barrel (endcap) of the CMS detector. All regions are required to contain events with exactly one photon passing the identification criteria detailed above, but with looser requirements on the identification algorithm, in particular no requirements on I_{ch} and $\sigma_{i\eta i\eta}$. Additionally, events in all regions are required to pass all

JHEP04(2026)086

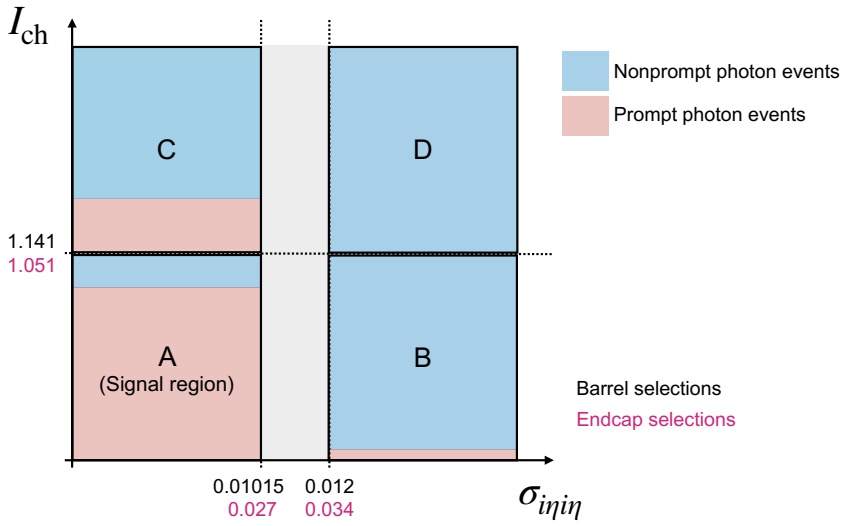

Figure 5. Schematic representation of the regions used to estimate the contribution from events with a nonprompt photon in the SR. The blue (light red) areas represent the fraction of events with a nonprompt (prompt) photon in each region. The area shaded in grey represents a gap between the regions, and events falling in that gap are excluded. The numbers in black on the axes represent the selections applied to separate the regions for events with a photon reconstructed in the ECAL barrel, while those in pink represent the selections applied to events with a photon reconstructed in the endcaps.

criteria of the signal event selection except for those on the number of jets. Two regions (C and D) form the measurement region, and the ratio between the nonprompt photon contributions in those regions is used to measure the probability that a nonprompt photon also passes the identification criteria and therefore ends up in the final selection, referred to as the misidentification rate (R_{misID}). In these regions, events are required to have at least one jet, or have two leptons of different flavours (eμ), to suppress the contribution from the DY+jets process. The remaining two regions (A and B) form the application region, with the same requirements on jet multiplicity as those described for the signal event selection, where the R_{misID} is applied in the form of a weight to photon events in region B in order to predict the number of nonprompt photon events in the SR (A).

In more detail, the measurement region contains events with one non-isolated photon, defined by requiring $1.141\ (1.051) \leq I_{\text{ch}} < 15$ for barrel (endcap) photons, and is further split into C with the same $\sigma_{i\eta i\eta}$ requirement as the SR, i.e. $\sigma_{i\eta i\eta} < 0.010\ (0.027)$ for barrel (endcap) photons; and a sideband D defined by inverting the $\sigma_{i\eta i\eta}$ requirement, i.e. $\sigma_{i\eta i\eta} > 0.012$ (0.034) for barrel (endcap) photons. With this definition, the events in D contain mostly nonprompt photons (about 99.5%). The misidentification rate is then measured by computing the ratio of data events in C to those in D in bins of p_{T} and η of the photon, since low-p_{T} and high-$|\eta|$ photons are more likely to be nonprompt. The small contribution from prompt photons in these regions is subtracted using simulated events. The application region contains events with isolated photons, i.e. with the requirement $I_{\text{ch}} < 1.141\ (1.051)$, and is further split into a region A that corresponds to the SR, and a sideband B defined by inverting the $\sigma_{i\eta i\eta}$ requirement. The gap between the two thresholds of the $\sigma_{i\eta i\eta}$ requirement ensures

JHEP04(2026)086

a higher contribution of nonprompt photons in both sideband regions. Figure 5 shows a scheme of the A, B, C, and D regions, illustrating the purity of each region in events with a nonprompt photon, computed from simulation. The contribution of nonprompt photons in A is estimated by computing $N_{\mathrm{A}} = R_{\mathrm{misID}}\, N_{\mathrm{B}}$. The R_{misID} values are computed separately for each data-taking period, to account for differences in the detector configuration.

The method described above relies on the condition that the variables chosen to define the four regions are fully independent of one another. In this analysis, it has been found in simulation that this assumption does not always hold true, especially for endcap photons. The physical reason lies in the fact that nonprompt photons tend to have both high values of $\sigma_{i\eta i\eta}$ and to be poorly isolated from charged particles around them, for instance if they originate from jets misreconstructed as photons. To address this issue, correction factors k_{MC} are calculated based on $\mathrm{t\bar{t}}$ simulated events using the same p_{T} and η binning as the R_{misID}. The correction factors are computed as the double ratio $(N_{\mathrm{A}}^{\mathrm{MC}}/N_{\mathrm{B}}^{\mathrm{MC}})/(N_{\mathrm{C}}^{\mathrm{MC}}/N_{\mathrm{D}}^{\mathrm{MC}})$, where $N_{\mathrm{X}}^{\mathrm{MC}}$ is the number of nonprompt photon events in each region X in $\mathrm{t\bar{t}}$ simulation. The correction factors are close to 1 for photons with low p_{T} and reconstructed in the barrel (the majority of events), but go up to 3 for some poorly populated bins in the higher p_{T} and/or higher rapidity regions. The number of nonprompt $\boldsymbol{\gamma}$ events in the SR is computed in each photon p_{T} and $|\eta|$ bin, indexed by i and j, respectively, by:

$$N_{\mathrm{A}}(\text{nonprompt } \boldsymbol{\gamma}) = \sum_{i,j} \left(N_{\mathrm{B}}^{ij}(\text{data}) - N_{\mathrm{B}}^{ij}(\text{prompt MC}) \right) R_{\mathrm{misID}}^{ij}\, k_{\mathrm{MC}}^{ij}. \tag{6.1}$$

The most significant contribution of nonprompt photon events in the SR arises from the $\mathrm{t\bar{t}}$ process, where an extra jet is misreconstructed as a photon. Therefore, in order to assess the consistency of this method, the R_{misID} is also computed on simulated $\mathrm{t\bar{t}}$ events, and subsequently applied to simulated $\mathrm{t\bar{t}}$ events with nonprompt photons in B, to estimate the number of nonprompt photon events in A. This is then compared to the distribution of simulated $\mathrm{t\bar{t}}$ events with nonprompt photons in A, which serves as a "closure test" to ensure the consistency of the method. Good agreement is observed in the normalized distributions, not only of the photon p_{T} and η, where these factors are derived, but of all the studied quantities. However, residual normalization differences were identified and are accounted for by applying a normalization uncertainty of 20% to the nonprompt photon background, corresponding to the largest relative differences observed between the distributions, in specific bins. In addition, an extra shape uncertainty is included in the fits to data, to capture slight trends observed in the closure tests for the specific variables that are included in the fits, that may not be adequately addressed by the normalization uncertainty.

7 Systematic uncertainties

Several sources of systematic uncertainties are considered, which affect the statistical interpretation of the results through their modification of the normalization and/or the shape of the templates for the signal and background processes. All sources of systematic uncertainty considered in this analysis are summarized in table 1, and are described below, grouped by experimental and theoretical uncertainties. Unless otherwise specified, the uncertainties are applied to all processes except the nonprompt photon background. The different components

JHEP04(2026)086

	Source	Correlation Period	Correlation Process
Experimental	Integrated luminosity	∼	✓
	Pileup reweighting	✓	✓
	L1 prefiring	✓	✓
	Electron/muon reconstruction and identification	✓	✓
	Photon reconstruction and identification	∼	✓
	b tagging	∼	✓
	JEC	∼	✓
	JER	×	✓
	Unclustered energy	✓	✓
	Trigger efficiencies	×	✓
	Limited size of simulated samples	×	∼
	Nonprompt photon estimation	∼	—
Theoretical	μ_R and μ_F scales	✓	∼
	PDF+α_S	✓	✓
	PS scales: ISR and FSR	✓	∼
	ME-PS matching (h_{damp})	✓	—
	NNLO QCD reweighting	✓	—
	Background normalization	✓	—
	Zγ+jets mormalization depending on jet multiplicity	✓	—
	t$\bar{t}\gamma$ production/decay fraction	✓	—

Table 1. Summary of the systematic uncertainty sources in the inclusive and differential t$\bar{t}\gamma$ cross section, t$\bar{t}\gamma$/t$\bar{t}$ ratio, and charge asymmetry measurements. The first column lists the source of the uncertainty, while the second (third) column indicates the treatment of correlations of the uncertainties between different data-taking periods (processes), where ✓ means fully correlated, ∼ means partially correlated (i.e. contains sub-sources that are either fully correlated or uncorrelated), × means uncorrelated, and — means not applicable.

were studied one by one to evaluate whether they were dependent on the data-taking period and signal/background process, and incorporated accordingly as a correlated or uncorrelated nuisance parameter.

- *Integrated luminosity*: The uncertainty in the integrated luminosity from the considered data-taking periods is propagated as a systematic uncertainty in the yields of all processes except the nonprompt photon contribution, estimated to be between 1.2 and 2.5% [74–76]. This uncertainty affects only the normalization of the processes and is partially correlated across data-taking periods.

- *Pileup reweighting*: The uncertainty in the pileup is taken into account by using two sets of alternative event weights derived with a variation of 4.6% in the total inelastic

JHEP04(2026)086

cross section [53]. This uncertainty affects both the shape and normalization of the predictions.

- *L1 trigger inefficiency*: In 2016 and 2017 data, a problem in L1 triggers related to the ECAL and the muon systems during a portion of the data-taking period led to the selection of data events from the previous bunch crossing [59], and consequently to a loss of signal efficiency. To account for this, a correction factor is applied to simulated events, and the corresponding uncertainties are assigned, affecting both the shape and normalization of the predictions.

- *Lepton selection*: The uncertainties associated to the lepton reconstruction, identification, and isolation affect both the shape and normalization of the processes [56, 58]. Separate nuisance parameters are included for electrons and muons.

- *Photon selection*: The uncertainties in the photon identification and pixel seed veto are considered, which affect both the shape and normalization of the processes [56].

- *b tagging*: Uncertainties in the b tagging efficiency corrections are considered, which affect both the shape and normalization of the predictions. These factors are derived from two different regions: a heavy-flavour one, i.e. a QCD-enriched region, and a light-flavour one, i.e. a Z+jets-enriched region [66, 68].

- *Jet energy scale and resolution*: Uncertainties in the determination of the jet energy scale (JES) are taken into account by shifting the jet momenta in the simulation up and down, separately for several sources of uncertainty such as the overall energy scale, differences in flavour response, and residual differences between energy scale measurements. These corrections to the JES are denoted jet energy corrections (JEC). The JEC uncertainties are also propagated to the $p_{\mathrm{T}}^{\mathrm{miss}}$. These uncertainties affect both the shape and normalization of the predictions. Some of the sources are treated as uncorrelated per data-taking period, while others are correlated for all periods, depending on whether the underlying effect depends on the different detector configurations across periods. Uncertainties in the jet energy resolution (JER) are evaluated by increasing or decreasing the variation of jet energies between the reconstructed and particle levels, or by randomly modifying the measured jet energy by a small amount in case no matching particle-level jet could be found [70].

- *Unclustered energy*: An uncertainty in $p_{\mathrm{T}}^{\mathrm{miss}}$ is derived by varying the energies of reconstructed particles not clustered into jets within their respective resolutions [69], affecting both the shape and normalization of the predictions.

- *Trigger efficiencies*: Uncertainties in the trigger efficiency corrections are considered, affecting both the shape and normalization of the predictions.

- *Limited size of MC simulation samples*: The uncertainty originating from a finite number of simulated events is accounted for using the Beeston-Barlow "lite" method [77].

JHEP04(2026)086

- *Nonprompt photon background*: Shape and normalization uncertainties are applied to account for the residual mismatches in the nonprompt photon estimation. These are built by comparing the distributions obtained with the ABCD method with those obtained directly from the simulation, as detailed in section 6, and are considered as partly correlated between data-taking periods.

Uncertainties arising from generator parameters and settings affect both the shape and normalization of the templates and are incorporated into the statistical analysis. To avoid double counting of pure normalization uncertainties, the templates containing the "up" and "down" variations of these parameters are normalized to the same cross section as the nominal ones, in the full phase space before any event selection, for all processes. These uncertainties are listed below:

- *Renormalization and factorization scales*: The uncertainties in the choice of renormalization and factorization scales (μ_F and μ_R) are considered for the $t\bar{t}\gamma$, $t\bar{t}$, and $Z\gamma$+jets processes. These uncertainties are estimated by varying each scale up and down independently, by a factor of two, and are treated as correlated between the $t\bar{t}\gamma$ production and $t\bar{t}$ processes, and uncorrelated between those and the $t\bar{t}\gamma$ decay and $Z\gamma$+jets processes. The choice to correlate or uncorrelate each process was based on how similar the simulated processes are in terms of their production mechanisms and order of perturbation theory at which they are generated.

- *PDF and* α_S: The impact of the uncertainties related to the PDFs and the variation of the strong coupling constant α_S for each simulated background and signal process is obtained using the corresponding variations in the NNPDF sets [49, 78]. In particular, one nuisance parameter per eigenvector is included.

- *PS scales*: Uncertainties in the PS simulation are accounted for by varying α_S independently for ISR and FSR by a factor of 1/2 and 2, for all processes. The ISR uncertainties are treated as uncorrelated between double- and single-top quark processes, while the FSR uncertainties are treated as correlated for all processes involving top quarks. Both uncertainties are treated as uncorrelated between processes involving and not involving top quarks.

- *ME-PS matching* (h_{damp}): In the POWHEG generator, the scale that separates the phase space of the first QCD emission into soft and hard parts is controlled by the h_{damp} parameter. The nominal value in the CP5 tune [48] is $h_{damp} = 1.379\,m_t$ and the uncertainties are estimated with varied values of $2.305\,m_t$ and $0.874\,m_t$, for the $t\bar{t}$ simulation sample only.

- *NNLO QCD reweighting*: The $t\bar{t}$ simulation sample is reweighted such that the top quark p_T spectrum matches that from a fixed-order ME calculation at NNLO in QCD, as described in section 3. The difference between the results obtained with this sample and with the unweighted version is taken as a systematic uncertainty.

Additionally, theoretical uncertainties in the total cross sections of the background processes are considered as systematic uncertainties in the yield predictions. In particular, 20% is

JHEP04(2026)086

estimated for tWγ and 30% for the remaining backgrounds, as used in ref. [15]. For the Zγ+jets process, a large uncertainty is assigned as a function of the number of jets, ranging from 50 to 150%, as it was observed that the modelling of this process is significantly worse for larger jet multiplicities [79]. These large uncertainties are constrained using the data, by including the Zγ+jets CR in all the fits. An additional uncertainty of 20% is applied to the ratio between the $t\bar{t}\gamma$ production and decay components; this uncertainty does not modify the total cross section, but only the relative contributions of the two processes. The choice of 20% is based on the observed differences between the $t\bar{t}\gamma$ sample produced with MadGraph5_aMC@NLO and the alternative sample produced with POWHEG, as described in section 3, but it was checked that the results are stable with respect to this choice. The impact of all systematic uncertainties on the results are discussed in sections 9, 10, and 11.

8 Statistical analysis

All results are extracted via a maximum likelihood fit to data, in the $t\bar{t}\gamma$ SR and Zγ+jets CR simultaneously, where systematic uncertainties are accounted for as nuisance parameters. The likelihood function is built from the product of Poisson probabilities $\mathcal{P}$ over N bins, calculated as functions of the number of data events n_i and the expected number of signal and background events ν_i in a given bin i. This is multiplied by an auxiliary function π, which controls the constraint of the nuisance parameter θ_k, given a set of nuisance parameters $\boldsymbol{\theta}$ of length M.

The likelihood function reads:

$$L(\mathbf{n}|\mu,\boldsymbol{\theta}) = \prod_{i=1}^{N} \mathcal{P}(n_i|\nu_i(\mu,\boldsymbol{\theta})) \prod_{k=1}^{M} \pi(\theta_k), \tag{8.1}$$

where the vector $\mathbf{n} = n_1, \ldots, n_N$ represents the observed number of events in each bin, $\boldsymbol{\theta}$ represents the set of nuisance parameters, and μ are the parameters of interest (POIs) to be measured. In the inclusive measurement of the cross section, the POI is a single parameter, i.e. the $t\bar{t}\gamma$ cross section modifier $\mu_{t\bar{t}\gamma} = \sigma^{\text{obs}}_{t\bar{t}\gamma}/\sigma^{\text{exp}}_{t\bar{t}\gamma}$, with $\sigma^{\text{obs}}_{t\bar{t}\gamma}$ and $\sigma^{\text{exp}}_{t\bar{t}\gamma}$ being the observed and expected $t\bar{t}\gamma$ cross sections, respectively. The fits are implemented with COMBINE [80].

In differential measurements, where cross sections are measured in bins of a chosen observable, a set of POIs is used instead, with one POI per bin. Each observable of interest x is divided into N bins at the generator level. A likelihood-based unfolding technique is used to correct for the finite resolution and limited acceptance of the detector, which cause the measured distribution to be distorted and the values of x to deviate from the ones at the generator level. In practice, we perform a fit to extract a cross section modifier μ_l for each generator-level bin l, and multiply it by σ^{exp}_l taken from the predictions, which results in the measured value of σ_l. The binning is chosen for each observable such that the purity (fraction of reconstructed events observed in the reconstruction-level bin x^{reco}_i that were also generated in the generator-level bin x_i) and stability (fraction of reconstructed events generated in the generator-level bin x_i that are also observed in the reconstruction-level bin x^{reco}_i) are above 50%, and the condition number for the response matrices comparing the generator- and reconstruction-level quantities are reasonably small. The condition number is a measure of the stability of the unfolding problem. Typically, numbers of the order of 10 or below guarantee that the unfolding can be performed without applying any regularization technique [81].

JHEP04(2026)086

For the inclusive and differential measurements of R_γ, in addition to the $t\bar{t}\gamma$ SR and the $Z\gamma$+jets CR, two separate regions enriched in $t\bar{t}$ and DY+jets events are defined. These regions are constructed similarly to the $t\bar{t}\gamma$ SR and the $Z\gamma$+jets CR, respectively, except that events are required to have no associated reconstructed photons. We refer to the $t\bar{t}\gamma$ and $t\bar{t}$ SRs with the subscripts "$t\bar{t}, 1\gamma$" and "$t\bar{t}, 0\gamma$", respectively. We perform a simultaneous fit to the $t\bar{t}$ cross section modifier $\mu_{t\bar{t}}$ and to the R_γ modifier $\mu_{R_\gamma} = R_\gamma/R_\gamma^{\text{exp}}$ in the four regions, where:

$$R_\gamma = \frac{\sigma_{t\bar{t},1\gamma}}{\sigma_{t\bar{t},0\gamma} + \sigma_{t\bar{t},1\gamma}}, \tag{8.2}$$

and R_γ^{exp} is the expected value of R_γ, computed using the simulated samples.

The top quark charge asymmetry at the LHC can be defined as:

$$A_C = \frac{\sigma(\Delta|y| > 0) - \sigma(\Delta|y| < 0)}{\sigma(\Delta|y| > 0) + \sigma(\Delta|y| < 0)}, \tag{8.3}$$

where $\Delta|y| = |y(t)| - |y(\bar{t})|$ is the difference in absolute rapidity between the top quark and antiquark, and σ is the associated cross section. For the measurement of this quantity, events are divided in two categories, according to the observable $\Delta|y|$ being positive or negative, and the charge asymmetry is extracted directly from a maximum likelihood fit to a distribution of this observable in the $t\bar{t}\gamma$ SR, as shown in figure 3, and in the $Z\gamma$+jets CR. The two signal categories are used to build two separate signal templates, and the cross section modifiers for one of the signals is reparametrized to be a function of the charge asymmetry. This way, the charge asymmetry is extracted directly, with all the uncertainties and respective correlations being taken into account in the fit.

9 Cross section measurements

9.1 Cross section definition

The $t\bar{t}\gamma$ cross section is measured in two different phase spaces: a fiducial phase space defined at the particle level after hadronization, and a broader phase space defined at the parton level. Both phase spaces are defined in terms of the generator-level objects. For the parton-level phase space, events are required to have two leptons in the final state, originating from top quark decays, and exactly one final-state photon with p_T greater than 20 GeV and $|\eta| < 2.5$, which is isolated from all other final-state particles with p_T larger than 5 GeV (leptons, other photons, and hadrons), excluding neutrinos, by $\Delta R > 0.1$. These photons must not originate from the hadronization process. No further requirements are imposed on any other objects.

Concerning the particle-level object definition [82], leptons are required to originate from the prompt decays of the W boson (or from the decay of a τ lepton which in turn originates from the W boson) and satisfy $p_T > 15$ GeV and $|\eta| < 2.5$. The momenta of photons within a $\Delta R = 0.1$ cone around leptons are added to the respective leptons. Photons are required to not originate from the hadronization process, have p_T greater than 20 GeV, $|\eta| < 2.5$, and that the sum of p_T of all particles surrounding the photon within $\Delta R = 0.4$ is less than 50% of the photon p_T. Photons separated from leptons by $\Delta R < 0.4$ are excluded.

JHEP04(2026)086

Criteria	Lepton	Photon	Jet	b jet
p_{T} [GeV]	>15	>20	>30	>30
$\lvert\eta\rvert$	<2.5	<2.5	<2.4	<2.4
Number	2	1	≥2	≥1
Origin	Prompt	Not from hadrons	—	—
Others	OS, $m(\ell\ell) > 30\,\mathrm{GeV}$	$\Delta R(\gamma, \ell) > 0.4$	$\Delta R(\gamma/\ell, \mathrm{jet}) > 0.4$	—

Table 2. Definition of the fiducial phase space.

Particle-level jets are clustered with the anti-k_{T} algorithm with a distance parameter of 0.4, and are required to satisfy $p_{\mathrm{T}} > 30\,\mathrm{GeV}$ and $|\eta| < 2.4$, and to be separated from leptons by $\Delta R > 0.4$. Particle-level b jets are identified as jets that have a b quark matched to them through a hadron ghost-matching technique [83], where for each b hadron, an additional collinear four-vector of infinitesimal magnitude is included in the jet clustering, and each jet that includes such a "ghost" is identified as a b jet. The fiducial phase space contains signal events with at least two leptons with opposite-sign charges (OS), exactly one photon, and at least two jets, of which at least one must be a b jet. Additionally, a requirement on the invariant mass of the dilepton system, $m(\ell\ell) > 30\,\mathrm{GeV}$ is applied. The fiducial phase space definition is summarized in table 2. This selection reduces the total predicted $\mathrm{t\bar{t}}\gamma$ fiducial cross section (including the production and decay components) when compared to the parton level phase space, from $1118 \pm 194\,\mathrm{fb}$ to $126 \pm 19\,\mathrm{fb}$, using the nominal prediction defined in section 3. The uncertainties include the choice of μ_{R} and μ_{F}, PS, and the PDF uncertainties.

9.2 Fixed-order predictions

All results are compared to the predictions from simulation. In addition, the particle-level results are compared to a set of fixed-order calculations. To obtain them, NLO QCD corrections to the $\mathrm{pp} \to \mathrm{t\bar{t}}\gamma$ process in the dilepton decay channel are computed, taking into account higher-order effects in both the $\mathrm{t\bar{t}}$ production and top quark decays, using the narrow-width-approximation (NWA) [5, 84]. In this approach, all unstable particles are treated as on shell and NLO spin correlation effects are preserved throughout the calculation. In addition, the effects of photon emission from the charged top quark decay products (part of the $\mathrm{t\bar{t}}\gamma$ decay process) are consistently included. The same applies to gluon radiation encountered in the NLO QCD corrections.

The five-flavour scheme is considered, and non-diagonal elements of the Cabibbo-Kobayashi-Maskawa matrix are neglected. The calculation is performed within the HELAC-NLO MC framework [85], which is interfaced to the RECOLA [86, 87] programme for the calculation of tree-level and one-loop matrix elements, together with the COLLIER [88] library for the numerical evaluation of one-loop scalar and tensor integrals. The calculation of the real emission part is performed with the Nagy-Soper subtraction scheme [89] with its extension to the NWA [90] and a phase-space restriction on the subtraction terms [91]. In addition, the parameter in the phase-space restriction is varied to cross check the computation of the real correction part. The numerical input parameters and the photon isolation prescription for this calculation are adapted from ref. [92] to match the fiducial phase space of the analysis.

JHEP04(2026)086

Specifically, we employ a hybrid approach where we first use a rather inclusive smooth-photon isolation condition, as introduced in ref. [28], with $\varepsilon_\gamma = 1$, $n = 1$, and $R = 0.05$. Afterwards, a fixed-cone isolation condition is applied where the event is rejected unless the scalar sum of p_T of all partons in the final-state within a cone of radius $R = 0.4$ centered around the photon candidate is smaller than half of the photon p_T. Events are required to have at least two jets and at least one jet originating from a b quark, matching the fiducial phase space selections of the analysis; however, the jets obtained from the calculation are before hadronization, and therefore do not correspond exactly to the particle-level jets defined in section 9.1. This effect is not explicitly corrected for in the unfolding procedure, but is expected to be small.

9.3 Inclusive measurements

We extract the inclusive $\mathrm{t\bar{t}}\gamma$ cross section in the particle-level fiducial phase space by performing a maximum likelihood fit using two distributions: the ΔR between the photon and the closest lepton in the SR, shown in figure 2 (lower right), and the number of jets in the $\mathrm{Z}\gamma$+jets CR. The variable in the SR is chosen because it provides good separation between the $\mathrm{t\bar{t}}\gamma$ production and decay components. The measured cross section modifier is $\mu_{\mathrm{t\bar{t}}\gamma} = 1.09 \pm 0.18$. The uncertainty in this value and other cross section modifiers throughout the paper includes both the uncertainty in the measurement and the one on the theoretical cross section used to normalize it. The resulting fiducial cross section is $\sigma_{\mathrm{t\bar{t}}\gamma} = 137 \pm 3\,(\mathrm{stat}) \pm 7\,(\mathrm{syst})\,\mathrm{fb}$. This value is consistent with the prediction of $126 \pm 19\,\mathrm{fb}$ obtained from simulation, where the uncertainty includes the choice of μ_R and μ_F, PS, and the PDF uncertainties. The leading sources of systematic uncertainty in the measurement are those related to the normalization of the nonprompt photon background and the photon identification. Other experimental sources such as luminosity, b tagging, and the normalization of the $\mathrm{tW}\gamma$ and $\mathrm{Z}\gamma$+jets backgrounds also play an important role, as well as the uncertainty in the fraction between the $\mathrm{t\bar{t}}\gamma$ production and decay components. The fit was also performed using as input alternative distributions, such as the photon or the leading lepton p_T ($p_T(\ell_1)$), and the results were found to be consistent, with the same or larger uncertainties.

The $\mathrm{t\bar{t}}\gamma$ production component is more sensitive to potential new physics effects than the decay component. Therefore, its cross section is also extracted in a separate fit, where the $\mathrm{t\bar{t}}\gamma$ decay component is treated as background and accounted for as a free parameter of the fit. In this case, we obtain a cross section modifier of $\mu^{\mathrm{prod}}_{\mathrm{t\bar{t}}\gamma} = 0.98 \pm 0.12$, corresponding to a fiducial cross section of $\sigma^{\mathrm{prod}}_{\mathrm{t\bar{t}}\gamma} = 56 \pm 2\,(\mathrm{stat}) \pm 4\,(\mathrm{syst})\,\mathrm{fb}$, consistent with the expectation from the nominal simulation, $57 \pm 5\,\mathrm{fb}$. The fitted $\mathrm{t\bar{t}}\gamma$ decay normalization factor is $\mu^{\mathrm{decay}}_{\mathrm{t\bar{t}}\gamma} = 1.21 \pm 0.28$, which has a small (5%) anticorrelation with the $\mathrm{t\bar{t}}\gamma$ production cross section. This normalization factor can be translated into a measured cross section of $\sigma^{\mathrm{decay}}_{\mathrm{t\bar{t}}\gamma} = 84 \pm 5\,\mathrm{fb}$, in agreement with the nominal simulation prediction of $70 \pm 16\,\mathrm{fb}$ for the $\mathrm{t\bar{t}}\gamma$ decay component. The leading sources of systematic uncertainty are the same as those for the measurement of the combined production+decay $\mathrm{t\bar{t}}\gamma$ cross section.

An assessment of the quality of the fit to the production component of $\mathrm{t\bar{t}}\gamma$ is shown in figure 6 through the postfit deviations of nuisance parameters from their prefit values ("pulls") as well as their postfit reduction in uncertainty ("constraints"). The nuisance parameters are ranked by the impact that shifting their fitted values would have on the central value

JHEP04(2026)086

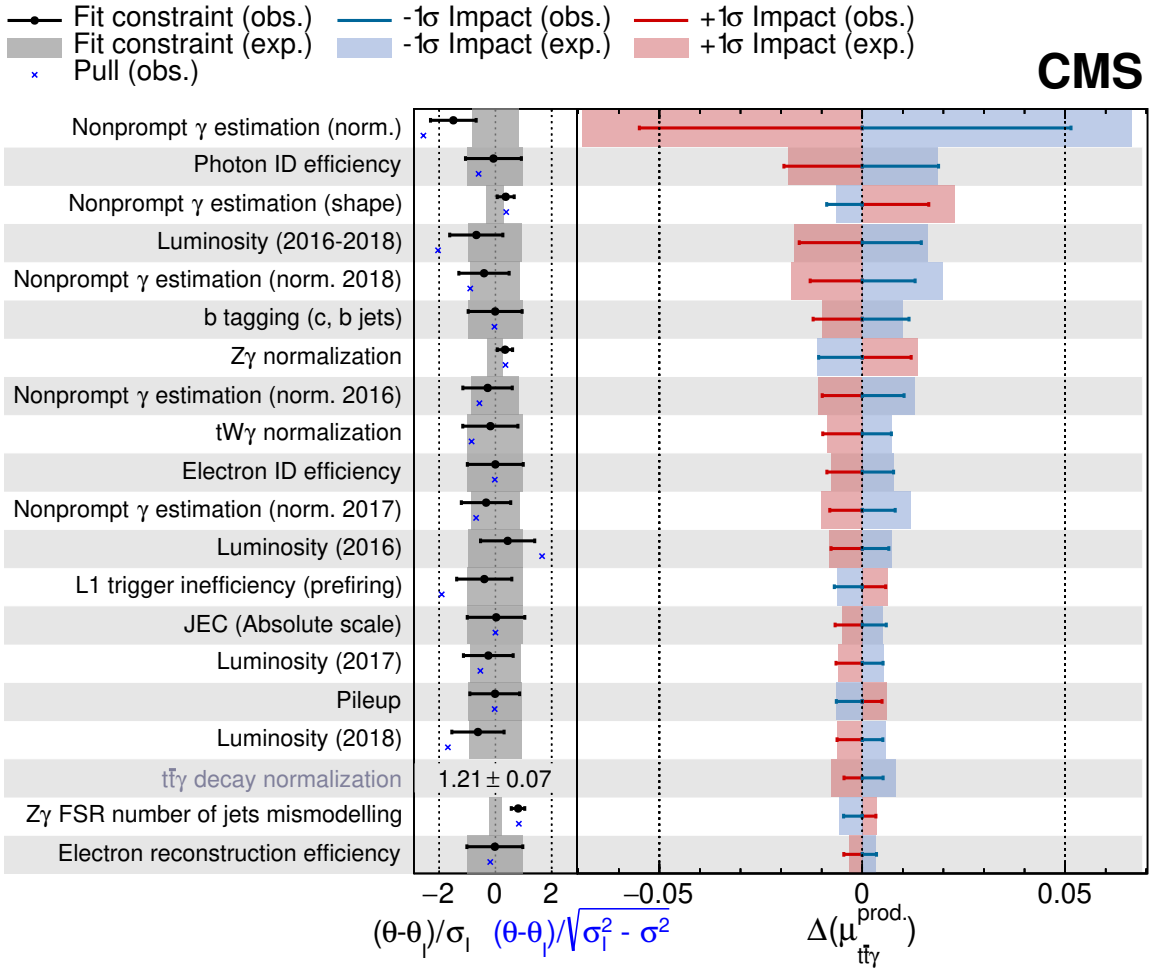

Figure 6. Impacts $\Delta(\mu^{\text{prod}}_{\text{t}\bar{\text{t}}\gamma})$ (right column) and fit pulls and constraints (middle column) of the twenty most important nuisance parameters (listed in the left column) in the fit to extract the cross section of the $\text{t}\bar{\text{t}}\gamma$ production component. In the middle column, two different pull definitions are presented: the difference between the postfit value of each nuisance parameter θ and its prefit value θ_I, normalized either by the initial size of the uncertainty σ_I (in black and gray) or by $\sqrt{{\sigma_I}^2 - \sigma^2}$ (in blue) [93], where σ is the postfit size of the uncertainty. For the first definition, the uncertainty on this quantity is also reported and calculated as σ/σ_I, effectively giving the constraints on the nuisance parameters. The contraints are shown as gray horizontal bands (black horizontal lines) for the expected (observed) fit. In the impacts column, the red and blue horizontal bands (lines) show the expected (observed) impact of each nuisance parameter on the cross section modifier, defined as the change in $\mu^{\text{prod}}_{\text{t}\bar{\text{t}}\gamma}$ when the nuisance parameter is shifted by one standard deviation from its fitted value.

JHEP04(2026)086

of the cross section modifier. In the figure, if the data-taking period is specified alongside the uncertainty name, it indicates that this component of the uncertainty is uncorrelated between periods. Similarly, if "norm." or "shape" is specified alongside the uncertainty name, it indicates an uncertainty modifying only the normalization or only the shape of the template histograms, respectively. The normalization of the $\mathrm{t\bar{t}}\gamma$ decay component is an unconstrained nuisance in the fit, and its value and uncertainty after the fit are shown in the respective row, instead of the constraint. Only the uncertainty on the measurement is quoted in the figure, not the uncertainty on the theoretical prediction used to normalize the $\mathrm{t\bar{t}}\gamma$ decay component. A goodness of fit test is performed using the saturated model [94], and the p-value is found to be 0.71, indicating a good agreement between the data and the postfit predictions.

9.4 Differential measurements

Additionally, we report the measurement of the differential $\mathrm{t\bar{t}}\gamma$ cross section as a function of several observables of interest at parton and particle level. At the parton level, the cross section is measured as a function of $p_{\mathrm{T}}(\mathrm{t}_1)$, the ΔR between the photon and the closest top quark (min. $\Delta R(\gamma, \mathrm{t})$), the ΔR between the photon and the $\mathrm{t\bar{t}}$ system ($\Delta R(\gamma, \mathrm{t\bar{t}})$), and $m(\mathrm{t\bar{t}})$. The observables chosen for the measurements at the particle level are $p_{\mathrm{T}}(\ell_1)$, $p_{\mathrm{T}}(\gamma)$, and the $\Delta\phi$ between the two charged leptons ($\Delta\phi(\ell, \ell)$). Observables such as the p_{T} of particles are sensitive to new physics in the tails of the distributions. Angular variables, on the other hand, are sensitive to the spin correlations of the top quark pair, to the coupling between the top quark and the photon, and to the modelling of the origin of the photon. Moreover, angular observables can be used to probe the charge-parity (CP) structure of the SM [9]. Measurements at the parton level are performed in a broader phase space, whereas those at the particle level are performed on particle-level objects in a fiducial phase space, as described in section 9.1.

In the unfolding process, the condition numbers of the response matrices relating reconstructed and parton level quantities were computed for all variables, and the largest number was found to be 11.4, for $p_{\mathrm{T}}(\mathrm{t}_1)$, well within the range of stability. Each differential measurement is the result of a fit to two distributions: that of the variable of interest in the SR and the number of jets in the $\mathrm{Z}\gamma$+jets CR.

The absolute and normalized differential cross sections at the parton level are displayed in figures 7 and 8, while those at the particle level are shown in figures 9 and 10. The purple and blue lines represent the predictions using the two modelling options described in section 3, while the hashed bands show the theoretical uncertainty in those predictions, coming from the choice of μ_{R} and μ_{F}, and the choice of PDFs including α_{S} variations. For particle-level measurements, the results are also compared to the fixed-order prediction introduced in section 9.2, shown in gray. The measurements are limited by the statistical uncertainties in most bins, with the exception of the most populated bins in some distributions. The leading systematic uncertainties affecting the unfolded data are those in the photon and electron identification, as well as the nonprompt photon contribution. The normalizations of the $\mathrm{tW}\gamma$ process and other backgrounds also play a significant role.

In terms of normalization, good agreement of the data with the nominal simulation is observed, while the alternative simulation model systematically overpredicts the data. The

JHEP04(2026)086

normalized cross sections show, however, that the shape of the data is well described by both models for the invariant masses and p_{T} observables, while for angular observables some trends are observed. The latter are especially sensitive to the modelling of the photon origin, showing that no model describes the photon emission perfectly. In general, it can be concluded that the alternative simulation model, which relies on the PS to model the photon emissions from the top quark decay products, does not describe the data well, while the nominal simulation, which relies on the ME calculations at LO, provides a better, though not ideal, description.

The fixed-order predictions are in good agreement with the data both in terms of shape and normalization, especially for the angular observables, where they are expected to be more accurate, providing a better description when compared to both simulation models.

10 Inclusive and differential ratio measurements

In order to extract the R_γ modifier $\mu_{R_\gamma} = R_\gamma / R_\gamma^{\mathrm{exp}}$ introduced in eq. (8.2), the distributions of the p_{T} of the leading lepton for the "$\mathrm{t\bar{t}}, 1\gamma$" region and the "$\mathrm{t\bar{t}}, 0\gamma$" region, and the number of jets distributions in the two CRs are fitted simultaneously. The CRs are the Zγ+jets CR and a DY+jets CR, built similarly to the "$\mathrm{t\bar{t}}, 0\gamma$" region, but selecting events with same-flavour leptons and $m(\ell\ell)$ within 15 GeV of m_{Z}. The fit is performed to four distributions: that of the $p_{\mathrm{T}}(\ell_1)$ in the "$\mathrm{t\bar{t}}, 1\gamma$" and the "$\mathrm{t\bar{t}}, 0\gamma$" regions, and the number of jets in the Zγ+jets and DY+jets CRs. The distributions after the fit are shown in figure 11. In this section, "$\mathrm{t\bar{t}}\gamma$" refers to the sum of the $\mathrm{t\bar{t}}\gamma$ production and decay processes. This measurement is performed in the extended phase space used for the parton-level measurements but without the photon requirement, where the predicted value of the ratio is 0.0127 ± 0.0008, computed using the nominal simulation samples. The uncertainty on this value comes from variations in the ME μ_{R} and μ_{F}, and PDFs, including α_{S} variations, all treated as uncorrelated between the $\mathrm{t\bar{t}}$ and $\mathrm{t\bar{t}}\gamma$ samples. In this measurement, the contribution from $\mathrm{t\bar{t}}$ with nonprompt photons in the "$\mathrm{t\bar{t}}, 1\gamma$" region is estimated from simulation, unlike in the cross section measurements, where it is part of the nonprompt-photon background that is taken from data. This procedure ensures that correlations between the $\mathrm{t\bar{t}}\gamma$ and $\mathrm{t\bar{t}}$ process without associated photons are properly accounted for. The residual nonprompt-photon background is then estimated from data after subtracting the $\mathrm{t\bar{t}}$ contribution obtained from simulation.

We measure $\mu_{R_\gamma} = 1.05 \pm 0.06$, corresponding to an inclusive ratio of $R_\gamma = 0.0133 \pm 0.0002\,(\mathrm{stat}) \pm 0.0005\,(\mathrm{syst})$, compatible with the prediction. The $\mathrm{t\bar{t}}$ normalization factor is found to be $\mu_{\mathrm{t\bar{t}}} = 1.008 \pm 0.015$, consistent with the predictions at NNLO in QCD. The systematic uncertainties with the largest impact in the R_γ measurement are those related to the photon identification and the estimation of the nonprompt photon background (with an impact of about 2% each), followed by modelling uncertainties such as FSR and the μ_{F} choice, and the normalization of the Zγ+jets and other minor backgrounds (with impacts below 1% each).

Similarly, we perform a differential measurement of R_γ as a function of $p_{\mathrm{T}}(\mathrm{t}_1)$, at the parton level, and of the $p_{\mathrm{T}}(\ell_1)$, at the particle level. The absolute differential cross section ratios are displayed in figure 12. Each result is extracted from a fit to four distributions: that of the variable of interest in the "$\mathrm{t\bar{t}}, 1\gamma$" and the "$\mathrm{t\bar{t}}, 0\gamma$" regions, and the number of jets in

JHEP04(2026)086

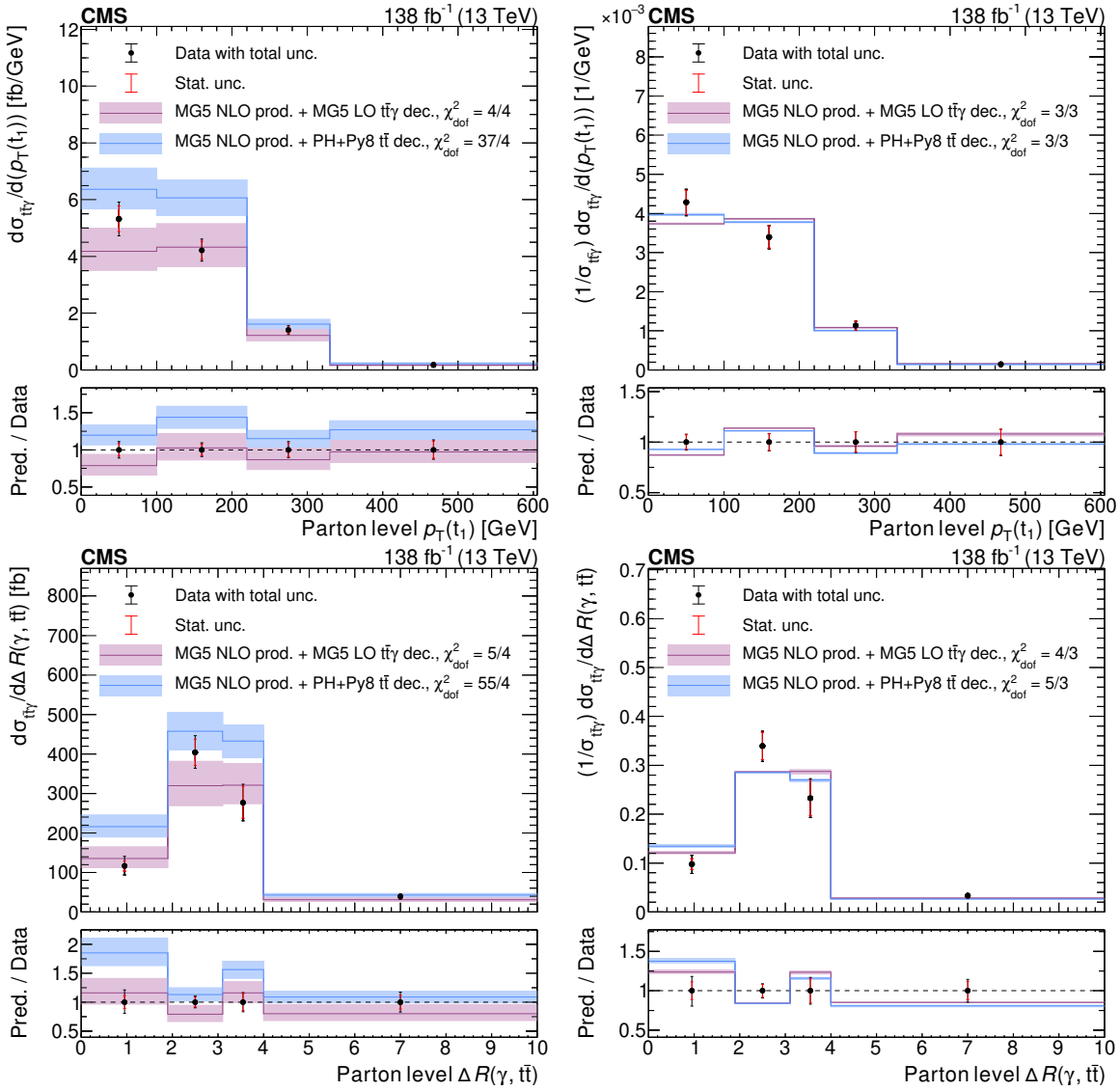

Figure 7. Absolute (left) and normalized (right) differential $t\bar{t}\gamma$ cross sections at the parton level as a function of $p_T(t_1)$ (upper) and $\Delta R(\gamma, t\bar{t})$ (lower). The purple (blue) lines show the predictions from the nominal (alternative) simulation, and the lighter purple (blue) shaded areas represent the theoretical uncertainties in the predictions. In the legends, "MG5" refers to MadGraph5_aMC@NLO, while "PH+Py8" refers to POWHEG and PYTHIA. The theoretical uncertainties include the choice of μ_R and μ_F and PDFs, including α_S variations. The black points represent the measured values, with the total uncertainty, while the red error bar shows the results considering only the statistical uncertainty.

JHEP04(2026)086

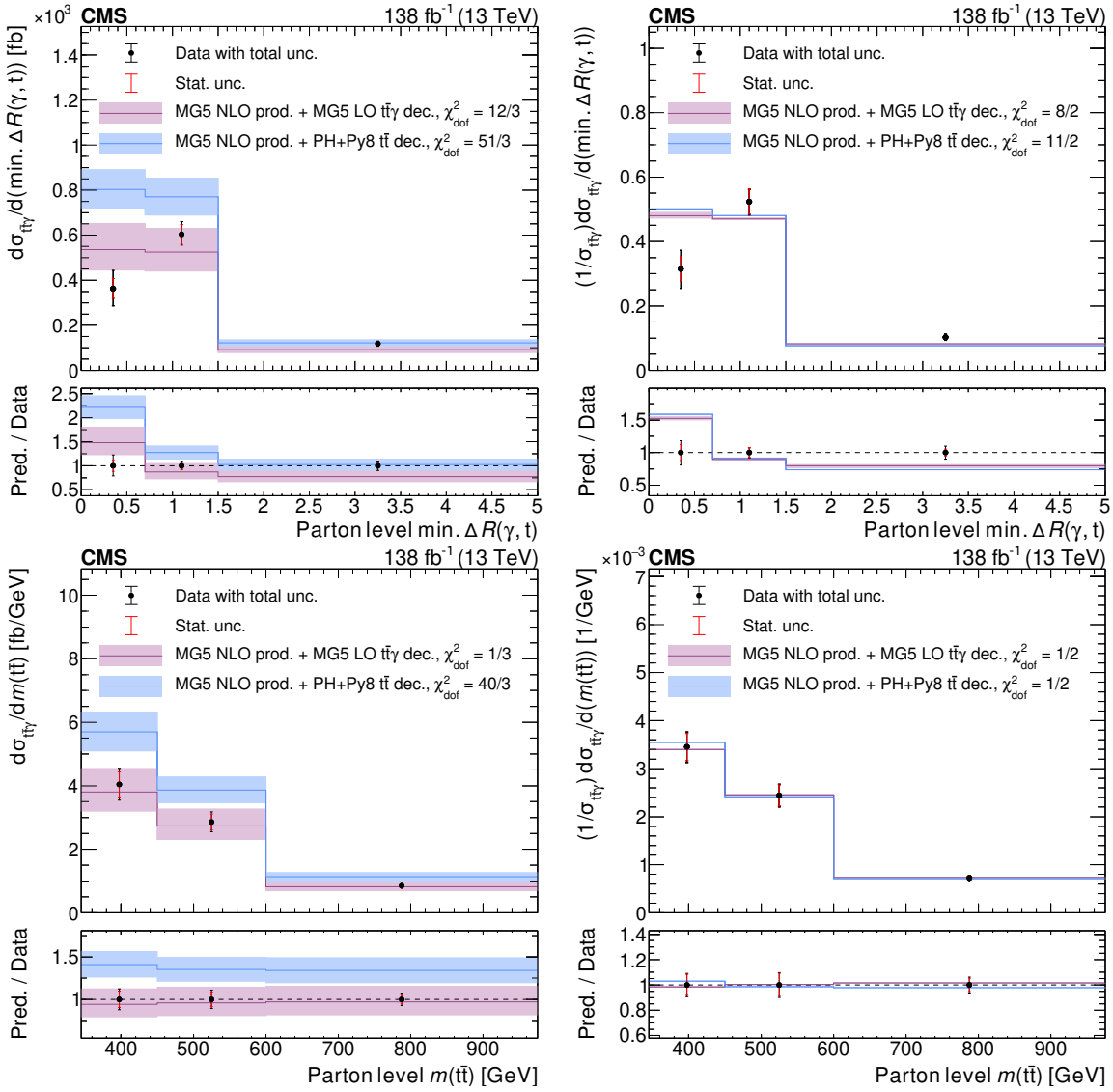

Figure 8. Absolute (left) and normalized (right) differential $t\bar{t}\gamma$ cross sections at the parton level as a function of the min. $\Delta R(\gamma, t)$ (upper) and $m(t\bar{t})$ (lower). The purple (blue) lines show the predictions from the nominal (alternative) simulation, and the lighter purple (blue) shaded areas represent the theoretical uncertainties in the predictions. In the legends, "MG5" refers to MadGraph5_aMC@NLO, while "PH+Py8" refers to POWHEG and PYTHIA. The theoretical uncertainties include the choice of μ_R and μ_F and PDFs, including α_S variations. The black points represent the measured values, with the total uncertainty, while the red error bar shows the results considering only the statistical uncertainty.

JHEP04(2026)086

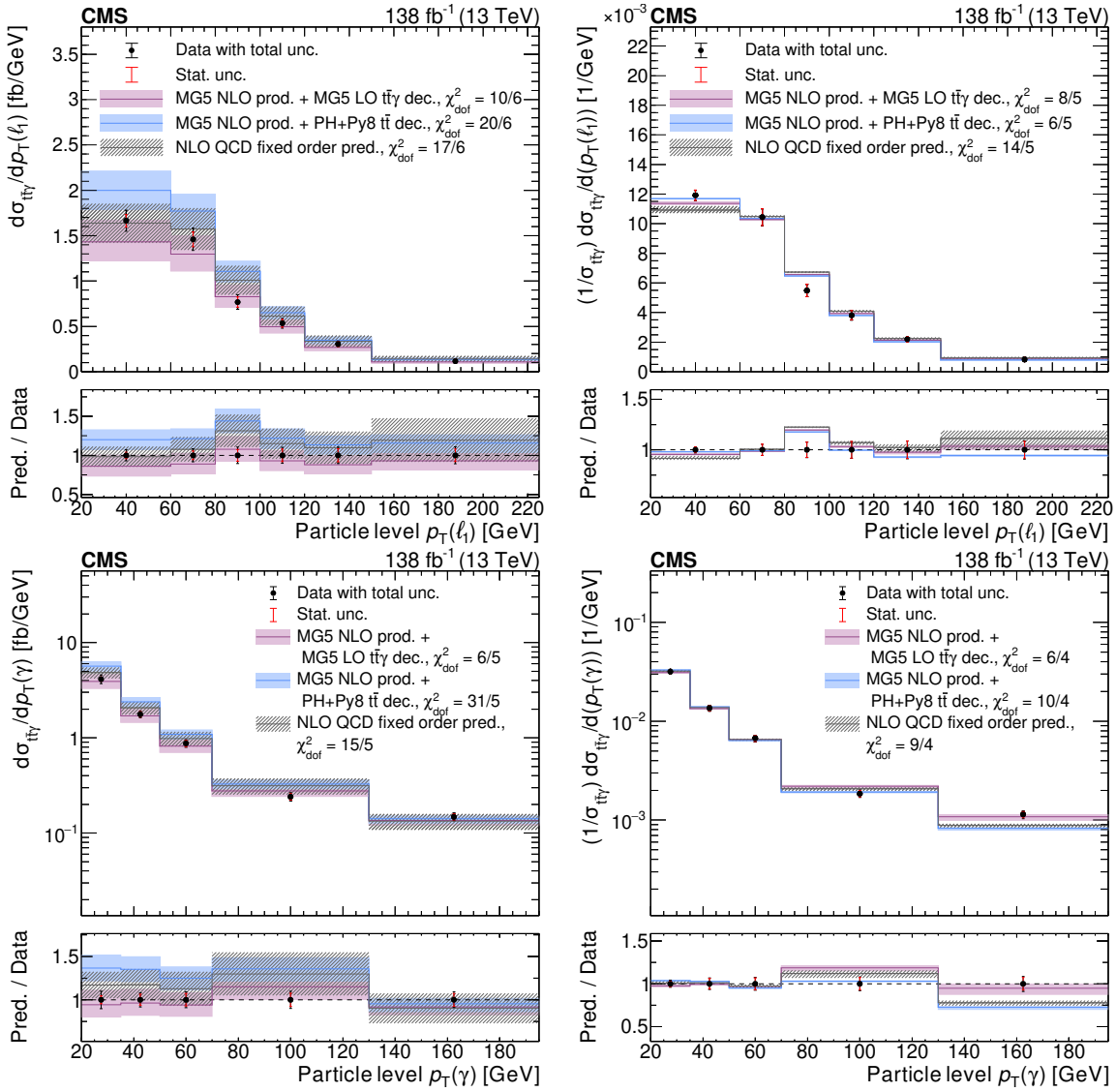

Figure 9. Absolute (left) and normalized (right) differential $t\bar{t}\gamma$ cross sections at the particle level as a function of $p_T(\ell_1)$ (upper) and $p_T(\gamma)$ (lower). The purple (blue) lines show the predictions from the nominal (alternative) simulation, and the lighter purple (blue) shaded areas represent the theoretical uncertainty in the predictions. The gray lines and bands represent the fixed-order prediction and their respective uncertainty. In the legends, "MG5" refers to MadGraph5_aMC@NLO, while "PH+Py8" refers to POWHEG and PYTHIA. The theoretical uncertainty includes the choice of μ_R and μ_F and PDFs, including α_S variations. The black points represent the measured values, with the total uncertainty, while the red error bar shows the results considering only the statistical uncertainty.

JHEP04(2026)086

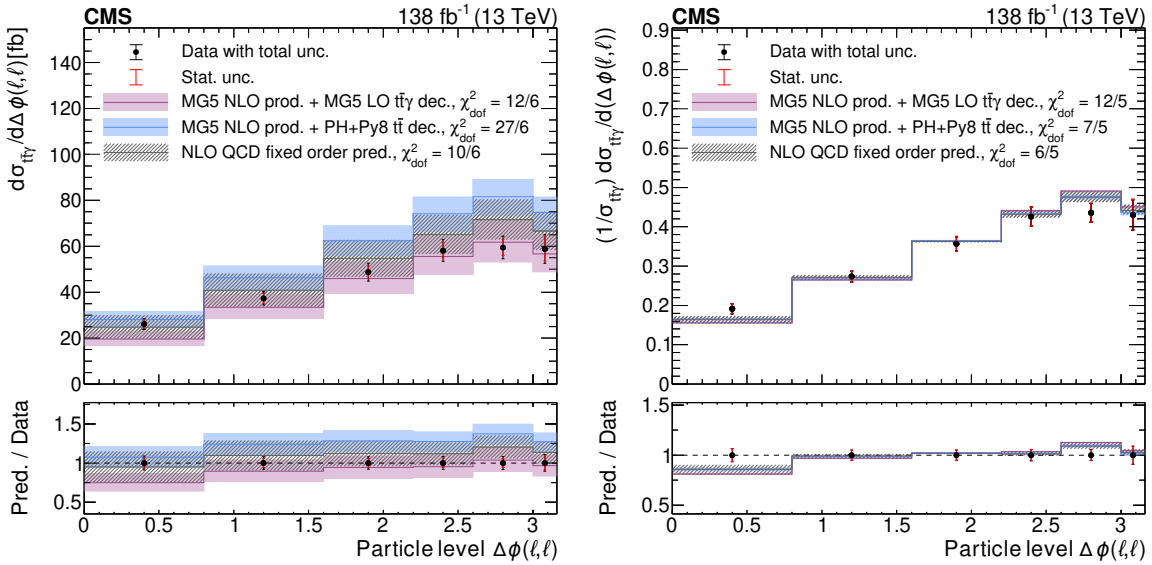

Figure 10. Absolute (left) and normalized (right) differential $t\bar{t}\gamma$ cross sections at the particle level as a function of the $\Delta\phi(\ell,\ell)$. The purple (blue) lines show the predictions from the nominal (alternative) simulation, and the lighter purple (blue) shaded areas represent the theoretical uncertainty in the predictions. The gray lines and bands represent the fixed-order prediction and their respective uncertainty. In the legends, "MG5" refers to MadGraph5_aMC@NLO, while "PH+Py8" refers to POWHEG and PYTHIA. The theoretical uncertainty include the choice of μ_R and μ_F and PDFs, including α_S variations. The black points represent the measured values, with the total uncertainty, while the red error bar shows the results considering only the statistical uncertainty.

the Zγ+jets and DY+jets CRs. The results are in agreement with the nominal prediction and with the fixed-order calculation, while the alternative prediction overpredicts the data. These results are limited by the statistical uncertainty. The systematic uncertainties with the largest contribution are those in the photon identification efficiency and in the reweighting of the top quark p_T distribution to NNLO in QCD.

11 Measurement of the top quark charge asymmetry in $t\bar{t}\gamma$

The top quark charge asymmetry in $t\bar{t}\gamma$ production is measured in the extended phase space at the parton level, through a fit to the difference in absolute rapidity between the top quark and antiquark in the SR, shown in figure 3, and the jet multiplicity in the Zγ+jets CR. The fit procedure and parametrization are described in section 8. The measured value of the charge asymmetry is $A_C = (-1.2 \pm 4.1\,(\text{stat}) \pm 0.9\,(\text{syst}))\%$, consistent with the expectation of $(-0.4 \pm 0.1)\%$, obtained from the MadGraph5_aMC@NLO MC simulation of $t\bar{t}\gamma$ production, where the uncertainty accounts for the choice of μ_R and μ_F, and PDFs, including α_S variations. The $t\bar{t}\gamma$ decay process is simulated without including any charge asymmetry. The precision of this measurement is heavily limited by the statistical uncertainty, both of the data and the simulated signal samples, and further investigations will be needed as new data become available, in order to have sensitivity to new physics scenarios that might alter the expected value.

JHEP04(2026)086

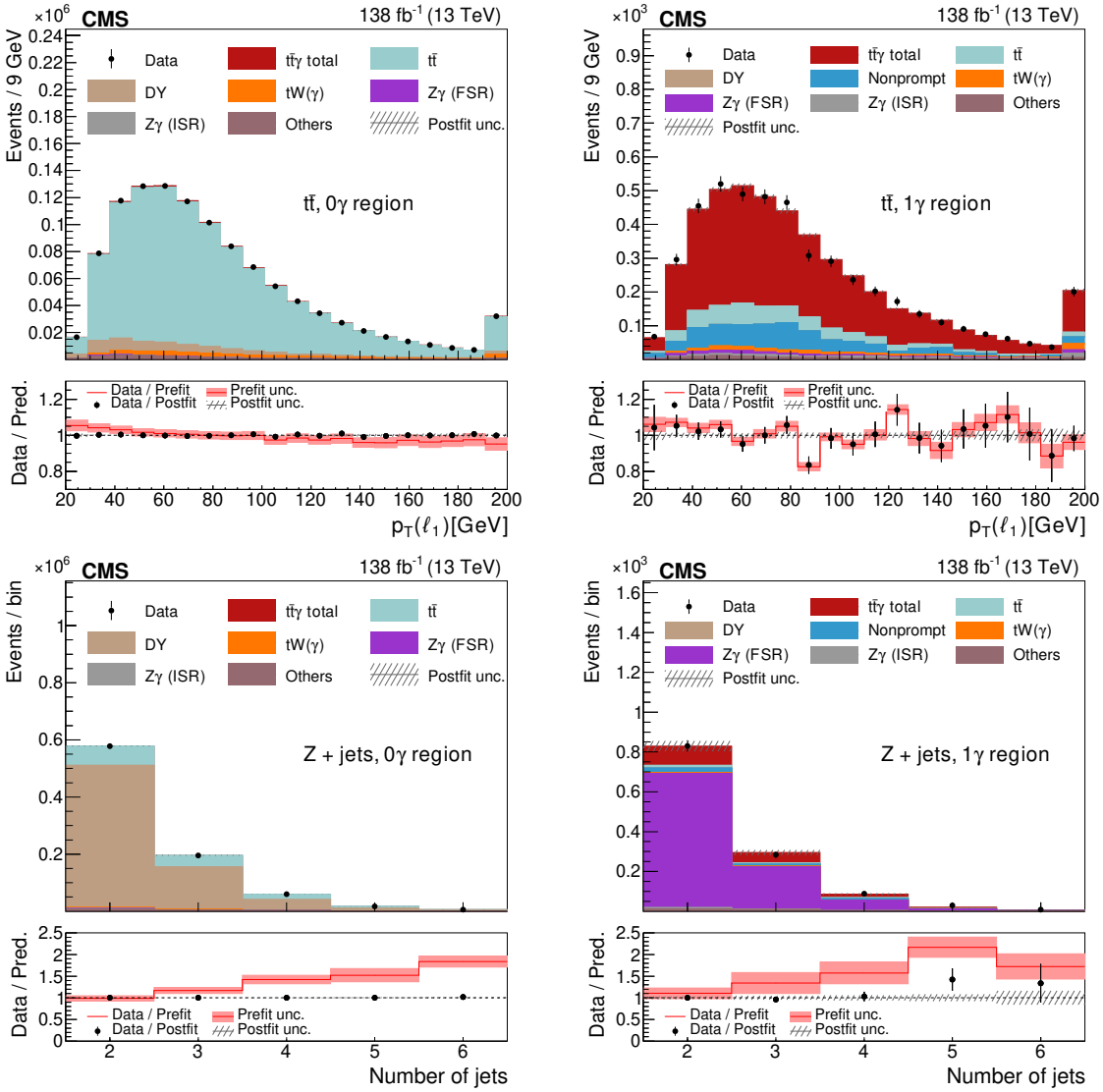

Figure 11. Distribution of the p_T of the leading lepton for the "$t\bar{t}, 0\gamma$" region (upper left) and the "$t\bar{t}, 1\gamma$" SR (upper right), and the number of jets for the DY+jets (lower left) and $Z\gamma$+jets (lower right) CRs after the fit. The hatched area indicates the total uncertainty in the prediction. The lower panels show the ratio of the data to the sum of the postfit predictions (points) and the ratio of the data to the sum of the prefit predictions (red line).

12 Summary

A comprehensive study of the top quark pair ($t\bar{t}$) production in association with a photon (γ) at the LHC is presented, using data collected by the CMS experiment in 2016–2018 at a centre-of-mass energy of 13 TeV, and corresponding to an integrated luminosity of 138 fb^{-1}. Inclusive and differential measurements are performed in the dilepton decay channels, in a fiducial region at the particle level including events with photon transverse momentum larger than 20 GeV.

JHEP04(2026)086

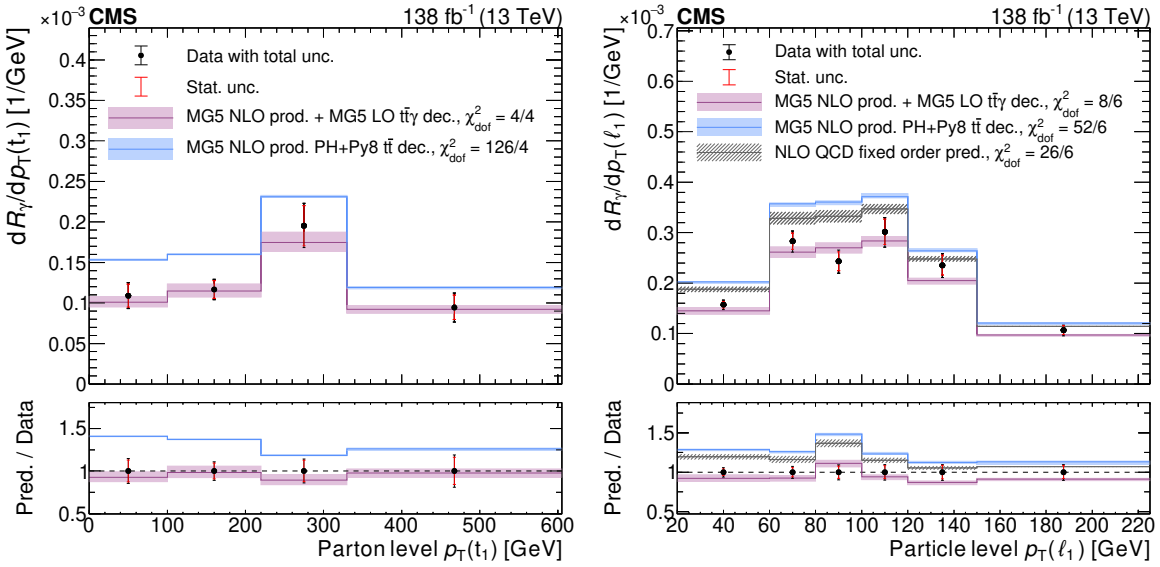

Figure 12. Absolute differential measurements of R_γ as a function of $p_T(t_1)$ at the parton level (left) and $p_T(\ell_1)$ at the particle level (right). The purple (blue) lines show the predictions from the nominal (alternative) simulation, and the lighter purple (blue) shaded areas represent the theoretical uncertainties in the predictions. The gray lines and bands represent the fixed-order predictions and their respective uncertainties. In the legends, "MG5" refers to MadGraph5_aMC@NLO, while "PH+Py8" refers to POWHEG and PYTHIA. The theoretical uncertainties include the choice of μ_R and μ_F and PDFs, including α_S variations. The black points represent the measured values, with the total uncertainty, while the red error bar shows the results considering only the statistical uncertainty.

The inclusive fiducial cross section, defined at the particle level, for $t\bar{t}\gamma$ with a photon radiated at any stage of the process is $137 \pm 3\,(\text{stat}) \pm 7\,(\text{syst})$ fb, while the cross section for events with a photon radiated at the production stage of the process is $56 \pm 2\,(\text{stat}) \pm 4\,(\text{syst})$ fb. The measured cross sections agree with the predictions from the standard model (SM) for the combined $t\bar{t}\gamma$ process and for the $t\bar{t}\gamma$ process with photons from the production stage.

The cross section is also measured differentially, in bins of seven different observables, related to the kinematic properties and topology of the photon, the leptons, and the top quarks reconstructed in the event. Measurements are performed at the particle or parton level, in different phase spaces, depending on the observable. The predictions from simulation accurately describe the shape of the measured cross sections. The $t\bar{t}\gamma/t\bar{t}$ cross section ratio is measured for the first time, inclusively and differentially. The inclusive ratio is found to be $0.0133 \pm 0.0002\,(\text{stat}) \pm 0.0005\,(\text{syst})$, in a phase space defined at the parton level, in agreement with the nominal predictions from simulation. The differential ratios are well described by the predictions, within the total uncertainty. The top quark charge asymmetry in $t\bar{t}\gamma$ events is also measured in a phase space defined at the parton level to be $(-1.2 \pm 4.1\,(\text{stat}) \pm 0.9\,(\text{syst}))\%$, compatible with both the SM prediction at next-to-leading order in quantum chromodynamics and with no asymmetry.

JHEP04(2026)086

Acknowledgments

We congratulate our colleagues in the CERN accelerator departments for the excellent performance of the LHC and thank the technical and administrative staffs at CERN and at other CMS institutes for their contributions to the success of the CMS effort. In addition, we gratefully acknowledge the computing centres and personnel of the Worldwide LHC Computing Grid and other centres for delivering so effectively the computing infrastructure essential to our analyses. Finally, we acknowledge the enduring support for the construction and operation of the LHC, the CMS detector, and the supporting computing infrastructure provided by the following funding agencies: SC (Armenia), BMBWF and FWF (Austria); FNRS and FWO (Belgium); CNPq, CAPES, FAPERJ, FAPERGS, and FAPESP (Brazil); MES and BNSF (Bulgaria); CERN; CAS, MoST, and NSFC (China); MINCIENCIAS (Colombia); MSES and CSF (Croatia); RIF (Cyprus); SENESCYT (Ecuador); ERC PRG, TARISTU24-TK10 and MoER TK202 (Estonia); Academy of Finland, MEC, and HIP (Finland); CEA and CNRS/IN2P3 (France); SRNSF (Georgia); BMFTR, DFG, and HGF (Germany); GSRI (Greece); NKFIH (Hungary); DAE and DST (India); IPM (Iran); SFI (Ireland); INFN (Italy); MSIT and NRF (Republic of Korea); MES (Latvia); LMTLT (Lithuania); MOE and UM (Malaysia); BUAP, CINVESTAV, CONACYT, LNS, SEP, and UASLP-FAI (Mexico); MOS (Montenegro); MBIE (New Zealand); PAEC (Pakistan); MES, NSC, and NAWA (Poland); FCT (Portugal); MESTD (Serbia); MICIU/AEI and PCTI (Spain); MOSTR (Sri Lanka); Swiss Funding Agencies (Switzerland); MST (Taipei); MHESI (Thailand); TUBITAK and TENMAK (Türkiye); NASU (Ukraine); STFC (United Kingdom); DOE and NSF (U.S.A.).

Individuals have received support from the Marie-Curie programme and the European Research Council and Horizon 2020 Grant, contract Nos. 675440, 724704, 752730, 758316, 765710, 824093, 101115353, 101002207, 101001205, and COST Action CA16108 (European Union); the Leventis Foundation; the Alfred P. Sloan Foundation; the Alexander von Humboldt Foundation; the Science Committee, project no. 22rl-037 (Armenia); the Fonds pour la Formation à la Recherche dans l'Industrie et dans l'Agriculture (FRIA) and Fonds voor Wetenschappelijk Onderzoek contract No. 1228724N (Belgium); the Beijing Municipal Science & Technology Commission, No. Z191100007219010, the Fundamental Research Funds for the Central Universities, the Ministry of Science and Technology of China under Grant No. 2023YFA1605804, the Natural Science Foundation of China under Grant No. 12061141002, 12535004, and USTC Research Funds of the Double First-Class Initiative No. YD2030002017 (China); the Ministry of Education, Youth and Sports (MEYS) of the Czech Republic; the Shota Rustaveli National Science Foundation, grant FR-22-985 (Georgia); the Deutsche Forschungsgemeinschaft (DFG), among others, under Germany's Excellence Strategy – EXC 2121 "Quantum Universe" – 390833306, and under project number 400140256 – GRK2497; the Hellenic Foundation for Research and Innovation (HFRI), Project Number 2288 (Greece); the Hungarian Academy of Sciences, the New National Excellence Program – ÚNKP, the NKFIH research grants K 131991, K 133046, K 138136, K 143460, K 143477, K 146913, K 146914, K 147048, 2020-2.2.1-ED-2021-00181, TKP2021-NKTA-64, and 2021-4.1.2-NEMZ_KI-2024-00036 (Hungary); the Council of Science and Industrial Research, India; ICSC – National Research Centre for High Performance Computing, Big Data and Quantum Computing, FAIR – Future Artificial Intelligence Research, and CUP I53D23001070006 (Mission 4 Component 1),

JHEP04(2026)086

funded by the NextGenerationEU program (Italy); the Latvian Council of Science; the Ministry of Education and Science, project no. 2022/WK/14, and the National Science Center, contracts Opus 2021/41/B/ST2/01369, 2021/43/B/ST2/01552, 2023/49/B/ST2/03273, and the NAWA contract BPN/PPO/2021/1/00011 (Poland); the Fundação para a Ciência e a Tecnologia, grant CEECIND/01334/2018 (Portugal); the National Priorities Research Program by Qatar National Research Fund; MICIU/AEI/10.13039/501100011033, ERDF/EU, "European Union NextGenerationEU/PRTR", and Programa Severo Ochoa del Principado de Asturias (Spain); the Chulalongkorn Academic into Its 2nd Century Project Advancement Project, the National Science, Research and Innovation Fund program IND_FF_68_369_2300_097, and the Program Management Unit for Human Resources & Institutional Development, Research and Innovation, grant B39G680009 (Thailand); the Kavli Foundation; the Nvidia Corporation; the SuperMicro Corporation; the Welch Foundation, contract C-1845; and the Weston Havens Foundation (U.S.A.).

Data Availability Statement. Release and preservation of data used by the CMS Collaboration as the basis for publications is guided by the CMS data preservation, re-use and open access policy.

Code Availability Statement. The CMS core software is publicly available on GitHub.

References

[1] U. Baur, A. Juste, L.H. Orr and D. Rainwater, *Probing electroweak top quark couplings at hadron colliders*, *Phys. Rev. D* **71** (2005) 054013 [hep-ph/0412021] [INSPIRE].

[2] A.O. Bouzas and F. Larios, *Electromagnetic dipole moments of the Top quark*, *Phys. Rev. D* **87** (2013) 074015 [arXiv:1212.6575] [INSPIRE].

[3] M. Schulze and Y. Soreq, *Pinning down electroweak dipole operators of the top quark*, *Eur. Phys. J. C* **76** (2016) 466 [arXiv:1603.08911] [INSPIRE].

[4] G. Bevilacqua et al., *Hard Photons in Hadroproduction of Top Quarks with Realistic Final States*, *JHEP* **10** (2018) 158 [arXiv:1803.09916] [INSPIRE].

[5] G. Bevilacqua et al., *Off-shell vs on-shell modelling of top quarks in photon associated production*, *JHEP* **03** (2020) 154 [arXiv:1912.09999] [INSPIRE].

[6] J. Bergner and M. Schulze, *The top quark charge asymmetry in $t\bar{t}\gamma$ production at the LHC*, *Eur. Phys. J. C* **79** (2019) 189 [arXiv:1812.10535] [INSPIRE].

[7] J.A. Aguilar-Saavedra, E. Álvarez, A. Juste and F. Rubbo, *Shedding light on the $t\bar{t}$ asymmetry: the photon handle*, *JHEP* **04** (2014) 188 [arXiv:1402.3598] [INSPIRE].

[8] D. Stremmer and M. Worek, *Associated production of a top-quark pair with two isolated photons at the LHC through NLO in QCD*, *JHEP* **08** (2023) 179 [arXiv:2306.16968] [INSPIRE].

[9] G. Bevilacqua et al., *Precise predictions for $t\bar{t}\gamma/t\bar{t}$ cross section ratios at the LHC*, *JHEP* **01** (2019) 188 [arXiv:1809.08562] [INSPIRE].

JHEP04(2026)086

[10] D. Barducci et al., *Interpreting top-quark LHC measurements in the standard-model effective field theory*, arXiv:1802.07237 [INSPIRE].

[11] CDF collaboration, *Evidence for $t\bar{t}\gamma$ Production and Measurement of $\sigma_t\bar{t}\gamma/\sigma_t\bar{t}$*, *Phys. Rev. D* **84** (2011) 031104 [arXiv:1106.3970] [INSPIRE].

[12] ATLAS collaboration, *Observation of top-quark pair production in association with a photon and measurement of the $t\bar{t}\gamma$ production cross section in pp collisions at $\sqrt{s} = 7$ TeV using the ATLAS detector*, *Phys. Rev. D* **91** (2015) 072007 [arXiv:1502.00586] [INSPIRE].

[13] ATLAS collaboration, *Measurement of the $t\bar{t}\gamma$ production cross section in proton-proton collisions at $\sqrt{s} = 8$ TeV with the ATLAS detector*, *JHEP* **11** (2017) 086 [arXiv:1706.03046] [INSPIRE].

[14] CMS collaboration, *Measurement of the semileptonic $t\bar{t}$ + γ production cross section in pp collisions at $\sqrt{s} = 8$ TeV*, *JHEP* **10** (2017) 006 [arXiv:1706.08128] [INSPIRE].

[15] CMS collaboration, *Measurement of the inclusive and differential $t\bar{t}\gamma$ cross sections in the dilepton channel and effective field theory interpretation in proton-proton collisions at $\sqrt{s} = 13$ TeV*, *JHEP* **05** (2022) 091 [arXiv:2201.07301] [INSPIRE].

[16] CMS collaboration, *Measurement of the inclusive and differential $\mathrm{t\bar{t}}\gamma$ cross sections in the single-lepton channel and EFT interpretation at $\sqrt{s}$ = 13 TeV*, *JHEP* **12** (2021) 180 [arXiv:2107.01508] [INSPIRE].

[17] ATLAS collaboration, *Measurements of inclusive and differential fiducial cross-sections of $t\bar{t}\gamma$ production in leptonic final states at $\sqrt{s} = 13$ TeV in ATLAS*, *Eur. Phys. J. C* **79** (2019) 382 [arXiv:1812.01697] [INSPIRE].

[18] ATLAS collaboration, *Measurements of inclusive and differential cross-sections of combined $t\bar{t}\gamma$ and $tW\gamma$ production in the eμ channel at 13 TeV with the ATLAS detector*, *JHEP* **09** (2020) 049 [arXiv:2007.06946] [INSPIRE].

[19] ATLAS collaboration, *Measurements of inclusive and differential cross-sections of $t\bar{t}\gamma$ production in pp collisions at $\sqrt{s} = 13$ TeV with the ATLAS detector*, *JHEP* **10** (2024) 191 [arXiv:2403.09452] [INSPIRE].

[20] ATLAS collaboration, *Measurement of the charge asymmetry in top-quark pair production in association with a photon with the ATLAS experiment*, *Phys. Lett. B* **843** (2023) 137848 [arXiv:2212.10552] [INSPIRE].

[21] HEPData record for this analysis, (2025) DOI:10.17182/hepdata.157848.

[22] CMS collaboration, *The CMS Experiment at the CERN LHC*, 2008 *JINST* **3** S08004 [INSPIRE].

[23] CMS collaboration, *Development of the CMS detector for the CERN LHC Run 3*, 2024 *JINST* **19** P05064 [arXiv:2309.05466] [INSPIRE].

[24] CMS collaboration, *Performance of the CMS Level-1 trigger in proton-proton collisions at $\sqrt{s} = 13$ TeV*, 2020 *JINST* **15** P10017 [arXiv:2006.10165] [INSPIRE].

[25] CMS collaboration, *The CMS trigger system*, 2017 *JINST* **12** P01020 [arXiv:1609.02366] [INSPIRE].

[26] CMS collaboration, *Performance of the CMS high-level trigger during LHC Run 2*, 2024 *JINST* **19** P11021 [arXiv:2410.17038] [INSPIRE].

[27] J. Alwall et al., *The automated computation of tree-level and next-to-leading order differential cross sections, and their matching to parton shower simulations*, *JHEP* **07** (2014) 079 [arXiv:1405.0301] [INSPIRE].

JHEP04(2026)086

[28] S. Frixione, *Isolated photons in perturbative QCD*, *Phys. Lett. B* **429** (1998) 369 [hep-ph/9801442] [INSPIRE].

[29] P. Artoisenet, R. Frederix, O. Mattelaer and R. Rietkerk, *Automatic spin-entangled decays of heavy resonances in Monte Carlo simulations*, *JHEP* **03** (2013) 015 [arXiv:1212.3460] [INSPIRE].

[30] S. Frixione et al., *Automated simulations beyond the Standard Model: supersymmetry*, *JHEP* **12** (2019) 008 [arXiv:1907.04898] [INSPIRE].

[31] P. Nason, *A new method for combining NLO QCD with shower Monte Carlo algorithms*, *JHEP* **11** (2004) 040 [hep-ph/0409146] [INSPIRE].

[32] S. Frixione, P. Nason and C. Oleari, *Matching NLO QCD computations with Parton Shower simulations: the POWHEG method*, *JHEP* **11** (2007) 070 [arXiv:0709.2092] [INSPIRE].

[33] S. Alioli, P. Nason, C. Oleari and E. Re, *A general framework for implementing NLO calculations in shower Monte Carlo programs: the POWHEG BOX*, *JHEP* **06** (2010) 043 [arXiv:1002.2581] [INSPIRE].

[34] M. Czakon and A. Mitov, *Top++: A Program for the Calculation of the Top-Pair Cross-Section at Hadron Colliders*, *Comput. Phys. Commun.* **185** (2014) 2930 [arXiv:1112.5675] [INSPIRE].

[35] M. Beneke, P. Falgari, S. Klein and C. Schwinn, *Hadronic top-quark pair production with NNLL threshold resummation*, *Nucl. Phys. B* **855** (2012) 695 [arXiv:1109.1536] [INSPIRE].

[36] M. Cacciari et al., *Top-pair production at hadron colliders with next-to-next-to-leading logarithmic soft-gluon resummation*, *Phys. Lett. B* **710** (2012) 612 [arXiv:1111.5869] [INSPIRE].

[37] M. Czakon and A. Mitov, *NNLO corrections to top-pair production at hadron colliders: the all-fermionic scattering channels*, *JHEP* **12** (2012) 054 [arXiv:1207.0236] [INSPIRE].

[38] M. Czakon and A. Mitov, *NNLO corrections to top pair production at hadron colliders: the quark-gluon reaction*, *JHEP* **01** (2013) 080 [arXiv:1210.6832] [INSPIRE].

[39] M. Czakon, P. Fiedler and A. Mitov, *Total Top-Quark Pair-Production Cross Section at Hadron Colliders Through* $O(\alpha_S^4)$, *Phys. Rev. Lett.* **110** (2013) 252004 [arXiv:1303.6254] [INSPIRE].

[40] M. Czakon et al., *Top-pair production at the LHC through NNLO QCD and NLO EW*, *JHEP* **10** (2017) 186 [arXiv:1705.04105] [INSPIRE].

[41] M. Czakon, D. Heymes and A. Mitov, *fastNLO tables for NNLO top-quark pair differential distributions*, arXiv:1704.08551 [INSPIRE].

[42] M. Czakon, D. Heymes and A. Mitov, *High-precision differential predictions for top-quark pairs at the LHC*, *Phys. Rev. Lett.* **116** (2016) 082003 [arXiv:1511.00549] [INSPIRE].

[43] M. Czakon, D. Heymes and A. Mitov, *Dynamical scales for multi-TeV top-pair production at the LHC*, *JHEP* **04** (2017) 071 [arXiv:1606.03350] [INSPIRE].

[44] T. Sjöstrand et al., *An introduction to PYTHIA 8.2*, *Comput. Phys. Commun.* **191** (2015) 159 [arXiv:1410.3012] [INSPIRE].

[45] CMS collaboration, *Measurement of the top quark mass using proton-proton data at* $\sqrt{s} = 7$ *and* 8 *TeV*, *Phys. Rev. D* **93** (2016) 072004 [arXiv:1509.04044] [INSPIRE].

[46] P. Skands, S. Carrazza and J. Rojo, *Tuning PYTHIA 8.1: the Monash 2013 Tune*, *Eur. Phys. J. C* **74** (2014) 3024 [arXiv:1404.5630] [INSPIRE].

[47] CMS collaboration, *Event generator tunes obtained from underlying event and multiparton scattering measurements*, *Eur. Phys. J. C* **76** (2016) 155 [arXiv:1512.00815] [INSPIRE].

JHEP04(2026)086

[48] CMS collaboration, *Extraction and validation of a new set of CMS PYTHIA8 tunes from underlying-event measurements*, *Eur. Phys. J. C* **80** (2020) 4 [arXiv:1903.12179] [INSPIRE].

[49] NNPDF collaboration, *Parton distributions from high-precision collider data*, *Eur. Phys. J. C* **77** (2017) 663 [arXiv:1706.00428] [INSPIRE].

[50] J. Alwall et al., *Comparative study of various algorithms for the merging of parton showers and matrix elements in hadronic collisions*, *Eur. Phys. J. C* **53** (2008) 473 [arXiv:0706.2569] [INSPIRE].

[51] R. Frederix and S. Frixione, *Merging meets matching in MC@NLO*, *JHEP* **12** (2012) 061 [arXiv:1209.6215] [INSPIRE].

[52] GEANT4 collaboration, *GEANT4 — A Simulation Toolkit*, *Nucl. Instrum. Meth. A* **506** (2003) 250 [INSPIRE].

[53] CMS collaboration, *Measurement of the inelastic proton-proton cross section at* $\sqrt{s} = 13$ *TeV*, *JHEP* **07** (2018) 161 [arXiv:1802.02613] [INSPIRE].

[54] D. Contardo et al., *Technical proposal for the Phase-II upgrade of the Compact Muon Solenoid*, CERN-LHCC-2015-010 (2015) [DOI:10.17181/CERN.VU8I.D59J] [INSPIRE].

[55] CMS collaboration, *Particle-flow reconstruction and global event description with the CMS detector*, 2017 *JINST* **12** P10003 [arXiv:1706.04965] [INSPIRE].

[56] CMS collaboration, *Electron and photon reconstruction and identification with the CMS experiment at the CERN LHC*, 2021 *JINST* **16** P05014 [arXiv:2012.06888] [INSPIRE].

[57] CMS collaboration, *ECAL 2016 refined calibration and Run 2 summary plots*, CMS Detector Performance Note CMS-DP-2020-021 (2020).

[58] CMS collaboration, *Performance of the CMS muon detector and muon reconstruction with proton-proton collisions at* $\sqrt{s} = 13$ *TeV*, 2018 *JINST* **13** P06015 [arXiv:1804.04528] [INSPIRE].

[59] CMS collaboration, *Performance of the CMS electromagnetic calorimeter in pp collisions at* $\sqrt{s} = 13$ *TeV*, 2024 *JINST* **19** P09004 [arXiv:2403.15518] [INSPIRE].

[60] CMS collaboration, *Electron and photon performance in CMS with the full 2016 data sample*, CMS Detector Performance Note CMS-DP-2017-004 (2017).

[61] CMS collaboration, *Performance of electron and photon reconstruction in Run 2 with the CMS experiment*, CMS Detector Performance Note CMS-DP-2020-037 (2020).

[62] M. Cacciari, G.P. Salam and G. Soyez, *The anti-*k_t *jet clustering algorithm*, *JHEP* **04** (2008) 063 [arXiv:0802.1189] [INSPIRE].

[63] M. Cacciari, G.P. Salam and G. Soyez, *FastJet User Manual*, *Eur. Phys. J. C* **72** (2012) 1896 [arXiv:1111.6097] [INSPIRE].

[64] CMS collaboration, *Jet algorithms performance in 13 TeV data*, CMS-PAS-JME-16-003 (2017) [INSPIRE].

[65] CMS collaboration, *Determination of Jet Energy Calibration and Transverse Momentum Resolution in CMS*, 2011 *JINST* **6** P11002 [arXiv:1107.4277] [INSPIRE].

[66] CMS collaboration, *Identification of heavy-flavour jets with the CMS detector in pp collisions at 13 TeV*, 2018 *JINST* **13** P05011 [arXiv:1712.07158] [INSPIRE].

[67] E. Bols et al., *Jet flavour classification using DeepJet*, 2020 *JINST* **15** P12012 [arXiv:2008.10519] [INSPIRE].

JHEP04(2026)086

[68] CMS collaboration, *Performance summary of AK4 jet b tagging with data from proton-proton collisions at 13 TeV with the CMS detector*, CMS Detector Performance Note CMS-DP-2023-005 (2023).

[69] CMS collaboration, *Performance of missing transverse momentum reconstruction in proton-proton collisions at $\sqrt{s} = 13$ TeV using the CMS detector*, 2019 *JINST* **14** P07004 [arXiv:1903.06078] [INSPIRE].

[70] CMS collaboration, *Jet energy scale and resolution in the CMS experiment in pp collisions at 8 TeV*, 2017 *JINST* **12** P02014 [arXiv:1607.03663] [INSPIRE].

[71] CMS collaboration, *Review of top quark mass measurements in CMS*, *Phys. Rept.* **1115** (2025) 116 [arXiv:2403.01313] [INSPIRE].

[72] Particle Data Group collaboration, *Review of particle physics*, *Phys. Rev. D* **110** (2024) 030001 [INSPIRE].

[73] CMS collaboration, *Measurement of the top quark polarization and $t\bar{t}$ spin correlations using dilepton final states in proton-proton collisions at $\sqrt{s} = 13$ TeV*, *Phys. Rev. D* **100** (2019) 072002 [arXiv:1907.03729] [INSPIRE].

[74] CMS collaboration, *Precision luminosity measurement in proton-proton collisions at $\sqrt{s} = 13$ TeV in 2015 and 2016 at CMS*, *Eur. Phys. J. C* **81** (2021) 800 [arXiv:2104.01927] [INSPIRE].

[75] CMS collaboration, *CMS luminosity measurement for the 2017 data-taking period at $\sqrt{s} = 13$ TeV*, CMS-PAS-LUM-17-004 (2018) [INSPIRE].

[76] CMS collaboration, *CMS luminosity measurement for the 2018 data-taking period at $\sqrt{s} = 13$ TeV*, CMS-PAS-LUM-18-002 (2019) [INSPIRE].

[77] R.J. Barlow and C. Beeston, *Fitting using finite Monte Carlo samples*, *Comput. Phys. Commun.* **77** (1993) 219 [INSPIRE].

[78] NNPDF collaboration, *Parton distributions for the LHC Run II*, *JHEP* **04** (2015) 040 [arXiv:1410.8849] [INSPIRE].

[79] CMS collaboration, *Measurement of the electroweak production of $Z\gamma$ and two jets in proton-proton collisions at $\sqrt{s} = 13$ TeV and constraints on anomalous quartic gauge couplings*, *Phys. Rev. D* **104** (2021) 072001 [arXiv:2106.11082] [INSPIRE].

[80] CMS collaboration, *The CMS Statistical Analysis and Combination Tool: Combine*, *Comput. Softw. Big Sci.* **8** (2024) 19 [arXiv:2404.06614] [INSPIRE].

[81] V. Blobel, *Unfolding methods in particle physics*, in *Proc. 2011 Workshop on Statistical Issues Related to Discovery Claims in Search Experiments and Unfolding (PHYSTAT 2011): Geneva, Switzerland, January 17–20, 2011*, p. 240, 2011, [DOI:10.5170/CERN-2011-006].

[82] CMS collaboration, *Object definitions for top quark analyses at the particle level*, CMS Note CMS-NOTE-2017-004 (2017).

[83] M. Cacciari, G.P. Salam and G. Soyez, *The catchment area of jets*, *JHEP* **04** (2008) 005 [arXiv:0802.1188] [INSPIRE].

[84] D. Stremmer and M. Worek, *Complete NLO corrections to top-quark pair production with isolated photons*, *JHEP* **07** (2024) 091 [arXiv:2403.03796] [INSPIRE].

[85] G. Bevilacqua et al., *HELAC-NLO*, *Comput. Phys. Commun.* **184** (2013) 986 [arXiv:1110.1499] [INSPIRE].

JHEP04(2026)086

[86] S. Actis et al., *RECOLA: REcursive Computation of One-Loop Amplitudes*, *Comput. Phys. Commun.* **214** (2017) 140 [arXiv:1605.01090] [INSPIRE].

[87] S. Actis et al., *Recursive generation of one-loop amplitudes in the Standard Model*, *JHEP* **04** (2013) 037 [arXiv:1211.6316] [INSPIRE].

[88] A. Denner, S. Dittmaier and L. Hofer, *Collier: a fortran-based Complex One-Loop LIbrary in Extended Regularizations*, *Comput. Phys. Commun.* **212** (2017) 220 [arXiv:1604.06792] [INSPIRE].

[89] G. Bevilacqua, M. Czakon, M. Kubocz and M. Worek, *Complete Nagy-Soper subtraction for next-to-leading order calculations in QCD*, *JHEP* **10** (2013) 204 [arXiv:1308.5605] [INSPIRE].

[90] G. Bevilacqua, M. Lupattelli, D. Stremmer and M. Worek, *Study of additional jet activity in top quark pair production and decay at the LHC*, *Phys. Rev. D* **107** (2023) 114027 [arXiv:2212.04722] [INSPIRE].

[91] M. Czakon, H.B. Hartanto, M. Kraus and M. Worek, *Matching the Nagy-Soper parton shower at next-to-leading order*, *JHEP* **06** (2015) 033 [arXiv:1502.00925] [INSPIRE].

[92] D. Stremmer and M. Worek, *NLO QCD predictions for $t\bar{t}\gamma$ with realistic photon isolation*, *JHEP* **01** (2025) 156 [arXiv:2411.02196] [INSPIRE].

[93] L. Demortier and L. Lyons, *Everything you always wanted to know about pulls*, Tech. Rep. CDF/ANAL/PUBLIC/5776, CDF (2002).

[94] E. Gross and O. Vitells, *Trial factors for the look elsewhere effect in high energy physics*, *Eur. Phys. J. C* **70** (2010) 525 [arXiv:1005.1891] [INSPIRE].

JHEP04(2026)086

The CMS collaboration

A. Hayrapetyan[1], V. Makarenko[1], A. Tumasyan[1,a], W. Adam[2], J.W. Andrejkovic[2], L. Benato[2], T. Bergauer[2], M. Dragicevic[2], C. Giordano[2], P.S. Hussain[2], M. Jeitler[2,b], N. Krammer[2], A. Li[2], D. Liko[2], M. Matthewman[2], I. Mikulec[2], J. Schieck[2,b], D. Schwarz[2], R. Schöfbeck[2,b], M. Shooshtari[2], M. Sonawane[2], W. Waltenberger[2], C.-E. Wulz[2,b], T. Janssen[3], H. Kwon[3], D. Ocampo Henao[3], T. Van Laer[3], P. Van Mechelen[3], J. Bierkens[4], N. Breugelmans[4], J. D'Hondt[4], S. Dansana[4], A. De Moor[4], M. Delcourt[4], F. Heyen[4], Y. Hong[4], P. Kashko[4], S. Lowette[4], I. Makarenko[4], D. Müller[4], J. Song[4], S. Tavernier[4], M. Tytgat[4,c], G.P. Van Onsem[4], S. Van Putte[4], D. Vannerom[4], B. Bilin[5], B. Clerbaux[5], A.K. Das[5], I. De Bruyn[5], G. De Lentdecker[5], H. Evard[5], L. Favart[5], P. Gianneios[5], A. Khalilzadeh[5], F.A. Khan[5], A. Malara[5], M.A. Shahzad[5], L. Thomas[5], M. Vanden Bemden[5], C. Vander Velde[5], P. Vanlaer[5], F. Zhang[5], M. De Coen[6], D. Dobur[6], G. Gokbulut[6], J. Knolle[6], D. Marckx[6], K. Skovpen[6], A.M. Tomaru[6], N. Van Den Bossche[6], J. van der Linden[6], J. Vandenbroeck[6], L. Wezenbeek[6], S. Bein[7], A. Benecke[7], A. Bethani[7], G. Bruno[7], A. Cappati[7], J. De Favereau De Jeneret[7], C. Delaere[7], F. Gameiro Casalinho[7], A. Giammanco[7], A.O. Guzel[7], V. Lemaitre[7], J. Lidrych[7], P. Malek[7], P. Mastrapasqua[7], S. Turkcapar[7], G.A. Alves[8], M. Barroso Ferreira Filho[8], E. Coelho[8], C. Hensel[8], T. Menezes De Oliveira[8], C. Mora Herrera[8], P. Rebello Teles[8], M. Soeiro[8], E.J. Tonelli Manganote[8,d], A. Vilela Pereira[8,e], W.L. Aldá Júnior[9], H. Brandao Malbouisson[9], W. Carvalho[9], J. Chinellato[9,f], M. Costa Reis[9], E.M. Da Costa[9], G.G. Da Silveira[9,g], D. De Jesus Damiao[9], S. Fonseca De Souza[9], R. Gomes De Souza[9], S. S. Jesus[9], T. Laux Kuhn[9,g], M. Macedo[9], K. Mota Amarilo[9], L. Mundim[9], H. Nogima[9], J.P. Pinheiro[9], A. Santoro[9], A. Sznajder[9], M. Thiel[9], F. Torres Da Silva De Araujo[9,h], C.A. Bernardes[10,g], F. Damas[10], E.M. Gregores[10], B. Lopes Da Costa[10], I. Maietto Silverio[10], P.G. Mercadante[10], S.F. Novaes[10], B. Orzari[10], Sandra S. Padula[10], V. Scheurer[10], T.R. Fernandez Perez Tomei[10], A. Aleksandrov[11], G. Antchev[11], P. Danev[11], R. Hadjiiska[11], P. Iaydjiev[11], M. Shopova[11], G. Sultanov[11], A. Dimitrov[12], L. Litov[12], B. Pavlov[12], P. Petkov[12], A. Petrov[12], S. Keshri[13], D. Laroze[13], S. Thakur[13], W. Brooks[14], T. Cheng[15], T. Javaid[15], L. Wang[15], L. Yuan[15], Z. Hu[16], Z. Liang[16], J. Liu[16], X. Wang[16], H. Yang[16], G.M. Chen[17,i], H.S. Chen[17,i], M. Chen[17,i], Y. Chen[17], Q. Hou[17], X. Hou[17], F. Iemmi[17], C.H. Jiang[17], A. Kapoor[17,j], H. Liao[17], G. Liu[17], Z.-A. Liu[17,k], J.N. Song[17,k], S. Song[17], J. Tao[17], C. Wang[17,i], J. Wang[17], H. Zhang[17], J. Zhao[17], A. Agapitos[18], Y. Ban[18], A. Carvalho Antunes De Oliveira[18], S. Deng[18], B. Guo[18], Q. Guo[18], C. Jiang[18], A. Levin[18], C. Li[18], Q. Li[18], Y. Mao[18], S. Qian[18], S.J. Qian[18], X. Qin[18], C. Quaranta[18], X. Sun[18], D. Wang[18], J. Wang[18], M. Zhang[18], Y. Zhao[18], C. Zhou[18], S. Yang[19], Z. You[20], K. Jaffel[21], N. Lu[21], G. Bauer[22,l,m], Z. Cui[22,m], B. Li[22,n], H. Wang[22], K. Yi[22,o], J. Zhang[22], Y. Li[23], Z. Lin[24], C. Lu[24], M. Xiao[24,p], C. Avila[25], D.A. Barbosa Trujillo[25], A. Cabrera[25], C. Florez[25], J. Fraga[25], J.A. Reyes Vega[25], C. Rendón[26], M. Rodriguez[26], A.A. Ruales Barbosa[26], J.D. Ruiz Alvarez[26], N. Godinovic[27], D. Lelas[27], A. Sculac[27], M. Kovac[28], A. Petkovic[28], T. Sculac[28], P. Bargassa[29], V. Brigljevic[29], B.K. Chitroda[29], D. Ferencek[29], K. Jakovcic[29], A. Starodumov[29], T. Susa[29], A. Attikis[30], K. Christoforou[30],

JHEP04(2026)086

C. Leonidou[30], C. Nicolaou[30], L. Paizanos[30], F. Ptochos[30], P.A. Razis[30], H. Rykaczewski[30], H. Saka[30], A. Stepennov[30], M. Finger[31,†], M. Finger Jr.[31], E. Ayala[32], E. Carrera Jarrin[33], B. El-mahdy[34,q], S. Khalil[34,r], A. Hussein[35], H. Mohammed[35], K. Ehataht[36], M. Kadastik[36], T. Lange[36], C. Nielsen[36], J. Pata[36], M. Raidal[36], N. Seeba[36], L. Tani[36], E. Brücken[37], A. Milieva[37], K. Osterberg[37], M. Voutilainen[37], F. Garcia[38], P. Inkaew[38], K.T.S. Kallonen[38], R. Kumar Verma[38], T. Lampén[38], K. Lassila-Perini[38], B. Lehtela[38], S. Lehti[38], T. Lindén[38], N.R. Mancilla Xinto[38], M. Myllymäki[38], M.m. Rantanen[38], S. Saariokari[38], N.T. Toikka[38], J. Tuominiemi[38], N. Bin Norjoharuddeen[39], H. Kirschenmann[39], P. Luukka[39], H. Petrow[39], M. Besancon[40], F. Couderc[40], M. Dejardin[40], D. Denegri[40], P. Devouge[40], J.L. Faure[40], F. Ferri[40], P. Gaigne[40], S. Ganjour[40], P. Gras[40], G. Hamel de Monchenault[40], M. Kumar[40], V. Lohezic[40], Y. Maidannyk[40], J. Malcles[40], F. Orlandi[40], L. Portales[40], S. Ronchi[40], M.Ö. Sahin[40], A. Savoy-Navarro[40,s], P. Simkina[40], M. Titov[40], M. Tornago[40], R. Amella Ranz[41], F. Beaudette[41], G. Boldrini[41], P. Busson[41], C. Charlot[41], M. Chiusi[41], T.D. Cuisset[41], O. Davignon[41], A. De Wit[41], T. Debnath[41], I.T. Ehle[41], S. Ghosh[41], A. Gilbert[41], R. Granier de Cassagnac[41], L. Kalipoliti[41], M. Manoni[41], M. Nguyen[41], S. Obraztsov[41], C. Ochando[41], R. Salerno[41], J.B. Sauvan[41], Y. Sirois[41], G. Sokmen[41], L. Urda Gómez[41], A. Zabi[41], A. Zghiche[41], J.-L. Agram[42,t], J. Andrea[42], D. Bloch[42], J.-M. Brom[42], E.C. Chabert[42], C. Collard[42], G. Coulon[42], S. Falke[42], U. Goerlach[42], R. Haeberle[42], A.-C. Le Bihan[42], M. Meena[42], O. Poncet[42], G. Saha[42], P. Vaucelle[42], A. Di Florio[43], D. Amram[44], S. Beauceron[44], B. Blancon[44], G. Boudoul[44], N. Chanon[44], D. Contardo[44], P. Depasse[44], H. El Mamouni[44], J. Fay[44], S. Gascon[44], M. Gouzevitch[44], C. Greenberg[44], G. Grenier[44], B. Ille[44], E. Jourd'Huy[44], M. Lethuillier[44], B. Massoteau[44], L. Mirabito[44], A. Purohit[44], M. Vander Donckt[44], J. Xiao[44], G. Adamov[45], I. Lomidze[45], Z. Tsamalaidze[45,u], V. Botta[46], S. Consuegra Rodríguez[46], L. Feld[46], K. Klein[46], M. Lipinski[46], D. Meuser[46], P. Nattland[46], V. Oppenländer[46], A. Pauls[46], D. Pérez Adán[46], N. Röwert[46], M. Teroerde[46], C. Daumann[47], S. Diekmann[47], A. Dodonova[47], N. Eich[47], D. Eliseev[47], F. Engelke[47], J. Erdmann[47], M. Erdmann[47], B. Fischer[47], T. Hebbeker[47], K. Hoepfner[47], F. Ivone[47], A. Jung[47], N. Kumar[47], M.y. Lee[47], F. Mausolf[47], M. Merschmeyer[47], A. Meyer[47], F. Nowotny[47], A. Pozdnyakov[47], W. Redjeb[47], H. Reithler[47], U. Sarkar[47], V. Sarkisovi[47], A. Schmidt[47], C. Seth[47], A. Sharma[47], J.L. Spah[47], V. Vaulin[47], M. Worek[47,v], S. Zaleski[47], M.R. Beckers[48], C. Dziwok[48], G. Flügge[48], N. Hoeflich[48], T. Kress[48], A. Nowack[48], O. Pooth[48], A. Stahl[48], A. Zotz[48], H. Aarup Petersen[49], A. Abel[49], M. Aldaya Martin[49], J. Alimena[49], S. Amoroso[49], Y. An[49], I. Andreev[49], J. Bach[49], S. Baxter[49], M. Bayatmakou[49], H. Becerril Gonzalez[49], O. Behnke[49], A. Belvedere[49], F. Blekman[49,w], K. Borras[49,x], A. Campbell[49], S. Chatterjee[49], L.X. Coll Saravia[49], G. Eckerlin[49], D. Eckstein[49], E. Gallo[49,w], A. Geiser[49], V. Guglielmi[49], M. Guthoff[49], A. Hinzmann[49], L. Jeppe[49], M. Kasemann[49], C. Kleinwort[49], R. Kogler[49], M. Komm[49], D. Krücker[49], W. Lange[49], D. Leyva Pernia[49], K.-Y. Lin[49], K. Lipka[49,y], W. Lohmann[49,z], J. Malvaso[49], R. Mankel[49], I.-A. Melzer-Pellmann[49], M. Mendizabal Morentin[49], A.B. Meyer[49], G. Milella[49], K. Moral Figueroa[49], A. Mussgiller[49], L.P. Nair[49], J. Niedziela[49], A. Nürnberg[49], J. Park[49], E. Ranken[49], A. Raspereza[49], D. Rastorguev[49], L. Rygaard[49],

JHEP04(2026)086

M. Scham[49,aa,ab], S. Schnake[49,x], C. Schwanenberger[49,w], P. Schütze[49], D. Selivanova[49], K. Sharko[49], M. Shchedrolosiev[49], D. Stafford[49], M. Torkian[49], F. Vazzoler[49], A. Ventura Barroso[49], R. Walsh[49], D. Wang[49], Q. Wang[49], K. Wichmann[49], L. Wiens[49,x], C. Wissing[49], Y. Yang[49], S. Zakharov[49], A. Zimermmane Castro Santos[49], A.R. Alves Andrade[50], M. Antonello[50], S. Bollweg[50], M. Bonanomi[50], K. El Morabit[50], Y. Fischer[50], M. Frahm[50], E. Garutti[50], A. Grohsjean[50], A.A. Guvenli[50], J. Haller[50], D. Hundhausen[50], G. Kasieczka[50], P. Keicher[50], R. Klanner[50], W. Korcari[50], T. Kramer[50], C.c. Kuo[50], F. Labe[50], J. Lange[50], A. Lobanov[50], L. Moureaux[50], A. Nigamova[50], K. Nikolopoulos[50], A. Paasch[50], K.J. Pena Rodriguez[50], N. Prouvost[50], B. Raciti[50], M. Rieger[50], D. Savoiu[50], P. Schleper[50], M. Schröder[50], J. Schwandt[50], M. Sommerhalder[50], H. Stadie[50], G. Steinbrück[50], R. Ward[50], B. Wiederspan[50], M. Wolf[50], S. Brommer[51], E. Butz[51], Y.M. Chen[51], T. Chwalek[51], A. Dierlamm[51], G.G. Dincer[51], U. Elicabuk[51], N. Faltermann[51], M. Giffels[51], A. Gottmann[51], F. Hartmann[51,ac], M. Horzela[51], F. Hummer[51], U. Husemann[51], J. Kieseler[51], M. Klute[51], R. Kunnilan Muhammed Rafeek[51], O. Lavoryk[51], J.M. Lawhorn[51], A. Lintuluoto[51], S. Maier[51], M. Mormile[51], Th. Müller[51], E. Pfeffer[51], M. Presilla[51], G. Quast[51], K. Rabbertz[51], B. Regnery[51], R. Schmieder[51], N. Shadskiy[51], I. Shvetsov[51], H.J. Simonis[51], L. Sowa[51], L. Stockmeier[51], D. Stremmer[51,ad], K. Tauqeer[51], M. Toms[51], B. Topko[51], N. Trevisani[51], C. Verstege[51], T. Voigtländer[51], R.F. Von Cube[51], J. Von Den Driesch[51], M. Wassmer[51], R. Wolf[51], W.D. Zeuner[51], X. Zuo[51], G. Anagnostou[52], G. Daskalakis[52], A. Kyriakis[52], G. Melachroinos[53], Z. Painesis[53], I. Paraskevas[53], N. Saoulidou[53], K. Theofilatos[53], E. Tziaferi[53], E. Tzovara[53], K. Vellidis[53], I. Zisopoulos[53], T. Chatzistavrou[54], G. Karapostoli[54], K. Kousouris[54], E. Siamarkou[54], G. Tsipolitis[54], I. Bestintzanos[55], I. Evangelou[55], C. Foudas[55], P. Katsoulis[55], P. Kokkas[55], P.G. Kosmoglou Kioseoglou[55], N. Manthos[55], I. Papadopoulos[55], J. Strologas[55], D. Druzhkin[56], C. Hajdu[56], D. Horvath[56,ae,af], K. Márton[56], A.J. Rádl[56,ag], F. Sikler[56], V. Veszpremi[56], M. Csanád[57], K. Farkas[57], A. Fehérkuti[57,ah], M.M.A. Gadallah[57,ai], Á. Kadlecsik[57], M. León Coello[57], G. Pásztor[57], G.I. Veres[57], B. Ujvari[58], G. Zilizi[58], G. Bencze[59], S. Czellar[59], J. Molnar[59], Z. Szillasi[59], T. Csorgo[60,ah], F. Nemes[60,ah], T. Novak[60], I. Szanyi[60,aj], S. Bansal[61], S.B. Beri[61], V. Bhatnagar[61], G. Chaudhary[61], S. Chauhan[61], N. Dhingra[61,ak], A. Kaur[61], A. Kaur[61], H. Kaur[61], M. Kaur[61], S. Kumar[61], T. Sheokand[61], J.B. Singh[61], A. Singla[61], A. Bhardwaj[62], A. Chhetri[62], B.C. Choudhary[62], A. Kumar[62], A. Kumar[62], M. Naimuddin[62], S. Phor[62], K. Ranjan[62], M.K. Saini[62], P. Palni[63], S. Acharya[64,al], B. Gomber[64], B. Sahu[64,al], S. Mukherjee[65], S. Bhattacharya[66], S. Das Gupta[66], S. Dutta[66], S. Dutta[66], S. Sarkar[66], M.M. Ameen[67], P.K. Behera[67], S. Chatterjee[67], G. Dash[67], A. Dattamunsi[67], P. Jana[67], P. Kalbhor[67], S. Kamble[67], J.R. Komaragiri[67,am], T. Mishra[67], P.R. Pujahari[67], A.K. Sikdar[67], R.K. Singh[67], P. Verma[67], S. Verma[67], A. Vijay[67], B.K. Sirasva[68], L. Bhatt[69], S. Dugad[69], G.B. Mohanty[69], M. Shelake[69], P. Suryadevara[69], A. Bala[70], S. Banerjee[70], S. Barman[70,an], R.M. Chatterjee[70], M. Guchait[70], Sh. Jain[70], A. Jaiswal[70], B.M. Joshi[70], S. Kumar[70], M. Maity[70,an], G. Majumder[70], K. Mazumdar[70], S. Parolia[70], R. Saxena[70], A. Thachayath[70], S. Bahinipati[71,ao], D. Maity[71,ap], P. Mal[71], K. Naskar[71,ap], A. Nayak[71,ap], S. Nayak[71], K. Pal[71], R. Raturi[71], P. Sadangi[71], S.K. Swain[71],

JHEP04(2026)086

S. Varghese[71,ap], D. Vats[71,ap], A. Alpana[72], S. Dube[72], P. Hazarika[72], B. Kansal[72], A. Laha[72], R. Sharma[72], S. Sharma[72], K.Y. Vaish[72], S. Ghosh[73], H. Bakhshiansohi[74,aq], A. Jafari[74,ar], V. Sedighzadeh Dalavi[74], M. Zeinali[74,as], S. Bashiri[75], S. Chenarani[75,at], S.M. Etesami[75], Y. Hosseini[75], M. Khakzad[75], E. Khazaie[75], M. Mohammadi Najafabadi[75], S. Tizchang[75,au], M. Felcini[76], M. Grunewald[76], M. Abbrescia[77a,77b], M. Barbieri[77a,77b], M. Buonsante[77a,77b], A. Colaleo[77a,77b], D. Creanza[77a,77c], N. De Filippis[77a,77c], M. De Palma[77a,77b], W. Elmetenawee[77a,77b,av], N. Ferrara[77a,77c], L. Fiore[77a], L. Longo[77a], M. Louka[77a,77b], G. Maggi[77a,77c], M. Maggi[77a], I. Margjeka[77a], V. Mastrapasqua[77a,77b], S. My[77a,77b], F. Nenna[77a,77b], S. Nuzzo[77a,77b], A. Pellecchia[77a,77b], A. Pompili[77a,77b], G. Pugliese[77a,77c], R. Radogna[77a,77b], D. Ramos[77a], A. Ranieri[77a], L. Silvestris[77a], F.M. Simone[77a,77c], A. Stamerra[77a,77b], Ü. Sözbilir[77a], D. Troiano[77a,77b], R. Venditti[77a,77b], P. Verwilligen[77a], A. Zaza[77a,77b], G. Abbiendi[78a], C. Battilana[78a,78b], D. Bonacorsi[78a,78b], P. Capiluppi[78a,78b], F.R. Cavallo[78a], M. Cuffiani[78a,78b], G.M. Dallavalle[78a], T. Diotalevi[78a,78b], F. Fabbri[78a], R. Farinelli[78a], D. Fasanella[78a], P. Giacomelli[78a], C. Grandi[78a], L. Guiducci[78a,78b], S. Lo Meo[78a,aw], M. Lorusso[78a,78b], L. Lunerti[78a], S. Marcellini[78a], F.L. Navarria[78a,78b], G. Paggi[78a,78b], A. Perrotta[78a], F. Primavera[78a,78b], A.M. Rossi[78a,78b], S. Rossi Tisbeni[78a,78b], T. Rovelli[78a,78b], G.P. Siroli[78a,78b], S. Costa[79a,79b,ax], A. Di Mattia[79a], A. Lapertosa[79a], R. Potenza[79a,79b], A. Tricomi[79a,79b,ax], J. Altork[80a,80b], P. Assiouras[80a], G. Barbagli[80a], G. Bardelli[80a], M. Bartolini[80a,80b], A. Calandri[80a,80b], B. Camaiani[80a,80b], A. Cassese[80a], R. Ceccarelli[80a], V. Ciulli[80a,80b], C. Civinini[80a], R. D'Alessandro[80a,80b], L. Damenti[80a,80b], E. Focardi[80a,80b], T. Kello[80a], G. Latino[80a,80b], P. Lenzi[80a,80b], M. Lizzo[80a], M. Meschini[80a], S. Paoletti[80a], A. Papanastassiou[80a,80b], G. Sguazzoni[80a], L. Viliani[80a], L. Benussi[81], S. Bianco[81], S. Meola[81,ay], D. Piccolo[81], M. Alves Gallo Pereira[82a], F. Ferro[82a], E. Robutti[82a], S. Tosi[82a,82b], A. Benaglia[83a], F. Brivio[83a], V. Camagni[83a,83b], F. Cetorelli[83a,83b], F. De Guio[83a,83b], M.E. Dinardo[83a,83b], P. Dini[83a], S. Gennai[83a], R. Gerosa[83a,83b], A. Ghezzi[83a,83b], P. Govoni[83a,83b], L. Guzzi[83a], M.R. Kim[83a], G. Lavizzari[83a,83b], M.T. Lucchini[83a,83b], M. Malberti[83a], S. Malvezzi[83a], A. Massironi[83a], D. Menasce[83a], L. Moroni[83a], M. Paganoni[83a,83b], S. Palluotto[83a,83b], D. Pedrini[83a], A. Perego[83a,83b], G. Pizzati[83a,83b], T. Tabarelli de Fatis[83a,83b], S. Buontempo[84a], C. Di Fraia[84a,84b], F. Fabozzi[84a,84c], L. Favilla[84a,84d], A.O.M. Iorio[84a,84b], L. Lista[84a,84b,az], P. Paolucci[84a,ac], B. Rossi[84a], P. Azzi[85a], N. Bacchetta[85a,ba], A. Bergnoli[85a], D. Bisello[85a,85b], P. Bortignon[85a,85c], G. Bortolato[85a,85b], A.C.M. Bulla[85a,85c], R. Carlin[85a,85b], P. Checchia[85a], T. Dorigo[85a,bb], U. Gasparini[85a,85b], S. Giorgetti[85a], E. Lusiani[85a], M. Margoni[85a,85b], A.T. Meneguzzo[85a,85b], J. Pazzini[85a,85b], P. Ronchese[85a,85b], R. Rossin[85a,85b], F. Simonetto[85a,85b], M. Tosi[85a,85b], A. Triossi[85a,85b], M. Zanetti[85a,85b], P. Zotto[85a,85b], A. Zucchetta[85a,85b], G. Zumerle[85a,85b], A. Braghieri[86a], S. Calzaferri[86a], P. Montagna[86a,86b], M. Pelliccioni[86a], V. Re[86a], C. Riccardi[86a,86b], P. Salvini[86a], I. Vai[86a,86b], P. Vitulo[86a,86b], S. Ajmal[87a,87b], M.E. Ascioti[87a,87b], G.M. Bilei[87a], C. Carrivale[87a,87b], D. Ciangottini[87a,87b], L. Della Penna[87a,87b], L. Fanò[87a,87b,†], V. Mariani[87a,87b], M. Menichelli[87a], F. Moscatelli[87a,bc], A. Rossi[87a,87b], A. Santocchia[87a,87b], D. Spiga[87a], T. Tedeschi[87a,87b], C. Aimè[88a,88b], C.A. Alexe[88a,88c], P. Asenov[88a,88b], P. Azzurri[88a], G. Bagliesi[88a], L. Bianchini[88a,88b], T. Boccali[88a],

JHEP04(2026)086

E. Bossini[88a], D. Bruschini[88a,88c], L. Calligaris[88a,88b], R. Castaldi[88a], F. Cattafesta[88a,88c], M.A. Ciocci[88a,88d], M. Cipriani[88a,88b], R. Dell'Orso[88a], S. Donato[88a,88b], R. Forti[88a,88b], A. Giassi[88a], F. Ligabue[88a,88c], A.C. Marini[88a,88b], D. Matos Figueiredo[88a], A. Messineo[88a,88b], S. Mishra[88a], V.K. Muraleedharan Nair Bindhu[88a,88b], S. Nandan[88a], F. Palla[88a], M. Riggirello[88a,88c], A. Rizzi[88a,88b], G. Rolandi[88a,88c], S. Roy Chowdhury[88a,bd], T. Sarkar[88a], A. Scribano[88a], P. Solanki[88a,88b], P. Spagnolo[88a], F. Tenchini[88a,88b], R. Tenchini[88a], G. Tonelli[88a,88b], N. Turini[88a,88d], F. Vaselli[88a,88c], A. Venturi[88a], P.G. Verdini[88a], P. Akrap[89a,89b], C. Basile[89a,89b], S.C. Behera[89a], F. Cavallari[89a], L. Cunqueiro Mendez[89a,89b], F. De Riggi[89a,89b], D. Del Re[89a,89b], E. Di Marco[89a], M. Diemoz[89a], F. Errico[89a], L. Frosina[89a,89b], R. Gargiulo[89a,89b], B. Harikrishnan[89a,89b], F. Lombardi[89a,89b], E. Longo[89a,89b], L. Martikainen[89a,89b], J. Mijuskovic[89a,89b], G. Organtini[89a,89b], N. Palmeri[89a,89b], R. Paramatti[89a,89b], S. Rahatlou[89a,89b], C. Rovelli[89a], F. Santanastasio[89a,89b], L. Soffi[89a], V. Vladimirov[89a,89b], N. Amapane[90a,90b], R. Arcidiacono[90a,90c], S. Argiro[90a,90b], M. Arneodo[90a,90c], N. Bartosik[90a,90c], R. Bellan[90a,90b], A. Bellora[90a,90b], C. Biino[90a], C. Borca[90a,90b], N. Cartiglia[90a], F. Cossio[90a], M. Costa[90a,90b], R. Covarelli[90a,90b], G. Dellacasa[90a], N. Demaria[90a], L. Finco[90a], M. Grippo[90a,90b], B. Kiani[90a,90b], L. Lanteri[90a,90b], F. Legger[90a], F. Luongo[90a,90b], C. Mariotti[90a], S. Maselli[90a], A. Mecca[90a,90b], L. Menzio[90a,90b], P. Meridiani[90a], E. Migliore[90a,90b], M. Monteno[90a], M.M. Obertino[90a,90b], G. Ortona[90a], L. Pacher[90a,90b], N. Pastrone[90a], M. Ruspa[90a,90c], F. Siviero[90a,90b], V. Sola[90a,90b], A. Solano[90a,90b], C. Tarricone[90a,90b], D. Trocino[90a], G. Umoret[90a,90b], R. White[90a,90b], J. Babbar[91a,91b], S. Belforte[91a], V. Candelise[91a,91b], M. Casarsa[91a], F. Cossutti[91a], K. De Leo[91a], G. Della Ricca[91a,91b], R. Delli Gatti[91a,91b], S. Dogra[92], J. Hong[92], J. Kim[92], T. Kim[92], D. Lee[92], H. Lee[92], J. Lee[92], S.W. Lee[92], C.S. Moon[92], Y.D. Oh[92], S. Sekmen[92], B. Tae[92], Y.C. Yang[92], M.S. Kim[93], G. Bak[94], P. Gwak[94], H. Kim[94], D.H. Moon[94], J. Seo[94], E. Asilar[95], F. Carnevali[95], J. Choi[95,be], T.J. Kim[95], Y. Ryou[95], S. Ha[96], S. Han[96], B. Hong[96], J. Kim[96], K. Lee[96], K.S. Lee[96], S. Lee[96], J. Yoo[96], J. Goh[97], J. Shin[97], S. Yang[97], Y. Kang[98], H. S. Kim[98], Y. Kim[98], S. Lee[98], J. Almond[99], J.H. Bhyun[99], J. Choi[99], J. Choi[99], W. Jun[99], H. Kim[99], J. Kim[99], T. Kim[99], Y. Kim[99], Y.W. Kim[99], S. Ko[99], H. Lee[99], J. Lee[99], J. Lee[99], B.H. Oh[99], S.B. Oh[99], J. Shin[99], U.K. Yang[99], I. Yoon[99], W. Jang[100], D.Y. Kang[100], D. Kim[100], S. Kim[100], B. Ko[100], J.S.H. Lee[100], Y. Lee[100], I.C. Park[100], Y. Roh[100], I.J. Watson[100], G. Cho[101], K. Hwang[101], B. Kim[101], S. Kim[101], K. Lee[101], H.D. Yoo[101], Y. Lee[102], I. Yu[102], T. Beyrouthy[103], Y. Gharbia[103], F. Alazemi[104], K. Dreimanis[105], O.M. Eberlins[105], A. Gaile[105], C. Munoz Diaz[105], D. Osite[105], G. Pikurs[105], R. Plese[105], A. Potrebko[105], M. Seidel[105], D. Sidiropoulos Kontos[105], N.R. Strautnieks[106], M. Ambrozas[107], A. Juodagalvis[107], S. Nargelas[107], A. Rinkevicius[107], G. Tamulaitis[107], I. Yusuff[108,bf], Z. Zolkapli[108], J.F. Benitez[109], A. Castaneda Hernandez[109], A. Cota Rodriguez[109], L.E. Cuevas Picos[109], H.A. Encinas Acosta[109], L.G. Gallegos Maríñez[109], J.A. Murillo Quijada[109], L. Valencia Palomo[109], G. Ayala[110], H. Castilla-Valdez[110], H. Crotte Ledesma[110], R. Lopez-Fernandez[110], J. Mejia Guisao[110], R. Reyes-Almanza[110], A. Sánchez Hernández[110], C. Oropeza Barrera[111], D.L. Ramirez Guadarrama[111], M. Ramírez García[111], I. Bautista[112], F.E. Neri Huerta[112], I. Pedraza[112], H.A. Salazar Ibarguen[112], C. Uribe Estrada[112],

JHEP04(2026)086

I. Bubanja[113], N. Raicevic[113], P.H. Butler[114], A. Ahmad[115], M.I. Asghar[115], A. Awais[115], M.I.M. Awan[115], W.A. Khan[115], V. Avati[116], L. Forthomme[116], L. Grzanka[116], M. Malawski[116], K. Piotrzkowski[116], M. Bluj[117], M. Górski[117], M. Kazana[117], M. Szleper[117], P. Zalewski[117], K. Bunkowski[118], K. Doroba[118], A. Kalinowski[118], M. Konecki[118], J. Krolikowski[118], A. Muhammad[118], P. Fokow[119], K. Pozniak[119], W. Zabolotny[119], M. Araujo[120], D. Bastos[120], C. Beirão Da Cruz E Silva[120], A. Boletti[120], M. Bozzo[120], T. Camporesi[120], G. Da Molin[120], M. Gallinaro[120], J. Hollar[120], N. Leonardo[120], G.B. Marozzo[120], A. Petrilli[120], M. Pisano[120], J. Seixas[120], J. Varela[120], J.W. Wulff[120], P. Adzic[121], L. Markovic[121], P. Milenovic[121], V. Milosevic[121], D. Devetak[122], M. Dordevic[122], J. Milosevic[122], L. Nadderd[122], V. Rekovic[122], M. Stojanovic[122], M. Alcalde Martinez[123], J. Alcaraz Maestre[123], J.A. Brochero Cifuentes[123], M. Cepeda[123], M. Cerrada[123], N. Colino[123], B. De La Cruz[123], A. Delgado Peris[123], A. Escalante Del Valle[123], Cristina F. Bedoya[123], D. Fernández Del Val[123], J.P. Fernández Ramos[123], J. Flix[123], M.C. Fouz[123], M. Gonzalez Hernandez[123], O. Gonzalez Lopez[123], S. Goy Lopez[123], J.M. Hernandez[123], M.I. Josa[123], J. Llorente Merino[123], Oliver M. Carretero[123], C. Martin Perez[123], E. Martin Viscasillas[123], D. Moran[123], C. M. Morcillo Perez[123], Á. Navarro Tobar[123], R. Paz Herrera[123], C. Perez Dengra[123], J. Puerta Pelayo[123], A. Pérez-Calero Yzquierdo[123], I. Redondo[123], J. Vazquez Escobar[123], J.F. de Trocóniz[124], B. Alvarez Gonzalez[125], J. Ayllon Torresano[125], A. Cardini[125], J. Cuevas[125], J. Del Riego Badas[125], D. Estrada Acevedo[125], J. Fernandez Menendez[125], S. Folgueras[125], I. Gonzalez Caballero[125], P. Leguina[125], M. Obeso Menendez[125], E. Palencia Cortezon[125], J. Prado Pico[125], A. Soto Rodríguez[125], C. Vico Villalba[125], P. Vischia[125], S. Blanco Fernández[126], I.J. Cabrillo[126], A. Calderon[126], J. Duarte Campderros[126], M. Fernandez[126], G. Gomez[126], C. Lasaosa García[126], R. Lopez Ruiz[126], C. Martinez Rivero[126], P. Martinez Ruiz del Arbol[126], F. Matorras[126], P. Matorras Cuevas[126], E. Navarrete Ramos[126], J. Piedra Gomez[126], C. Quintana San Emeterio[126], L. Scodellaro[126], I. Vila[126], R. Vilar Cortabitarte[126], J.M. Vizan Garcia[126], D.D.C. Wickramarathna[127], B. Kailasapathy[127,bg], W.G.D. Dharmaratna[128,bh], K. Liyanage[128], N. Perera[128], D. Abbaneo[129], C. Amendola[129], R. Ardino[129], E. Auffray[129], J. Baechler[129], D. Barney[129], J. Bendavid[129], M. Bianco[129], A. Bocci[129], L. Borgonovi[129], C. Botta[129], A. Bragagnolo[129], C.E. Brown[129], C. Caillol[129], G. Cerminara[129], P. Connor[129], D. d'Enterria[129], A. Dabrowski[129], A. David[129], A. De Roeck[129], M.M. Defranchis[129], M. Deile[129], M. Dobson[129], P.J. Fernández Manteca[129], B.A. Fontana Santos Alves[129], E. Fontanesi[129], W. Funk[129], A. Gaddi[129], S. Giani[129], D. Gigi[129], K. Gill[129], F. Glege[129], M. Glowacki[129], A. Gruber[129], J. Hegeman[129], J.K. Heikkilä[129], R. Hofsaess[129], B. Huber[129], T. James[129], P. Janot[129], O. Kaluzinska[129], O. Karacheban[129,z], G. Karathanasis[129], S. Laurila[129], P. Lecoq[129], E. Leutgeb[129], C. Lourenço[129], A.-M. Lyon[129], M. Magherini[129], L. Malgeri[129], M. Mannelli[129], A. Mehta[129], F. Meijers[129], J.A. Merlin[129], S. Mersi[129], E. Meschi[129], M. Migliorini[129], F. Monti[129], F. Moortgat[129], M. Mulders[129], M. Musich[129], I. Neutelings[129], S. Orfanelli[129], F. Pantaleo[129], M. Pari[129], G. Petrucciani[129], A. Pfeiffer[129], M. Pierini[129], M. Pitt[129], H. Qu[129], D. Rabady[129], A. Reimers[129], B. Ribeiro Lopes[129], F. Riti[129], P. Rosado[129], M. Rovere[129], H. Sakulin[129],

JHEP04(2026)086

R. Salvatico[129], S. Sanchez Cruz[129], S. Scarfi[129], M. Selvaggi[129], A. Sharma[129], K. Shchelina[129], P. Silva[129], P. Sphicas[129,bi], A.G. Stahl Leiton[129], A. Steen[129], S. Summers[129], D. Treille[129], P. Tropea[129], E. Vernazza[129], J. Wanczyk[129,bj], S. Wuchterl[129], M. Zarucki[129], P. Zehetner[129], P. Zejdl[129], G. Zevi Della Porta[129], T. Bevilacqua[130,bk], L. Caminada[130,bk], W. Erdmann[130], R. Horisberger[130], Q. Ingram[130], H.C. Kaestli[130], D. Kotlinski[130], C. Lange[130], U. Langenegger[130], L. Noehte[130,bk], T. Rohe[130], A. Samalan[130], T.K. Aarrestad[131], M. Backhaus[131], G. Bonomelli[131], C. Cazzaniga[131], K. Datta[131], P. De Bryas Dexmiers D'Archiacchiac[131,bj], A. De Cosa[131], G. Dissertori[131], M. Dittmar[131], M. Donegà[131], F. Eble[131], K. Gedia[131], F. Glessgen[131], C. Grab[131], T.G. Harte[131], N. Härringer[131], W. Lustermann[131], M. Malucchi[131], R.A. Manzoni[131], L. Marchese[131], A. Mascellani[131,bj], F. Nessi-Tedaldi[131], F. Pauss[131], V. Perovic[131], B. Ristic[131], R. Seidita[131], J. Steggemann[131,bj], A. Tarabini[131], D. Valsecchi[131], R. Wallny[131], C. Amsler[132,bl], F. Bilandzija[132], P. Bärtschi[132], M.F. Canelli[132], G. Celotto[132], K. Cormier[132], M. Huwiler[132], W. Jin[132], A. Jofrehei[132], B. Kilminster[132], T.H. Kwok[132], S. Leontsinis[132], V. Lukashenko[132], A. Macchiolo[132], F. Meng[132], M. Missiroli[132], J. Motta[132], P. Robmann[132], M. Senger[132], E. Shokr[132], F. Stäger[132], R. Tramontano[132], P. Viscone[132], D. Bhowmik[133], C.M. Kuo[133], P.K. Rout[133], S. Taj[133], P.C. Tiwari[133,am], L. Ceard[134], K.F. Chen[134], Z.g. Chen[134], A. De Iorio[134], W.-S. Hou[134], T.h. Hsu[134], Y.w. Kao[134], S. Karmakar[134], G. Kole[134], Y.y. Li[134], R.-S. Lu[134], E. Paganis[134], X.f. Su[134], J. Thomas-Wilsker[134], L.s. Tsai[134], D. Tsionou[134], H.y. Wu[134], E. Yazgan[134], C. Asawatangtrakuldee[135], N. Srimanobhas[135], Y. Maghrbi[136], D. Agyel[137], F. Dolek[137], I. Dumanoglu[137,bm], Y. Guler[137,bn], E. Gurpinar Guler[137,bn], C. Isik[137], O. Kara[137], A. Kayis Topaksu[137], Y. Komurcu[137], G. Onengut[137], K. Ozdemir[137,bo], B. Tali[137,bp], U.G. Tok[137], E. Uslan[137], I.S. Zorbakir[137], S. Sen[138], M. Yalvac[139,bq], B. Akgun[140], I.O. Atakisi[140,br], E. Gülmez[140], M. Kaya[140,bs], O. Kaya[140,bt], M.A. Sarkisla[140,bu], S. Tekten[140,bv], D. Boncukcu[141], A. Cakir[141], K. Cankocak[141,bm,bw], B. Hacisahinoglu[142], I. Hos[142,bx], B. Kaynak[142], S. Ozkorucuklu[142], O. Potok[142], H. Sert[142], C. Simsek[142], C. Zorbilmez[142], S. Cerci[143], C. Dozen[143,by], B. Isildak[143,bz], E. Simsek[143], D. Sunar Cerci[143], T. Yetkin[143,by], A. Boyaryntsev[144], O. Dadazhanova[144], B. Grynyov[144], L. Levchuk[145], J.J. Brooke[146], A. Bundock[146], F. Bury[146], E. Clement[146], D. Cussans[146], D. Dharmender[146], H. Flacher[146], J. Goldstein[146], H.F. Heath[146], M.-L. Holmberg[146], L. Kreczko[146], S. Paramesvaran[146], L. Robertshaw[146], M.S. Sanjrani[146,aq], J. Segal[146], V.J. Smith[146], A.H. Ball[147], K.W. Bell[147], A. Belyaev[147,ca], C. Brew[147], R.M. Brown[147], D.J.A. Cockerill[147], A. Elliot[147], K.V. Ellis[147], J. Gajownik[147], K. Harder[147], S. Harper[147], J. Linacre[147], K. Manolopoulos[147], M. Moallemi[147], D.M. Newbold[147], E. Olaiya[147], D. Petyt[147], T. Reis[147], A.R. Sahasransu[147], G. Salvi[147], T. Schuh[147], C.H. Shepherd-Themistocleous[147], I.R. Tomalin[147], K.C. Whalen[147], T. Williams[147], I. Andreou[148], R. Bainbridge[148], P. Bloch[148], O. Buchmuller[148], C.A. Carrillo Montoya[148], D. Colling[148], I. Das[148], P. Dauncey[148], G. Davies[148], M. Della Negra[148], S. Fayer[148], G. Fedi[148], G. Hall[148], H.R. Hoorani[148], A. Howard[148], G. Iles[148], C.R. Knight[148], P. Krueper[148], J. Langford[148], K.H. Law[148], J. León Holgado[148], L. Lyons[148], A.-M. Magnan[148], B. Maier[148], S. Mallios[148], A. Mastronikolis[148], M. Mieskolainen[148], J. Nash[148,cb], M. Pesaresi[148],

JHEP04(2026)086

P.B. Pradeep[148], B.C. Radburn-Smith[148], A. Richards[148], A. Rose[148], L. Russell[148], K. Savva[148], C. Seez[148], R. Shukla[148], A. Tapper[148], K. Uchida[148], G.P. Uttley[148], T. Virdee[148,ac], M. Vojinovic[148], N. Wardle[148], D. Winterbottom[148], J.E. Cole[149], A. Khan[149], P. Kyberd[149], I.D. Reid[149], S. Abdullin[150], A. Brinkerhoff[150], E. Collins[150], M.R. Darwish[150], J. Dittmann[150], K. Hatakeyama[150], V. Hegde[150], J. Hiltbrand[150], B. McMaster[150], J. Samudio[150], S. Sawant[150], C. Sutantawibul[150], J. Wilson[150], J.M. Hogan[151], R. Bartek[152], A. Dominguez[152], S. Raj[152], A.E. Simsek[152], S.S. Yu[152], B. Bam[153], A. Buchot Perraguin[153], S. Campbell[153], R. Chudasama[153], S.I. Cooper[153], C. Crovella[153], G. Fidalgo[153], S.V. Gleyzer[153], A. Khukhunaishvili[153], K. Matchev[153], E. Pearson[153], C.U. Perez[153], P. Rumerio[153,cc], E. Usai[153], R. Yi[153], S. Cholak[154], G. De Castro[154], Z. Demiragli[154], C. Erice[154], C. Fangmeier[154], C. Fernandez Madrazo[154], J. Fulcher[154], F. Golf[154], S. Jeon[154], J. O'Cain[154], I. Reed[154], J. Rohlf[154], K. Salyer[154], D. Sperka[154], D. Spitzbart[154], I. Suarez[154], A. Tsatsos[154], E. Wurtz[154], A.G. Zecchinelli[154], G. Barone[155], G. Benelli[155], D. Cutts[155], S. Ellis[155], L. Gouskos[155], M. Hadley[155], U. Heintz[155], K.W. Ho[155], T. Kwon[155], L. Lambrecht[155], G. Landsberg[155], K.T. Lau[155], J. Luo[155], S. Mondal[155], J. Roloff[155], T. Russell[155], S. Sagir[155,cd], X. Shen[155], M. Stamenkovic[155], N. Venkatasubramanian[155], S. Abbott[156], S. Baradia[156], B. Barton[156], R. Breedon[156], H. Cai[156], M. Calderon De La Barca Sanchez[156], E. Cannaert[156], M. Chertok[156], M. Citron[156], J. Conway[156], P.T. Cox[156], R. Erbacher[156], O. Kukral[156], G. Mocellin[156], S. Ostrom[156], I. Salazar Segovia[156], J.S. Tafoya Vargas[156], W. Wei[156], S. Yoo[156], K. Adamidis[157], M. Bachtis[157], D. Campos[157], R. Cousins[157], A. Datta[157], G. Flores Avila[157], J. Hauser[157], M. Ignatenko[157], M.A. Iqbal[157], T. Lam[157], Y.f. Lo[157], E. Manca[157], A. Nunez Del Prado[157], D. Saltzberg[157], V. Valuev[157], R. Clare[158], J.W. Gary[158], G. Hanson[158], A. Aportela[159], A. Arora[159], J.G. Branson[159], S. Cittolin[159], S. Cooperstein[159], B. D'Anzi[159], D. Diaz[159], J. Duarte[159], L. Giannini[159], Y. Gu[159], J. Guiang[159], V. Krutelyov[159], R. Lee[159], J. Letts[159], H. Li[159], M. Masciovecchio[159], F. Mokhtar[159], S. Mukherjee[159], M. Pieri[159], D. Primosch[159], M. Quinnan[159], V. Sharma[159], M. Tadel[159], E. Vourliotis[159], F. Würthwein[159], A. Yagil[159], Z. Zhao[159], A. Barzdukas[160], L. Brennan[160], C. Campagnari[160], S. Carron Montero[160,ce], K. Downham[160], C. Grieco[160], M.M. Hussain[160], J. Incandela[160], M.W.K. Lai[160], A.J. Li[160], P. Masterson[160], J. Richman[160], S.N. Santpur[160], U. Sarica[160], R. Schmitz[160], F. Setti[160], J. Sheplock[160], D. Stuart[160], T.Á. Vámi[160], X. Yan[160], D. Zhang[160], A. Albert[161], S. Bhattacharya[161], A. Bornheim[161], O. Cerri[161], R. Kansal[161], J. Mao[161], H.B. Newman[161], G. Reales Gutiérrez[161], T. Sievert[161], M. Spiropulu[161], J.R. Vlimant[161], R.A. Wynne[161], S. Xie[161], J. Alison[162], S. An[162], M. Cremonesi[162], V. Dutta[162], E.Y. Ertorer[162], T. Ferguson[162], T.A. Gómez Espinosa[162], A. Harilal[162], A. Kallil Tharayil[162], M. Kanemura[162], C. Liu[162], M. Marchegiani[162], P. Meiring[162], T. Mudholkar[162], S. Murthy[162], P. Palit[162], K. Park[162], M. Paulini[162], A. Roberts[162], A. Sanchez[162], W. Terrill[162], J.P. Cumalat[163], W.T. Ford[163], A. Hart[163], S. Kwan[163], J. Pearkes[163], C. Savard[163], N. Schonbeck[163], K. Stenson[163], K.A. Ulmer[163], S.R. Wagner[163], N. Zipper[163], D. Zuolo[163], J. Alexander[164], X. Chen[164], J. Dickinson[164], A. Duquette[164], J. Fan[164], X. Fan[164], J. Grassi[164], S. Hogan[164], P. Kotamnives[164], J. Monroy[164], G. Niendorf[164], M. Oshiro[164], J.R. Patterson[164], A. Ryd[164], J. Thom[164],

JHEP04(2026)086

P. Wittich[164], R. Zou[164], L. Zygala[164], M. Albrow[165], M. Alyari[165], O. Amram[165], G. Apollinari[165], A. Apresyan[165], L.A.T. Bauerdick[165], D. Berry[165], J. Berryhill[165], P.C. Bhat[165], K. Burkett[165], J.N. Butler[165], A. Canepa[165], G.B. Cerati[165], H.W.K. Cheung[165], F. Chlebana[165], C. Cosby[165], G. Cummings[165], I. Dutta[165], V.D. Elvira[165], J. Freeman[165], A. Gandrakota[165], Z. Gecse[165], L. Gray[165], D. Green[165], A. Grummer[165], S. Grünendahl[165], D. Guerrero[165], O. Gutsche[165], R.M. Harris[165], T.C. Herwig[165], J. Hirschauer[165], V. Innocente[165], B. Jayatilaka[165], S. Jindariani[165], M. Johnson[165], U. Joshi[165], B. Klima[165], K.H.M. Kwok[165], S. Lammel[165], C. Lee[165], D. Lincoln[165], R. Lipton[165], T. Liu[165], K. Maeshima[165], D. Mason[165], P. McBride[165], P. Merkel[165], S. Mrenna[165], S. Nahn[165], J. Ngadiuba[165], D. Noonan[165], S. Norberg[165], V. Papadimitriou[165], N. Pastika[165], K. Pedro[165], C. Pena[165,cf], C.E. Perez Lara[165], F. Ravera[165], A. Reinsvold Hall[165,cg], L. Ristori[165], M. Safdari[165], E. Sexton-Kennedy[165], N. Smith[165], A. Soha[165], L. Spiegel[165], S. Stoynev[165], J. Strait[165], L. Taylor[165], S. Tkaczyk[165], N.V. Tran[165], L. Uplegger[165], E.W. Vaandering[165], C. Wang[165], I. Zoi[165], C. Aruta[166], P. Avery[166], D. Bourilkov[166], P. Chang[166], V. Cherepanov[166], R.D. Field[166], C. Huh[166], E. Koenig[166], M. Kolosova[166], J. Konigsberg[166], A. Korytov[166], G. Mitselmakher[166], K. Mohrman[166], A. Muthirakalayil Madhu[166], N. Rawal[166], S. Rosenzweig[166], V. Sulimov[166], Y. Takahashi[166], J. Wang[166], T. Adams[167], A. Al Kadhim[167], A. Askew[167], S. Bower[167], R. Goff[167], R. Hashmi[167], A. Hassani[167], R.S. Kim[167], T. Kolberg[167], G. Martinez[167], M. Mazza[167], H. Prosper[167], P.R. Prova[167], R. Yohay[167], B. Alsufyani[168], S. Butalla[168], S. Das[168], M. Hohlmann[168], M. Lavinsky[168], E. Yanes[168], M.R. Adams[169], N. Barnett[169], A. Baty[169], C. Bennett[169], R. Cavanaugh[169], R. Escobar Franco[169], O. Evdokimov[169], C.E. Gerber[169], H. Gupta[169], M. Hawksworth[169], A. Hingrajiya[169], D.J. Hofman[169], Z. Huang[169], J.h. Lee[169], C. Mills[169], S. Nanda[169], G. Nigmatkulov[169], B. Ozek[169], T. Phan[169], D. Pilipovic[169], R. Pradhan[169], E. Prifti[169], P. Roy[169], T. Roy[169], N. Singh[169], M.B. Tonjes[169], N. Varelas[169], M.A. Wadud[169], J. Yoo[169], M. Alhusseini[170], D. Blend[170], K. Dilsiz[170,ch], O.K. Köseyan[170], A. Mestvirishvili[170,ci], O. Neogi[170], H. Ogul[170,cj], Y. Onel[170], A. Penzo[170], C. Snyder[170], E. Tiras[170,ck], B. Blumenfeld[171], J. Davis[171], A.V. Gritsan[171], L. Kang[171], S. Kyriacou[171], P. Maksimovic[171], M. Roguljic[171], S. Sekhar[171], M.V. Srivastav[171], M. Swartz[171], A. Abreu[172], L.F. Alcerro Alcerro[172], J. Anguiano[172], S. Arteaga Escatel[172], P. Baringer[172], A. Bean[172], R. Bhattacharya[172], Z. Flowers[172], D. Grove[172], J. King[172], G. Krintiras[172], M. Lazarovits[172], C. Le Mahieu[172], J. Marquez[172], M. Murray[172], M. Nickel[172], S. Popescu[172,cl], C. Rogan[172], C. Royon[172], S. Rudrabhatla[172], S. Sanders[172], C. Smith[172], G. Wilson[172], B. Allmond[173], N. Islam[173], A. Ivanov[173], K. Kaadze[173], Y. Maravin[173], J. Natoli[173], G.G. Reddy[173], D. Roy[173], G. Sorrentino[173], A. Baden[174], A. Belloni[174], J. Bistany-riebman[174], S.C. Eno[174], N.J. Hadley[174], S. Jabeen[174], R.G. Kellogg[174], T. Koeth[174], B. Kronheim[174], S. Lascio[174], P. Major[174], A.C. Mignerey[174], C. Palmer[174], C. Papageorgakis[174], M.M. Paranjpe[174], E. Popova[174,cm], A. Shevelev[174], L. Zhang[174], C. Baldenegro Barrera[175], H. Bossi[175], S. Bright-Thonney[175], I.A. Cali[175], Y.c. Chen[175], P.c. Chou[175], M. D'Alfonso[175], J. Eysermans[175], C. Freer[175], G. Gomez-Ceballos[175], M. Goncharov[175], G. Grosso[175], P. Harris[175], D. Hoang[175], G.M. Innocenti[175], K. Ivanov[175], D. Kovalskyi[175], J. Krupa[175], L. Lavezzo[175],

JHEP04(2026)086

Y.-J. Lee[175], K. Long[175], C. Mcginn[175], A. Novak[175], M.I. Park[175], C. Paus[175], C. Reissel[175], C. Roland[175], G. Roland[175], S. Rothman[175], T.a. Sheng[175], G.S.F. Stephans[175], D. Walter[175], J. Wang[175], Z. Wang[175], B. Wyslouch[175], T. J. Yang[175], B. Crossman[176], W.J. Jackson[176], C. Kapsiak[176], M. Krohn[176], D. Mahon[176], J. Mans[176], B. Marzocchi[176], R. Rusack[176], O. Sancar[176], R. Saradhy[176], N. Strobbe[176], K. Bloom[177], D.R. Claes[177], G. Haza[177], J. Hossain[177], C. Joo[177], I. Kravchenko[177], A. Rohilla[177], J.E. Siado[177], W. Tabb[177], A. Vagnerini[177], A. Wightman[177], F. Yan[177], H. Bandyopadhyay[178], L. Hay[178], H.w. Hsia[178], I. Iashvili[178], A. Kalogeropoulos[178], A. Kharchilava[178], A. Mandal[178], M. Morris[178], D. Nguyen[178], S. Rappoccio[178], H. Rejeb Sfar[178], A. Williams[178], P. Young[178], D. Yu[178], G. Alverson[179], E. Barberis[179], J. Bonilla[179], B. Bylsma[179], M. Campana[179], J. Dervan[179], Y. Haddad[179], Y. Han[179], I. Israr[179], A. Krishna[179], M. Lu[179], N. Manganelli[179], R. Mccarthy[179], D.M. Morse[179], T. Orimoto[179], L. Skinnari[179], C.S. Thoreson[179], E. Tsai[179], D. Wood[179], S. Dittmer[180], K.A. Hahn[180], M. Mcginnis[180], Y. Miao[180], D.G. Monk[180], M.H. Schmitt[180], A. Taliercio[180], M. Velasco[180], J. Wang[180], G. Agarwal[181], R. Band[181], R. Bucci[181], S. Castells[181], A. Das[181], A. Ehnis[181], R. Goldouzian[181], M. Hildreth[181], K. Hurtado Anampa[181], T. Ivanov[181], C. Jessop[181], A. Karneyeu[181], K. Lannon[181], J. Lawrence[181], N. Loukas[181], L. Lutton[181], J. Mariano[181], N. Marinelli[181], I. Mcalister[181], T. McCauley[181], C. Mcgrady[181], C. Moore[181], Y. Musienko[181,cn], H. Nelson[181], M. Osherson[181], A. Piccinelli[181], R. Ruchti[181], A. Townsend[181], Y. Wan[181], M. Wayne[181], H. Yockey[181], A. Basnet[182], M. Carrigan[182], R. De Los Santos[182], L.S. Durkin[182], C. Hill[182], M. Joyce[182], M. Nunez Ornelas[182], D.A. Wenzl[182], B.L. Winer[182], B. R. Yates[182], H. Bouchamaoui[183], G. Dezoort[183], P. Elmer[183], A. Frankenthal[183], M. Galli[183], B. Greenberg[183], N. Haubrich[183], K. Kennedy[183], G. Kopp[183], Y. Lai[183], D. Lange[183], A. Loeliger[183], D. Marlow[183], I. Ojalvo[183], J. Olsen[183], F. Simpson[183], D. Stickland[183], C. Tully[183], S. Malik[184], R. Sharma[184], S. Chandra[185], R. Chawla[185], A. Gu[185], L. Gutay[185], M. Jones[185], A.W. Jung[185], D. Kondratyev[185], M. Liu[185], G. Negro[185], N. Neumeister[185], G. Paspalaki[185], S. Piperov[185], N.R. Saha[185], J.F. Schulte[185], F. Wang[185], A. Wildridge[185], W. Xie[185], Y. Yao[185], Y. Zhong[185], N. Parashar[186], A. Pathak[186], E. Shumka[186], D. Acosta[187], A. Agrawal[187], C. Arbour[187], T. Carnahan[187], P. Das[187], K.M. Ecklund[187], S. Freed[187], F.J.M. Geurts[187], T. Huang[187], I. Krommydas[187], N. Lewis[187], W. Li[187], J. Lin[187], O. Miguel Colin[187], B.P. Padley[187], R. Redjimi[187], J. Rotter[187], M. Wulansatiti[187], E. Yigitbasi[187], Y. Zhang[187], O. Bessidskaia Bylund[188], A. Bodek[188], P. de Barbaro[188,†], R. Demina[188], A. Garcia-Bellido[188], H.S. Hare[188], O. Hindrichs[188], N. Parmar[188], P. Parygin[188,cm], H. Seo[188], R. Taus[188], B. Chiarito[189], J.P. Chou[189], S.V. Clark[189], S. Donnelly[189], D. Gadkari[189], Y. Gershtein[189], E. Halkiadakis[189], C. Houghton[189], D. Jaroslawski[189], A. Kobert[189], S. Konstantinou[189], I. Laflotte[189], A. Lath[189], J. Martins[189], M. Perez Prada[189], B. Rand[189], J. Reichert[189], P. Saha[189], S. Salur[189], S. Schnetzer[189], S. Somalwar[189], R. Stone[189], S.A. Thayil[189], S. Thomas[189], J. Vora[189], D. Ally[190], A.G. Delannoy[190], S. Fiorendi[190], J. Harris[190], T. Holmes[190], A.R. Kanuganti[190], N. Karunarathna[190], J. Lawless[190], L. Lee[190], E. Nibigira[190], B. Skipworth[190], S. Spanier[190], D. Aebi[191], M. Ahmad[191], T. Akhter[191], K. Androsov[191], A. Bolshov[191], O. Bouhali[191,co],

JHEP04(2026)086

A. Cagnotta[191], V. D'Amante[191], R. Eusebi[191], P. Flanagan[191], J. Gilmore[191], Y. Guo[191], T. Kamon[191], S. Luo[191], R. Mueller[191], A. Safonov[191], N. Akchurin[192], J. Damgov[192], Y. Feng[192], N. Gogate[192], Y. Kazhykarim[192], K. Lamichhane[192], S.W. Lee[192], C. Madrid[192], A. Mankel[192], T. Peltola[192], I. Volobouev[192], E. Appelt[193], Y. Chen[193], S. Greene[193], A. Gurrola[193], W. Johns[193], R. Kunnawalkam Elayavalli[193], A. Melo[193], D. Rathjens[193], F. Romeo[193], P. Sheldon[193], S. Tuo[193], J. Velkovska[193], J. Viinikainen[193], J. Zhang[193], B. Cardwell[194], H. Chung[194], B. Cox[194], J. Hakala[194], G. Hamilton Ilha Machado[194], R. Hirosky[194], M. Jose[194], A. Ledovskoy[194], C. Mantilla[194], C. Neu[194], C. Ramón Álvarez[194], Z. Wu[194], S. Bhattacharya[195], P.E. Karchin[195], A. Aravind[196], S. Banerjee[196], K. Black[196], T. Bose[196], E. Chavez[196], S. Dasu[196], P. Everaerts[196], C. Galloni[196], H. He[196], M. Herndon[196], A. Herve[196], C.K. Koraka[196], S. Lomte[196], R. Loveless[196], A. Mallampalli[196], A. Mohammadi[196], S. Mondal[196], T. Nelson[196], G. Parida[196], D. Pinna[196], L. Pétré[196], A. Savin[196], V. Shang[196], V. Sharma[196], W.H. Smith[196], D. Teague[196], H.F. Tsoi[196], W. Vetens[196], A. Warden[196], S. Afanasiev[197], V. Alexakhin[197], Yu. Andreev[197], T. Aushev[197], D. Budkouski[197], R. Chistov[197], M. Danilov[197], T. Dimova[197], A. Ershov[197], S. Gninenko[197], I. Gorbunov[197], A. Gribushin[197], A. Kamenev[197], V. Karjavine[197], M. Kirsanov[197], V. Klyukhin[197], O. Kodolova[197,cp], V. Korenkov[197], I. Korsakov[197], A. Kozyrev[197], N. Krasnikov[197], A. Lanev[197], A. Malakhov[197], V. Matveev[197], A. Nikitenko[197,cq,cr], V. Palichik[197], V. Perelygin[197], S. Petrushanko[197], S. Polikarpov[197], O. Radchenko[197], M. Savina[197], V. Shalaev[197], S. Shmatov[197], S. Shulha[197], Y. Skovpen[197], K. Slizhevskiy[197], V. Smirnov[197], O. Teryaev[197], I. Tlisova[197], A. Toropin[197], N. Voytishin[197], A. Zarubin[197], I. Zhizhin[197], E. Boos[198], V. Bunichev[198], M. Dubinin[198,cf], L. Dudko[198], V. Kim[198,cn], V. Murzin[198], V. Oreshkin[198], V. Savrin[198], A. Snigirev[198], D. Sosnov[198]

[1] *Yerevan Physics Institute, Yerevan, Armenia*
[2] *Institut für Hochenergiephysik, Vienna, Austria*
[3] *Universiteit Antwerpen, Antwerpen, Belgium*
[4] *Vrije Universiteit Brussel, Brussel, Belgium*
[5] *Université Libre de Bruxelles, Bruxelles, Belgium*
[6] *Ghent University, Ghent, Belgium*
[7] *Université Catholique de Louvain, Louvain-la-Neuve, Belgium*
[8] *Centro Brasileiro de Pesquisas Fisicas, Rio de Janeiro, Brazil*
[9] *Universidade do Estado do Rio de Janeiro, Rio de Janeiro, Brazil*
[10] *Universidade Estadual Paulista, Universidade Federal do ABC, São Paulo, Brazil*
[11] *Institute for Nuclear Research and Nuclear Energy, Bulgarian Academy of Sciences, Sofia, Bulgaria*
[12] *University of Sofia, Sofia, Bulgaria*
[13] *Instituto De Alta Investigación, Universidad de Tarapacá, Casilla 7 D, Arica, Chile*
[14] *Universidad Tecnica Federico Santa Maria, Valparaiso, Chile*
[15] *Beihang University, Beijing, China*
[16] *Department of Physics, Tsinghua University, Beijing, China*
[17] *Institute of High Energy Physics, Beijing, China*
[18] *State Key Laboratory of Nuclear Physics and Technology, Peking University, Beijing, China*
[19] *State Key Laboratory of Nuclear Physics and Technology, Institute of Quantum Matter, South China Normal University, Guangzhou, China*
[20] *Sun Yat-Sen University, Guangzhou, China*
[21] *University of Science and Technology of China, Hefei, China*

JHEP04(2026)086

[22] Nanjing Normal University, Nanjing, China
[23] Institute of Modern Physics and Key Laboratory of Nuclear Physics and Ion-beam Application (MOE) — Fudan University, Shanghai, China
[24] Zhejiang University, Hangzhou, Zhejiang, China
[25] Universidad de Los Andes, Bogota, Colombia
[26] Universidad de Antioquia, Medellin, Colombia
[27] University of Split, Faculty of Electrical Engineering, Mechanical Engineering and Naval Architecture, Split, Croatia
[28] University of Split, Faculty of Science, Split, Croatia
[29] Institute Rudjer Boskovic, Zagreb, Croatia
[30] University of Cyprus, Nicosia, Cyprus
[31] Charles University, Prague, Czech Republic
[32] Escuela Politecnica Nacional, Quito, Ecuador
[33] Universidad San Francisco de Quito, Quito, Ecuador
[34] Academy of Scientific Research and Technology of the Arab Republic of Egypt, Egyptian Network of High Energy Physics, Cairo, Egypt
[35] Center for High Energy Physics (CHEP-FU), Fayoum University, El-Fayoum, Egypt
[36] National Institute of Chemical Physics and Biophysics, Tallinn, Estonia
[37] Department of Physics, University of Helsinki, Helsinki, Finland
[38] Helsinki Institute of Physics, Helsinki, Finland
[39] Lappeenranta-Lahti University of Technology, Lappeenranta, Finland
[40] IRFU, CEA, Université Paris-Saclay, Gif-sur-Yvette, France
[41] Laboratoire Leprince-Ringuet, CNRS/IN2P3, Ecole Polytechnique, Institut Polytechnique de Paris, Palaiseau, France
[42] Université de Strasbourg, CNRS, IPHC UMR 7178, Strasbourg, France
[43] Centre de Calcul de l'Institut National de Physique Nucleaire et de Physique des Particules, CNRS/IN2P3, Villeurbanne, France
[44] Institut de Physique des 2 Infinis de Lyon (IP2I), Villeurbanne, France
[45] Georgian Technical University, Tbilisi, Georgia
[46] RWTH Aachen University, I. Physikalisches Institut, Aachen, Germany
[47] RWTH Aachen University, III. Physikalisches Institut A, Aachen, Germany
[48] RWTH Aachen University, III. Physikalisches Institut B, Aachen, Germany
[49] Deutsches Elektronen-Synchrotron, Hamburg, Germany
[50] University of Hamburg, Hamburg, Germany
[51] Karlsruher Institut fuer Technologie, Karlsruhe, Germany
[52] Institute of Nuclear and Particle Physics (INPP), NCSR Demokritos, Aghia Paraskevi, Greece
[53] National and Kapodistrian University of Athens, Athens, Greece
[54] National Technical University of Athens, Athens, Greece
[55] University of Ioánnina, Ioánnina, Greece
[56] HUN-REN Wigner Research Centre for Physics, Budapest, Hungary
[57] MTA-ELTE Lendület CMS Particle and Nuclear Physics Group, Eötvös Loránd University, Budapest, Hungary
[58] Faculty of Informatics, University of Debrecen, Debrecen, Hungary
[59] HUN-REN ATOMKI — Institute of Nuclear Research, Debrecen, Hungary
[60] Karoly Robert Campus, MATE Institute of Technology, Gyongyos, Hungary
[61] Panjab University, Chandigarh, India
[62] University of Delhi, Delhi, India
[63] Indian Institute of Technology Mandi (IIT-Mandi), Himachal Pradesh, India
[64] University of Hyderabad, Hyderabad, India
[65] Indian Institute of Technology Kanpur, Kanpur, India
[66] Saha Institute of Nuclear Physics, HBNI, Kolkata, India
[67] Indian Institute of Technology Madras, Madras, India
[68] IISER Mohali, India, Mohali, India

JHEP04(2026)086

[69] Tata Institute of Fundamental Research-A, Mumbai, India
[70] Tata Institute of Fundamental Research-B, Mumbai, India
[71] National Institute of Science Education and Research, An OCC of Homi Bhabha National Institute, Bhubaneswar, Odisha, India
[72] Indian Institute of Science Education and Research (IISER), Pune, India
[73] Indian Institute of Technology Hyderabad, Telangana, India
[74] Isfahan University of Technology, Isfahan, Iran
[75] Institute for Research in Fundamental Sciences (IPM), Tehran, Iran
[76] University College Dublin, Dublin, Ireland
[77a] INFN Sezione di Bari, Bari, Italy
[77b] Università di Bari, Bari, Italy
[77c] Politecnico di Bari, Bari, Italy
[78a] INFN Sezione di Bologna, Bologna, Italy
[78b] Università di Bologna, Bologna, Italy
[79a] INFN Sezione di Catania, Catania, Italy
[79b] Università di Catania, Catania, Italy
[80a] INFN Sezione di Firenze, Firenze, Italy
[80b] Università di Firenze, Firenze, Italy
[81] INFN Laboratori Nazionali di Frascati, Frascati, Italy
[82a] INFN Sezione di Genova, Genova, Italy
[82b] Università di Genova, Genova, Italy
[83a] INFN Sezione di Milano-Bicocca, Milano, Italy
[83b] Università di Milano-Bicocca, Milano, Italy
[84a] INFN Sezione di Napoli, Napoli, Italy
[84b] Università di Napoli 'Federico II', Napoli, Italy
[84c] Università della Basilicata, Potenza, Italy
[84d] Scuola Superiore Meridionale (SSM), Napoli, Italy
[85a] INFN Sezione di Padova, Padova, Italy
[85b] Università di Padova, Padova, Italy
[85c] Universita degli Studi di Cagliari, Cagliari, Italy
[86a] INFN Sezione di Pavia, Pavia, Italy
[86b] Università di Pavia, Pavia, Italy
[87a] INFN Sezione di Perugia, Perugia, Italy
[87b] Università di Perugia, Perugia, Italy
[88a] INFN Sezione di Pisa, Pisa, Italy
[88b] Università di Pisa, Pisa, Italy
[88c] Scuola Normale Superiore di Pisa, Pisa, Italy
[88d] Università di Siena, Siena, Italy
[89a] INFN Sezione di Roma, Roma, Italy
[89b] Sapienza Università di Roma, Roma, Italy
[90a] INFN Sezione di Torino, Torino, Italy
[90b] Università di Torino, Torino, Italy
[90c] Università del Piemonte Orientale, Novara, Italy
[91a] INFN Sezione di Trieste, Trieste, Italy
[91b] Università di Trieste, Trieste, Italy
[92] Kyungpook National University, Daegu, Korea
[93] Department of Mathematics and Physics — GWNU, Gangneung, Korea
[94] Chonnam National University, Institute for Universe and Elementary Particles, Kwangju, Korea
[95] Hanyang University, Seoul, Korea
[96] Korea University, Seoul, Korea
[97] Kyung Hee University, Department of Physics, Seoul, Korea
[98] Sejong University, Seoul, Korea
[99] Seoul National University, Seoul, Korea

JHEP04(2026)086

[100] University of Seoul, Seoul, Korea
[101] Yonsei University, Department of Physics, Seoul, Korea
[102] Sungkyunkwan University, Suwon, Korea
[103] College of Engineering and Technology, American University of the Middle East (AUM), Dasman, Kuwait
[104] Kuwait University — College of Science — Department of Physics, Safat, Kuwait
[105] Riga Technical University, Riga, Latvia
[106] University of Latvia (LU), Riga, Latvia
[107] Vilnius University, Vilnius, Lithuania
[108] National Centre for Particle Physics, Universiti Malaya, Kuala Lumpur, Malaysia
[109] Universidad de Sonora (UNISON), Hermosillo, Mexico
[110] Centro de Investigacion y de Estudios Avanzados del IPN, Mexico City, Mexico
[111] Universidad Iberoamericana, Mexico City, Mexico
[112] Benemerita Universidad Autonoma de Puebla, Puebla, Mexico
[113] University of Montenegro, Podgorica, Montenegro
[114] University of Canterbury, Christchurch, New Zealand
[115] National Centre for Physics, Quaid-I-Azam University, Islamabad, Pakistan
[116] AGH University of Krakow, Krakow, Poland
[117] National Centre for Nuclear Research, Swierk, Poland
[118] Institute of Experimental Physics, Faculty of Physics, University of Warsaw, Warsaw, Poland
[119] Warsaw University of Technology, Warsaw, Poland
[120] Laboratório de Instrumentação e Física Experimental de Partículas, Lisboa, Portugal
[121] Faculty of Physics, University of Belgrade, Belgrade, Serbia
[122] VINCA Institute of Nuclear Sciences, University of Belgrade, Belgrade, Serbia
[123] Centro de Investigaciones Energéticas Medioambientales y Tecnológicas (CIEMAT), Madrid, Spain
[124] Universidad Autónoma de Madrid, Madrid, Spain
[125] Universidad de Oviedo, Instituto Universitario de Ciencias y Tecnologías Espaciales de Asturias (ICTEA), Oviedo, Spain
[126] Instituto de Física de Cantabria (IFCA), CSIC-Universidad de Cantabria, Santander, Spain
[127] University of Colombo, Colombo, Sri Lanka
[128] University of Ruhuna, Department of Physics, Matara, Sri Lanka
[129] CERN, European Organization for Nuclear Research, Geneva, Switzerland
[130] PSI Center for Neutron and Muon Sciences, Villigen, Switzerland
[131] ETH Zurich — Institute for Particle Physics and Astrophysics (IPA), Zurich, Switzerland
[132] Universität Zürich, Zurich, Switzerland
[133] National Central University, Chung-Li, Taiwan
[134] National Taiwan University (NTU), Taipei, Taiwan
[135] High Energy Physics Research Unit, Department of Physics, Faculty of Science, Chulalongkorn University, Bangkok, Thailand
[136] Tunis El Manar University, Tunis, Tunisia
[137] Çukurova University, Physics Department, Science and Art Faculty, Adana, Turkey
[138] Hacettepe University, Ankara, Turkey
[139] Middle East Technical University, Physics Department, Ankara, Turkey
[140] Bogazici University, Istanbul, Turkey
[141] Istanbul Technical University, Istanbul, Turkey
[142] Istanbul University, Istanbul, Turkey
[143] Yildiz Technical University, Istanbul, Turkey
[144] Institute for Scintillation Materials of National Academy of Science of Ukraine, Kharkiv, Ukraine
[145] National Science Centre, Kharkiv Institute of Physics and Technology, Kharkiv, Ukraine
[146] University of Bristol, Bristol, U.K.
[147] Rutherford Appleton Laboratory, Didcot, U.K.
[148] Imperial College, London, U.K.
[149] Brunel University, Uxbridge, U.K.
[150] Baylor University, Waco, Texas, U.S.A.

JHEP04(2026)086

[151] Bethel University, St. Paul, Minnesota, U.S.A.
[152] Catholic University of America, Washington, DC, U.S.A.
[153] The University of Alabama, Tuscaloosa, Alabama, U.S.A.
[154] Boston University, Boston, Massachusetts, U.S.A.
[155] Brown University, Providence, Rhode Island, U.S.A.
[156] University of California, Davis, Davis, California, U.S.A.
[157] University of California, Los Angeles, California, U.S.A.
[158] University of California, Riverside, Riverside, California, U.S.A.
[159] University of California, San Diego, La Jolla, California, U.S.A.
[160] University of California, Santa Barbara — Department of Physics, Santa Barbara, California, U.S.A.
[161] California Institute of Technology, Pasadena, California, U.S.A.
[162] Carnegie Mellon University, Pittsburgh, Pennsylvania, U.S.A.
[163] University of Colorado Boulder, Boulder, Colorado, U.S.A.
[164] Cornell University, Ithaca, New York, U.S.A.
[165] Fermi National Accelerator Laboratory, Batavia, Illinois, U.S.A.
[166] University of Florida, Gainesville, Florida, U.S.A.
[167] Florida State University, Tallahassee, Florida, U.S.A.
[168] Florida Institute of Technology, Melbourne, Florida, U.S.A.
[169] University of Illinois Chicago, Chicago, Illinois, U.S.A.
[170] The University of Iowa, Iowa City, Iowa, U.S.A.
[171] Johns Hopkins University, Baltimore, Maryland, U.S.A.
[172] The University of Kansas, Lawrence, Kansas, U.S.A.
[173] Kansas State University, Manhattan, Kansas, U.S.A.
[174] University of Maryland, College Park, Maryland, U.S.A.
[175] Massachusetts Institute of Technology, Cambridge, Massachusetts, U.S.A.
[176] University of Minnesota, Minneapolis, Minnesota, U.S.A.
[177] University of Nebraska-Lincoln, Lincoln, Nebraska, U.S.A.
[178] State University of New York at Buffalo, Buffalo, New York, U.S.A.
[179] Northeastern University, Boston, Massachusetts, U.S.A.
[180] Northwestern University, Evanston, Illinois, U.S.A.
[181] University of Notre Dame, Notre Dame, Indiana, U.S.A.
[182] The Ohio State University, Columbus, Ohio, U.S.A.
[183] Princeton University, Princeton, New Jersey, U.S.A.
[184] University of Puerto Rico, Mayaguez, Puerto Rico, U.S.A.
[185] Purdue University, West Lafayette, Indiana, U.S.A.
[186] Purdue University Northwest, Hammond, Indiana, U.S.A.
[187] Rice University, Houston, Texas, U.S.A.
[188] University of Rochester, Rochester, New York, U.S.A.
[189] Rutgers, The State University of New Jersey, Piscataway, New Jersey, U.S.A.
[190] University of Tennessee, Knoxville, Tennessee, U.S.A.
[191] Texas A&M University, College Station, Texas, U.S.A.
[192] Texas Tech University, Lubbock, Texas, U.S.A.
[193] Vanderbilt University, Nashville, Tennessee, U.S.A.
[194] University of Virginia, Charlottesville, Virginia, U.S.A.
[195] Wayne State University, Detroit, Michigan, U.S.A.
[196] University of Wisconsin — Madison, Madison, Wisconsin, U.S.A.
[197] An institute or international laboratory covered by a cooperation agreement with CERN
[198] An institute formerly covered by a cooperation agreement with CERN

[a] Also at Yerevan State University, Yerevan, Armenia
[b] Also at TU Wien, Vienna, Austria
[c] Also at Ghent University, Ghent, Belgium
[d] Also at FACAMP — Faculdades de Campinas, Sao Paulo, Brazil

JHEP04(2026)086

[e] Also at Universidade do Estado do Rio de Janeiro, Rio de Janeiro, Brazil
[f] Also at Universidade Estadual de Campinas, Campinas, Brazil
[g] Also at Federal University of Rio Grande do Sul, Porto Alegre, Brazil
[h] Also at The University of the State of Amazonas, Manaus, Brazil
[i] Also at University of Chinese Academy of Sciences, Beijing, China
[j] Also at China Center of Advanced Science and Technology, Beijing, China
[k] Also at University of Chinese Academy of Sciences, Beijing, China
[l] Also at School of Physics, Zhengzhou University, Zhengzhou, China
[m] Now at Henan Normal University, Xinxiang, China
[n] Also at University of Shanghai for Science and Technology, Shanghai, China
[o] Now at The University of Iowa, Iowa City, Iowa, U.S.A.
[p] Also at Center for High Energy Physics, Peking University, Beijing, China
[q] Also at Cairo University, Cairo, Egypt
[r] Also at Zewail City of Science and Technology, Zewail, Egypt
[s] Also at Purdue University, West Lafayette, Indiana, U.S.A.
[t] Also at Université de Haute Alsace, Mulhouse, France
[u] Also at Another institute or international laboratory covered by a cooperation agreement with CERN
[v] Also at Institut für Theoretische Teilchenphysik und Kosmologie, RWTH Aachen University, Aachen, Germany
[w] Also at University of Hamburg, Hamburg, Germany
[x] Also at RWTH Aachen University, III. Physikalisches Institut A, Aachen, Germany
[y] Also at Bergische University Wuppertal (BUW), Wuppertal, Germany
[z] Also at Brandenburg University of Technology, Cottbus, Germany
[aa] Also at Forschungszentrum Jülich, Juelich, Germany
[ab] Now at RWTH Aachen University, III. Physikalisches Institut A, Aachen, Germany
[ac] Also at CERN, European Organization for Nuclear Research, Geneva, Switzerland
[ad] Also at Institute for Theoretical Particle Physics, Karlsruhe Institute of Technology, Karlsruhe, Germany
[ae] Also at HUN-REN ATOMKI — Institute of Nuclear Research, Debrecen, Hungary
[af] Now at Universitatea Babes-Bolyai — Facultatea de Fizica, Cluj-Napoca, Romania
[ag] Also at MTA-ELTE Lendület CMS Particle and Nuclear Physics Group, Eötvös Loránd University, Budapest, Hungary
[ah] Also at HUN-REN Wigner Research Centre for Physics, Budapest, Hungary
[ai] Also at Physics Department, Faculty of Science, Assiut University, Assiut, Egypt
[aj] Also at The University of Kansas, Lawrence, Kansas, U.S.A.
[ak] Also at Punjab Agricultural University, Ludhiana, India
[al] Also at University of Hyderabad, Hyderabad, India
[am] Also at Indian Institute of Science (IISc), Bangalore, India
[an] Also at University of Visva-Bharati, Santiniketan, India
[ao] Also at IIT Bhubaneswar, Bhubaneswar, India
[ap] Also at Institute of Physics, Bhubaneswar, India
[aq] Also at Deutsches Elektronen-Synchrotron, Hamburg, Germany
[ar] Also at Isfahan University of Technology, Isfahan, Iran
[as] Also at Sharif University of Technology, Tehran, Iran
[at] Also at Department of Physics, University of Science and Technology of Mazandaran, Behshahr, Iran
[au] Also at Department of Physics, Faculty of Science, Arak University, ARAK, Iran
[av] Also at Helwan University, Cairo, Egypt
[aw] Also at Italian National Agency for New Technologies, Energy and Sustainable Economic Development, Bologna, Italy
[ax] Also at Centro Siciliano di Fisica Nucleare e di Struttura Della Materia, Catania, Italy
[ay] Also at Università degli Studi Guglielmo Marconi, Roma, Italy
[az] Also at Scuola Superiore Meridionale, Università di Napoli 'Federico II', Napoli, Italy
[ba] Also at Fermi National Accelerator Laboratory, Batavia, Illinois, U.S.A.
[bb] Also at Lulea University of Technology, Lulea, Sweden

JHEP04(2026)086

[bc] Also at Consiglio Nazionale delle Ricerche — Istituto Officina dei Materiali, Perugia, Italy
[bd] Also at UPES — University of Petroleum and Energy Studies, Dehradun, India
[be] Also at Institut de Physique des 2 Infinis de Lyon (IP2I), Villeurbanne, France
[bf] Also at Department of Applied Physics, Faculty of Science and Technology, Universiti Kebangsaan Malaysia, Bangi, Malaysia
[bg] Also at Trincomalee Campus, Eastern University, Sri Lanka, Nilaveli, Sri Lanka
[bh] Also at Saegis Campus, Nugegoda, Sri Lanka
[bi] Also at National and Kapodistrian University of Athens, Athens, Greece
[bj] Also at Ecole Polytechnique Fédérale Lausanne, Lausanne, Switzerland
[bk] Also at Universität Zürich, Zurich, Switzerland
[bl] Also at Stefan Meyer Institute for Subatomic Physics, Vienna, Austria
[bm] Also at Near East University, Research Center of Experimental Health Science, Mersin, Turkey
[bn] Also at Konya Technical University, Konya, Turkey
[bo] Also at Izmir Bakircay University, Izmir, Turkey
[bp] Also at Adiyaman University, Adiyaman, Turkey
[bq] Also at Bozok Universitetesi Rektörlügü, Yozgat, Turkey
[br] Also at Istanbul Sabahattin Zaim University, Istanbul, Turkey
[bs] Also at Marmara University, Istanbul, Turkey
[bt] Also at Milli Savunma University, Istanbul, Turkey
[bu] Also at Informatics and Information Security Research Center, Gebze/Kocaeli, Turkey
[bv] Also at Kafkas University, Kars, Turkey
[bw] Now at Istanbul Okan University, Istanbul, Turkey
[bx] Also at Istanbul University — Cerrahpasa, Faculty of Engineering, Istanbul, Turkey
[by] Also at Istinye University, Istanbul, Turkey
[bz] Also at Yildiz Technical University, Istanbul, Turkey
[ca] Also at School of Physics and Astronomy, University of Southampton, Southampton, U.K.
[cb] Also at Monash University, Faculty of Science, Clayton, Australia
[cc] Also at Università di Torino, Torino, Italy
[cd] Also at Karamanoğlu Mehmetbey University, Karaman, Turkey
[ce] Also at California Lutheran University;, Thousand Oaks, California, U.S.A.
[cf] Also at California Institute of Technology, Pasadena, California, U.S.A.
[cg] Also at United States Naval Academy, Annapolis, Maryland, U.S.A.
[ch] Also at Bingol University, Bingol, Turkey
[ci] Also at Georgian Technical University, Tbilisi, Georgia
[cj] Also at Sinop University, Sinop, Turkey
[ck] Also at Erciyes University, Kayseri, Turkey
[cl] Also at Horia Hulubei National Institute of Physics and Nuclear Engineering (IFIN-HH), Bucharest, Romania
[cm] Now at Another institute formerly covered by a cooperation agreement with CERN
[cn] Also at Another institute formerly covered by a cooperation agreement with CERN
[co] Also at Hamad Bin Khalifa University (HBKU), Doha, Qatar
[cp] Also at Yerevan Physics Institute, Yerevan, Armenia
[cq] Also at Imperial College, London, U.K.
[cr] Now at Yerevan Physics Institute, Yerevan, Armenia
[†] Deceased

JHEP04(2026)086